Riv. Mat. Univ. Parma (8) **1** (2009), 1-69

KAZUO AOKI and SHIGERU TAKATA

Fluid models and simulations of internal rarefied gas flows

Abstract. Fluid flows in small systems become increasingly important in various applications such as micromechanical systems. The present article focuses its attention on internal rarefied gas flows, in particular, flows induced by temperature fields, and summarizes some of the results that seem to be useful or interesting for applications to micromechanical systems. In the first half, after a brief description of the Boltzmann equation, its boundary-value problems for small Knudsen numbers are considered, and the results of the asymptotic theory that gives the recipe to obtain correct solutions via fluid-dynamic systems are summarized. Numerical analyses of flows induced by temperature fields at intermediate Knudsen numbers are also presented. In the latter half, potential applications of the flows caused by temperature fields are surveyed, with special emphasis on the Knudsen compressor and its variants. Convenient convection-diffusion systems for the Knudsen compressor are proposed, and the methods of numerical analysis of fundamental problems, such as Poiseuille flow and thermal transpiration, are reviewed in the connection to the convection-diffusion systems.

Keywords. Rarefied gas, Boltzmann equation, slip flow, thermal transpiration, thermal edge flow, Poiseuille flow, Knudsen compressor.

Mathematics Subject Classification (2000): 76P05, 82B40, 82C40, 82D05.

Received: November 13, 2008; accepted: February 9, 2009.

This research was partially supported by KAKENHI (Nos. 20360046 and 19560066) from JSPS.

Contents

1 - Introduction

Fluid flows in small systems become increasingly important in various applications such as micromechanical systems. In the case of gas flows in micro scales, the mean free path of the gas molecules is not negligibly small compared with the characteristic length of the systems. Therefore, the effect of gas rarefaction, which is peculiar to low-density gases, also manifests itself in this situation. In other words, the ordinary fluid dynamics is not applicable, and a microscopic approach based on kinetic theory is necessary.

In the present paper, we focus our attention to internal rarefied gas flows, in particular, flows induced by temperature fields, and summarize some of the results that seem to be useful or interesting for applications to micromechanical systems. The paper is organized as follows. To begin with, we summarize the Boltzmann equation in Sec. 2. Then, in Sec. 3, we consider boundary-value problems of the Boltzmann equation for small Knudsen numbers (near continuum regime) and summarize the results of the asymptotic theory that gives the recipe to obtain correct solutions via fluid-dynamic systems. Section 4 is devoted to numerical analysis of flows induced by temperature fields at intermediate Knudsen numbers (transition regime). In Sec. 5, we overview potential applications of the flows caused by temperature fields with special emphasis on the Knudsen compressor and its variants. Then, in Sec. 6, we propose convenient convection-diffusion systems for the Knudsen compressor. Section 7 is devoted to numerical analysis of fundamental problems, such as Poiseuille flow and thermal transpiration, that play important roles also in the convection-diffusion systems introduced in Sec. 6.

2 - Boltzmann equation

In this section, we summarize the Boltzmann equation and related equations, following [**1, 2**] basically. In this introductory section, we restrict ourselves to a simple monatomic gas and assume that there is no external force. However, in the later sections, more general cases, such as a gas mixture, will also be considered. Supplementary explanations will be given when necessary.

2.1 - *Notation*

To begin with, we summarize the notation used here. The t is the time variable, $\boldsymbol{X}$ (or X_i) the position vector in physical space, $\boldsymbol{\xi}$ (or ξ_i) the molecular velocity vector, $f(t,\boldsymbol{X},\boldsymbol{\xi})$ the velocity distribution function of the gas molecules, $\rho(t,\boldsymbol{X})$ the macroscopic mass density, $\boldsymbol{v}(t,\boldsymbol{X})$ [or $v_i(t,\boldsymbol{X})$] the flow velocity, $T(t,\boldsymbol{X})$ the temperature, $p_{ij}(t,\boldsymbol{X})$ the stress tensor, and $\boldsymbol{q}(t,\boldsymbol{X})$ [or $q_i(t,\boldsymbol{X})$] the heat-flow vector. We further introduce the following dimensionless variables.

$$
\begin{aligned}
&\hat{t} = t/t_0, && \boldsymbol{x} = \boldsymbol{X}/L, && \boldsymbol{\zeta} = \boldsymbol{\xi}/(2RT_0)^{1/2},\\
&\hat{f} = (2RT_0)^{3/2}\rho_0^{-1}f, && \hat{\rho} = \rho/\rho_0, &&\\
&\hat{\boldsymbol{v}} = \boldsymbol{v}/(2RT_0)^{1/2}, && \hat{T} = T/T_0, && \hat{p} = p/p_0,\\
&\hat{p}_{ij} = p_{ij}/p_0, && \hat{\boldsymbol{q}} = \boldsymbol{q}/p_0(2RT_0)^{1/2}, &&
\end{aligned}
\tag{1}
$$

where t_0 is the reference time, L the reference length, ρ_0 the reference density, T_0 the reference temperature, $p_0 = R\rho_0 T_0$ the reference pressure, and R the gas constant per unit mass ($R = k_B/m$ with m the mass of a molecule and k_B the Boltzmann constant). The x_i, ζ_i, $\hat{v}_i$, and $\hat{q}_i$ are also used for $\boldsymbol{x}$, $\boldsymbol{\zeta}$, $\hat{\boldsymbol{v}}$, and $\hat{\boldsymbol{q}}$.

2.2 - *Macroscopic quantities*

The macroscopic quantities ρ, $\boldsymbol{v}$, T, p, p_{ij}, and $\boldsymbol{q}$ are expressed as appropriate integrals of the velocity distribution function f. We summarize the expression in the dimensionless form.

$$
\begin{aligned}
&\hat{\rho} = \int \hat{f}\, d\boldsymbol{\zeta}, && \hat{\boldsymbol{v}} = (1/\hat{\rho})\int \boldsymbol{\zeta}\hat{f}\, d\boldsymbol{\zeta},\\
&\hat{T} = (2/3\hat{\rho})\int (\zeta_j - \hat{v}_j)^2 \hat{f}\, d\boldsymbol{\zeta}, && \hat{p} = \hat{\rho}\hat{T},\\
&\hat{p}_{ij} = 2\int (\zeta_i - \hat{v}_i)(\zeta_j - \hat{v}_j)\hat{f}\, d\boldsymbol{\zeta}, &&\\
&\hat{\boldsymbol{q}} = \int (\boldsymbol{\zeta} - \hat{\boldsymbol{v}})(\zeta_j - \hat{v}_j)^2 \hat{f}\, d\boldsymbol{\zeta}, &&
\end{aligned}
\tag{2}
$$

where the domain of integration with respect to $\boldsymbol{\zeta}$ is its whole space.

When the state of the gas is close to the equilibrium state at rest with density ρ_0 (or pressure p_0) and temperature T_0, the velocity distribution function f can be expressed as

$$
\begin{aligned}
&f = \rho_0 (2\pi R T_0)^{-3/2} \exp(-\xi_i^2/2RT_0)(1+\phi), \quad \text{or} \\
&\hat{f} = E(1+\phi), \qquad E = \pi^{-3/2}\exp(-\zeta_i^2),
\end{aligned}
\tag{3}
$$

where $|\phi|$ is a small quantity. Correspondingly, the dimensionless macroscopic quantities can be written as

$$
\begin{aligned}
&\hat{\rho} = 1+\omega, \qquad &&\hat{\boldsymbol{v}} = \boldsymbol{u}, \qquad &&\hat{T} = 1+\tau, \\
&\hat{p} = 1+P, \qquad &&\hat{p}_{ij} = \delta_{ij} + P_{ij}, \qquad &&\hat{\boldsymbol{q}} = \boldsymbol{Q},
\end{aligned}
\tag{4}
$$

where δ_{ij} is the Kronecker delta, and $|\omega|$, $|\boldsymbol{u}|$ (or $|u_i|$), $|\tau|$, $|P|$, $|P_{ij}|$, and $|\boldsymbol{Q}|$ (or $|Q_i|$) are small quantities. If $|\phi|$ and these small quantities are so small that their products may be neglected, Eq. (2) can be linearized and gives

$$
\begin{aligned}
&\omega = \int \phi E d\boldsymbol{\zeta}, \qquad &&\boldsymbol{u} = \int \boldsymbol{\zeta}\phi E d\boldsymbol{\zeta}, \\
&\tau = \frac{2}{3}\int \left(\zeta_j^2 - \frac{3}{2}\right)\phi E d\boldsymbol{\zeta}, \qquad &&P = \omega + \tau, \\
&P_{ij} = 2\int \zeta_i \zeta_j \phi E d\boldsymbol{\zeta}, \qquad &&\boldsymbol{Q} = \int \boldsymbol{\zeta}\zeta_j^2 \phi E d\boldsymbol{\zeta} - \frac{5}{2}\boldsymbol{u}.
\end{aligned}
\tag{5}
$$

2.3 - *Boltzmann equation*

The Boltzmann equation, written in terms of the dimensionless variables, is

$$
\mathrm{Sh}\frac{\partial \hat{f}}{\partial \hat{t}} + \boldsymbol{\zeta}\cdot\frac{\partial \hat{f}}{\partial \boldsymbol{x}} = \frac{2}{\sqrt{\pi}\,\mathrm{Kn}}\hat{J}(\hat{f},\hat{f}),
\tag{6}
$$

$$
\hat{J}(\hat{f},\hat{f}) = \int (\hat{f}'\hat{f}_*' - \hat{f}\hat{f}_*)\hat{B}\, d\Omega d\boldsymbol{\zeta}_*,
\tag{7}
$$

$$
\mathrm{Sh} = L/(2RT_0)^{1/2}t_0, \qquad \mathrm{Kn} = l_0/L.
\tag{8}
$$

Here, $\hat{J}(\hat{f},\hat{f})$ expresses the effect of molecular collision, and the symbols there are as follows: $\hat{f}'$, $\hat{f}_*'$, $\hat{f}$, and $\hat{f}_*$ stand for $\hat{f}(t, \boldsymbol{x}, \boldsymbol{\zeta})$ with $\boldsymbol{\zeta} = \boldsymbol{\zeta}'$, $\boldsymbol{\zeta}_*'$, $\boldsymbol{\zeta}$, and $\boldsymbol{\zeta}_*$, respectively, $\boldsymbol{\zeta}_*$ is the variable of integration corresponding to $\boldsymbol{\zeta}$, and $\boldsymbol{\zeta}'$ and $\boldsymbol{\zeta}_*'$ are defined by

$$
\begin{aligned}
&\boldsymbol{\zeta}' = \boldsymbol{\zeta} + (\boldsymbol{V}\cdot\boldsymbol{e})\boldsymbol{e}, \qquad &&\boldsymbol{\zeta}_*' = \boldsymbol{\zeta}_* - (\boldsymbol{V}\cdot\boldsymbol{e})\boldsymbol{e}, \\
&\boldsymbol{V} = \boldsymbol{\zeta}_* - \boldsymbol{\zeta},
\end{aligned}
\tag{9}
$$

where $\boldsymbol{e}$ is a unit vector; $\hat{B}$ is a nonnegative function of $|\boldsymbol{V}|$ and $|\boldsymbol{V}\cdot\boldsymbol{e}|$ depending on the molecular model (in general, $\hat{B}$ also depends on U_*/k_BT_0, where U_* is the characteristic size of the intermolecular potential [**1**]); $d\Omega$ is the solid-angle element around $\boldsymbol{e}$, and the domain of integration in Eq. (7) is all directions of $\boldsymbol{e}$ and the whole space of $\boldsymbol{\zeta}_*$. In Eq. (8), l_0 is the mean free path of the gas molecules in the equilibrium state at rest at density ρ_0 and temperature T_0, and Sh and Kn are the dimensionless parameters called the Strouhal number and the Knudsen number, respectively. For hard-sphere molecules, $\hat{B} = |\boldsymbol{V}\cdot\boldsymbol{e}|/4\sqrt{2\pi}$ and $l_0 = (\sqrt{2}\pi d_m^2\rho_0/m)^{-1}$ with m and d_m being the mass and the diameter of a molecule.

When $|\phi|$ [Eq. (3)] is small and the linearization (5) is valid, the Boltzmann equation (6) can be linearized and gives the following linearized Boltzmann equation.

$$\mathrm{Sh}\,\frac{\partial\phi}{\partial\hat{t}} + \boldsymbol{\zeta}\cdot\frac{\partial\phi}{\partial\boldsymbol{x}} = \frac{2}{\sqrt{\pi}\,\mathrm{Kn}}\,\mathcal{L}(\phi), \tag{10}$$

$$\mathcal{L}(\phi) = \int E_*(\phi' + \phi'_* - \phi - \phi_*)\hat{B}\,d\Omega\,d\boldsymbol{\zeta}_*, \tag{11}$$

where E_* is E in Eq. (3) with $\boldsymbol{\zeta} = \boldsymbol{\zeta}_*$, and ϕ', ϕ'_*, etc. stand for ϕ with $\boldsymbol{\zeta} = \boldsymbol{\zeta}'$, $\boldsymbol{\zeta}'_*$, etc.

The model collision term, called the BGK model, is often used in place of (7). The model is given by

$$\hat{J}(\hat{f}, \hat{f}) = \hat{\rho}\,(\hat{f}_e - \hat{f}), \tag{12}$$

$$\hat{f}_e = \frac{\hat{\rho}}{(\pi\hat{T})^{3/2}}\exp\Big(-\frac{(\zeta_j - \hat{v}_j)^2}{\hat{T}}\Big), \tag{13}$$

where $\hat{f}_e$ is the dimensionless form of the local equilibrium distribution, and $\hat{\rho}$, $\hat{\boldsymbol{v}}$, and $\hat{T}$ are given by Eq. (2). In this model, $l_0 = (2/\sqrt{\pi})(2RT_0)^{1/2}(A_c\rho_0)^{-1}$, where A_c is a constant ($A_c\rho_0$ is the corresponding collision frequency). For this model, the linearized collision term corresponding to Eq. (10) is

$$\mathcal{L}(\phi) = \omega + 2\boldsymbol{\zeta}\cdot\boldsymbol{u} + (\zeta_j^2 - 3/2)\tau - \phi, \tag{14}$$

where ω, $\boldsymbol{u}$, and τ are given by Eq. (5).

2.4 - *Boundary condition*

As the initial condition for the Boltzmann equation (6) [or (10)], we need to specify $\hat{f}$ (or ϕ) at the initial time.

Let $\boldsymbol{v}_w$ (or v_{wi}) and T_w be the velocity and temperature of the boundary, and $\hat{\boldsymbol{v}}_w$ (or $\hat{v}_{wi}$) and $\hat{T}_w$ be the corresponding dimensionless quantities, i.e.,

$$\hat{\boldsymbol{v}}_w = \boldsymbol{v}_w/(2RT_0)^{1/2}, \qquad \hat{T}_w = T_w/T_0. \tag{15}$$

The conventional boundary condition for Eq. (6) on the solid boundary is the Maxwell type condition, the dimensionless form of which is written as

$$\hat{f}(\zeta_i) = (1-a)\hat{f}(\zeta_i - 2[(\boldsymbol{\zeta}-\hat{\boldsymbol{v}}_w)\cdot\boldsymbol{n}]\,n_i) + a\frac{\hat{\rho}_w}{(\pi\hat{T}_w)^{3/2}}\exp\Big(-\frac{(\zeta_j-\hat{v}_{wj})^2}{\hat{T}_w}\Big), \qquad (\boldsymbol{\zeta}-\hat{\boldsymbol{v}}_w)\cdot\boldsymbol{n} > 0, \tag{16a}$$

$$\hat{\rho}_w = -\frac{2\sqrt{\pi}}{\hat{T}_w^{1/2}} \int\limits_{(\boldsymbol{\zeta}-\hat{\boldsymbol{v}}_w)\cdot\boldsymbol{n}<0} (\boldsymbol{\zeta}-\hat{\boldsymbol{v}}_w)\cdot\boldsymbol{n}\,\hat{f}(\zeta_i)d\boldsymbol{\zeta}, \tag{16b}$$

where $\boldsymbol{n}$ is the unit normal vector to the boundary, pointing to the gas, a ($0 \le a \le 1$) is the accommodation coefficient, and the independent variables $\hat{t}$ and $\boldsymbol{x}$ in $\hat{f}$ are not shown explicitly. The case $a = 1$ is called the diffuse reflection, and $a = 0$ the specular reflection. The condition for the linearized Boltzmann equation (10) corresponding to Eqs. (16a) and (16b) is

$$\phi(\zeta_i) = (1-a)\big[\phi(\zeta_i - 2[(\boldsymbol{\zeta}-\boldsymbol{u}_w)\cdot\boldsymbol{n}]\,n_i) + 4(\boldsymbol{\zeta}\cdot\boldsymbol{n})(\boldsymbol{u}_w\cdot\boldsymbol{n})\big] + a\big[\sigma_w + 2\boldsymbol{\zeta}\cdot\boldsymbol{u}_w + (\zeta_j^2 - 3/2)\tau_w\big], \qquad (\boldsymbol{\zeta}-\boldsymbol{u}_w)\cdot\boldsymbol{n} > 0, \tag{17a}$$

$$\sigma_w = \sqrt{\pi}\boldsymbol{u}_w\cdot\boldsymbol{n} - (1/2)\tau_w - 2\sqrt{\pi} \int\limits_{(\boldsymbol{\zeta}-\boldsymbol{u}_w)\cdot\boldsymbol{n}<0} (\boldsymbol{\zeta}-\boldsymbol{u}_w)\cdot\boldsymbol{n}\,\phi(\zeta_i)E d\boldsymbol{\zeta}, \tag{17b}$$

where $\hat{\boldsymbol{v}}_w = \boldsymbol{u}_w$ and $\hat{T}_w = 1 + \tau_w$. Note that $\hat{\boldsymbol{v}}_w\cdot\boldsymbol{n} = 0$ in Eqs. (16a) and (16b) [or $\boldsymbol{u}_w\cdot\boldsymbol{n} = 0$ in Eqs. (17a) and (17b)] for steady problems.

3 - Asymptotic Theory for Small Knudsen Numbers

In practical applications, slightly rarefied gas flows (gas flows with small Knudsen numbers) are often analyzed by the use of the Navier–Stokes equations and the slip boundary conditions. However, much attention is not paid to the validity of the use of this system. Furthermore, it is rather surprising that the formulas of the slip conditions derived by means of the elementary kinetic theory very long time ago are still in use. The systematic derivation of the fluid-dynamic description of slightly rarefied gas flows has been one of the important subjects in rarefied gas dynamics, and such treatment has been established for steady flows by Sone by means of a systematic asymptotic analysis of the Boltzmann equation

(asymptotic theory) [**3, 4, 5, 6, 7, 8, 9, 1, 2**]. This theory, which is of theoretical importance, also provides a convenient tool to compute slightly rarefied gas flows in view of the fact that direct numerical computations or simulations based on the Boltzmann and other kinetic equations become increasingly difficult as the Knudsen number becomes small.

According to the asymptotic theory, the overall behavior of the gas is described by a system of fluid-dynamic type equations and their appropriate boundary conditions, and the solution of this system undergoes a correction in a thin layer, with a few mean-free-path thick, adjacent to the boundary (the Knudsen layer). The explicit form of the fluid-dynamic type systems depends on the physical situation under consideration. In the present paper, we omit the course of the asymptotic analysis and give only part of the results because of the limited space. More specifically, we summarize the fluid-dynamic type systems that are sufficient to obtain the overall behavior, omitting the formulas of the local Knudsen-layer corrections. For the details, the reader is referred to [**1, 2,** 8].

Let us consider a gas around solid boundaries with arbitrary but smooth shape. We investigate the steady behavior of the gas when the Knudsen number Kn, defined by $\mathrm{Kn} = l_0/L$, is small, where l_0 is the reference mean free path of the gas molecules, and L is the reference length of the system. Let Ma be the Mach number and Re the Reynolds number, defined respectively by $\mathrm{Ma} = U/a_0$ and $\mathrm{Re} = \mu_0 UL/\rho_0$, where U, a_0, ρ_0, and μ_0 are, respectively, the reference values of the flow speed, sound speed, density, and viscosity [$a_0 = (5RT_0/3)^{1/2}$ with T_0 being the reference temperature]. Then, the three parameters are not independent, but are related as

$$\mathrm{Ma} \propto \mathrm{Kn}\,\mathrm{Re}. \tag{18}$$

3.1 - *The case of small* Re

The case where the Reynolds number is small, i.e., $\mathrm{Re} \ll \mathrm{Kn} \ll 1$, [thus, Ma is much smaller than Kn from Eq. (18)] is studied in [**3, 4, 6**]. Since Ma is a measure of deviation of the system from the reference equilibrium state at rest (with density ρ_0 and temperature T_0), the density ρ, flow velocity $\boldsymbol{v}$, temperature T, and pressure p are expressed as $\rho = \rho_0(1+\omega)$, $\boldsymbol{v} = (2RT_0)^{1/2}\boldsymbol{u}$, $T = T_0(1+\tau)$, and $p = p_0(1+P)$ with small deviations ω, $\boldsymbol{u}$ (or u_i), τ, and P, where $p_0 = R\rho_0 T_0$ is the reference pressure [see Eqs. (1) and (4)]. These deviations are expanded in power series of the Knudsen number, i.e.,

$$h = h_{(0)} + h_{(1)}\varepsilon + h_{(2)}\varepsilon^2 + \cdots, \qquad (h = \omega,\ \boldsymbol{u},\ \tau,\ \text{or } P), \tag{19}$$

$$\varepsilon = (\sqrt{\pi}/2)\,\mathrm{Kn}. \tag{20}$$

3.1.1 - Fluid-dynamic equations

The $h_{(m)}$ in Eq. (19) are governed by the following Stokes system of equations:

$$\frac{\partial P_{(0)}}{\partial x_i} = 0, \tag{21}$$

$$\frac{\partial u_{i(m)}}{\partial x_i} = 0, \tag{22a}$$

$$\frac{\partial P_{(m+1)}}{\partial x_i} = \gamma_1 \frac{\partial^2 u_{i(m)}}{\partial x_j^2}, \tag{22b}$$

$$\frac{\partial^2 \tau_{(m)}}{\partial x_j^2} = 0, \tag{22c}$$

$$\omega_{(m)} = P_{(m)} - \tau_{(m)}, \tag{22d}$$

$$(m = 0,\ 1,\ 2,\ \ldots),$$

where x_i is the system of dimensionless coordinates [Eq. (1)], and γ_1 is a constant depending on the molecular model:

$$\gamma_1 = 1.270042, \tag{23}$$

for hard-sphere molecules, and

$$\gamma_1 = 1, \tag{24}$$

for the BGK model [Eq. (6) with Eq. (12) or Eq. (10) with Eq. (14)]. The γ_1 is related to the viscosity μ_0 corresponding to pressure p_0 and temperature T_0 as

$$\mu_0 = (\sqrt{\pi}/2)\gamma_1 p_0 (2RT_0)^{-1/2} l_0. \tag{25}$$

3.1.2 - Slip boundary conditions

Let $\boldsymbol{v}_w = (2RT_0)^{1/2}\boldsymbol{u}_w$ and $T_w = T_0(1 + \tau_w)$ be the velocity and temperature of the boundary, respectively, where $\boldsymbol{u}_w$ and τ_w are small deviations, and let $\boldsymbol{n}$ (or n_i) and $\boldsymbol{t}$ (or t_i) be the unit normal vector (pointing to the gas) and a unit tangential vector of the boundary, respectively ($\boldsymbol{u}_w \cdot \boldsymbol{n} = 0$ for steady problems). Then, the boundary conditions for Eqs. (22a)–(22d) on the boundary, which have been obtained up to the second order ($m = 2$), are given by

$$\boldsymbol{u}_{(0)} = \boldsymbol{u}_w, \qquad \tau_{(0)} = \tau_w, \tag{26}$$

$$u_{i(1)} t_i = k_0 S_{ij(0)} n_i t_j + K_1 G_{i(0)} t_i, \tag{27a}$$

$$u_{i(1)} n_i = 0, \tag{27b}$$

$$\tau_{(1)} = -d_1 G_{i(0)} n_i, \tag{27c}$$

$$u_{i(2)} t_i = k_0 S_{ij(1)} n_i t_j + a_1 \frac{\partial S_{ij(0)}}{\partial x_r} n_j n_r t_i + a_2 \bar{\kappa} S_{ij(0)} n_i t_j + a_3 \kappa_{ij} S_{jr(0)} n_r t_i + a_4 \frac{\partial G_{i(0)}}{\partial x_j} n_j t_i + a_5 \bar{\kappa} G_{i(0)} t_i + a_6 \kappa_{ij} G_{j(0)} t_i, \tag{28a}$$

$$u_{i(2)} n_i = b_1 \frac{\partial S_{ij(0)}}{\partial x_r} n_i n_j n_r + b_2 \Big(\frac{\partial G_{i(0)}}{\partial x_j} n_i n_j + 2 \bar{\kappa} G_{i(0)} n_i \Big), \tag{28b}$$

$$\tau_{(2)} = -d_1 G_{i(1)} n_i - d_4 \frac{\partial S_{ij(0)}}{\partial x_r} n_i n_j n_r - d_3 \frac{\partial G_{i(0)}}{\partial x_j} n_i n_j - d_5 \bar{\kappa} G_{i(0)} n_i, \tag{28c}$$

where

$$S_{ij(m)} = -\Big(\frac{\partial u_{i(m)}}{\partial x_j} + \frac{\partial u_{j(m)}}{\partial x_i} \Big), \tag{29a}$$

$$G_{i(m)} = -\frac{\partial \tau_{(m)}}{\partial x_i}, \tag{29b}$$

$$\bar{\kappa} = (\kappa_1 + \kappa_2)/2, \qquad \kappa_{ij} = \kappa_1 \ell_i \ell_j + \kappa_2 s_i s_j. \tag{29c}$$

Here, κ_1 and κ_2 are the principal curvatures of the boundary in the dimensionless x_i space, taken in such a manner that κ_β ($\beta = 1,\ 2$) is negative when the corresponding center of curvature lies in the gas; ℓ_i and s_i are the direction cosines of the principal directions corresponding to κ_1 and κ_2, respectively. Note that all the terms in the right-hand sides in Eqs. (27a)–(28c) are to be evaluated on the boundary.

The coefficients k_0, K_1, d_1, ... in Eqs. (27a)–(28c), which are called the slip coefficients, are the constants, the values of which depend on the molecular model and the reflection law on the boundary. For the BGK model under the diffuse reflection condition [Eqs. (17a) and (17b) with $a = 1$], they are given by

$$\begin{array}{lll} k_0 = -1.01619, & K_1 = -0.38316, & d_1 = 1.30272, \\ a_1 = 0.76632, & a_2 = 0.50000, & a_3 = -0.26632, \\ a_4 = 0.27922, & a_5 = 0.26693, & a_6 = -0.76644, \\ b_1 = 0.11684, & b_2 = 0.26693, & d_3 = 0, \\ d_4 = 0.11169, & d_5 = 1.82181. & \end{array} \tag{30}$$

For hard-sphere molecules and the diffuse reflection condition, the first-order slip coefficients and some of the second-order ones are obtained, that is,

$$\begin{array}{lll} k_0 = -1.2540, & K_1 = -0.6463, & d_1 = 2.4001, \\ a_4 = 0.0330, & b_1 = 0.1068, & b_2 = 0.4776. \end{array} \tag{31}$$

The numerical values given in Eqs. (30) and (31), the origins of which are some different papers, are taken from [**1, 2,** 8].

3.1.3 - Recipe for the solution

Although the system, in particular, the second-order boundary condition, appears to be complicated, its application is straightforward. The recipe would be obvious, but we give it just to make sure.

(i) From Eq. (21), $P_{(0)}$ is a constant, which is determined by an intrinsic condition of each problem.

(ii) Solve Eqs. (22a)–(22c) ($m = 0$) under the no-slip condition (26) to obtain $\boldsymbol{u}_{(0)}$, $P_{(1)}$, and $\tau_{(0)}$ and compute $\omega_{(0)}$ from Eq. (22d) ($m = 0$). (The additive constant in $P_{(1)}$ is determined by the intrinsic condition. The situation is the same for $P_{(2)}$ and $P_{(3)}$ in the steps below.)

(iii) Compute the right-hand sides of Eqs. (27a)–(27c) using the result in step (ii). Under the resultant boundary conditions (27a)–(27c), solve Eqs. (22a)–(22c) ($m = 1$) to obtain $\boldsymbol{u}_{(1)}$, $P_{(2)}$, and $\tau_{(1)}$. Then compute $\omega_{(1)}$ from Eq. (22d) ($m = 1$).

(iv) Compute the right-hand sides of Eqs. (28a)–(28c) using the result in steps (ii) and (iii). Under the resultant boundary conditions (28a)–(28c), solve Eqs. (22a)–(22c) ($m = 2$) to obtain $\boldsymbol{u}_{(2)}$, $P_{(3)}$, and $\tau_{(2)}$. Then compute $\omega_{(2)}$ from Eq. (22d) ($m = 2$).

3.1.4 - Remarks

Equations (22a), (22b), and (22c) are, respectively, the continuity equation, the Stokes equation of motion, and the energy equation [Eq. (22d) is the linearized equation of state; cf. Eq. (5)]. Their boundary conditions are the no-slip conditions in the leading order [Eq. (26)] and the conventional slip conditions in the first order [Eqs. (27a)–(27c)]. The latter consist of the velocity slip proportional to the shear (the k_0-term), that proportional to the temperature gradient along the boundary (the K_1-term), and the temperature jump proportional to the temperature gradient normal to the boundary (the d_1-term), where the shear and the temperature gradient are those of the leading-order solution. If the temperature of the boundary (τ_w) is not uniform, a slip flow is caused from the colder part to the hotter because of the K_1-term [note that $-G_{i(0)}t_i = (\partial\tau_{(0)}/\partial x_i)t_i$ is the gradient of τ_w along the boundary because of the second condition of Eq. (26)]. This slip flow is called the thermal creep, which is a typical effect of gas rarefaction [**10, 11, 12, 13, 14**]. This and related flows will play important roles in later sections. The second-order boundary conditions (28a)–(28c) consist of various terms. The terms containing $\bar{\kappa}$ and κ_{ij} indicate the effect of boundary curvature and disappear for planar boundaries. The term containing a_4 in Eq. (28a) can cause a slip flow of $O(\mathrm{Kn}^2)$ when the temperature gradient normal to the boundary is not uniform along it (even when the temperature of the boundary is uniform). This slip flow is called the thermal stress slip flow [**4, 15, 16, 17**].

The reader is referred to [**1, 2, 8**] for the physical mechanism of it as well as that of the thermal creep.

The fluid-dynamic system, Eqs. (21)–(22d) and (26)–(28c), gives the correct overall behavior of the gas up to $O(\mathrm{Kn}^2)$. But, when the local values of the physical quantities on (or near) the boundary is required, one needs to introduce the Knudsen-layer corrections to the overall solutions of $O(\mathrm{Kn})$ and of $O(\mathrm{Kn}^2)$. We also refer to [**1, 2, 8**] for the recipe to obtain the Knudsen-layer corrections.

It should be mentioned that a rigorous mathematical proof of the passage from the Boltzmann to the Stokes equations in the continuum limit was given by Golse and Levermore [**18**].

3.2 - *The case of* $\mathrm{Re} \sim 1$

Next, we consider the case where the Reynolds number is finite, i.e., $\mathrm{Re} = O(1)$ [thus, $\mathrm{Ma} = O(\mathrm{Kn})$ from Eq. (18)] [**4, 5, 6**]. Since the measure of deviation Ma from the reference equilibrium state is of the order of Kn, it is natural to assume that the deviations $\omega, \boldsymbol{u}, \tau$, and P [cf. Eqs. (1) and (4)] are of the order of Kn or ε. (In the case of $\mathrm{Re} \ll \mathrm{Kn} \ll 1$ considered in Sec. 3.1, these deviations were much smaller than Kn. In the case of $\mathrm{Re} = O(1)$, the ω, τ, and P can also be of the order of unity. We will comment on this case later.) That is, we put

$$\begin{aligned} &\rho = \rho_0(1 + \varepsilon\tilde{\omega}), \qquad &&\boldsymbol{v} = (2RT_0)^{1/2}\varepsilon\tilde{\boldsymbol{u}}, \\ &T = T_0(1 + \varepsilon\tilde{\tau}), \qquad &&p = p_0(1 + \varepsilon\tilde{P}), \end{aligned} \tag{32}$$

where $\tilde{\omega}$, $\tilde{\boldsymbol{u}}$, $\tilde{\tau}$, and $\tilde{P}$ are of $O(1)$. The latter quantities are expanded in ε [Eq. (20)] as

$$\tilde{h} = \tilde{h}_{(0)} + \tilde{h}_{(1)}\varepsilon + \cdots, \qquad (\tilde{h} = \tilde{\omega},\ \tilde{\boldsymbol{u}},\ \tilde{\tau},\ \text{or}\ \tilde{P}). \tag{33}$$

3.2.1 - Fluid-dynamic type equations

The fluid-dynamic type equations for $\tilde{h}_{(m)}$ in the leading and the first order are as follows.

$$\frac{\partial \tilde{P}_{(0)}}{\partial x_i} = 0, \tag{34}$$

$$\frac{\partial \tilde{u}_{i(0)}}{\partial x_i} = 0, \tag{35a}$$

$$\tilde{u}_{j(0)}\frac{\partial \tilde{u}_{i(0)}}{\partial x_j} = -\frac{1}{2}\frac{\partial \tilde{P}_{(1)}}{\partial x_i} + \frac{1}{2}\gamma_1\frac{\partial^2 \tilde{u}_{i(0)}}{\partial x_j^2}, \tag{35b}$$

$$\tilde{u}_{j(0)}\frac{\partial \tilde{\tau}_{(0)}}{\partial x_j} = \frac{1}{2}\gamma_2\frac{\partial^2 \tilde{\tau}_{(0)}}{\partial x_j^2}, \tag{35c}$$

$$\tilde{\omega}_{(0)} = \tilde{P}_{(0)} - \tilde{\tau}_{(0)}, \tag{35d}$$

$$\frac{\partial \tilde{u}_{j(1)}}{\partial x_j} = -\tilde{u}_{j(0)} \frac{\partial \omega_{(0)}}{\partial x_j}, \tag{36a}$$

$$\begin{aligned} &\tilde{u}_{j(0)} \frac{\partial \tilde{u}_{i(1)}}{\partial x_j} + (\tilde{\omega}_{(0)} \tilde{u}_{j(0)} + \tilde{u}_{j(1)}) \frac{\partial \tilde{u}_{i(0)}}{\partial x_j} \\ &\quad = -\frac{1}{2} \frac{\partial}{\partial x_i} \Big[\tilde{P}_{(2)} - \frac{1}{6} (\gamma_1 \gamma_2 - 4\gamma_3) \frac{\partial^2 \tilde{\tau}_{(0)}}{\partial x_j^2} \Big] \\ &\qquad + \frac{1}{2} \gamma_1 \frac{\partial^2 \tilde{u}_{i(1)}}{\partial x_j^2} + \frac{1}{2} \gamma_4 \frac{\partial}{\partial x_j} \Big[\tilde{\tau}_{(0)} \Big(\frac{\partial \tilde{u}_{i(0)}}{\partial x_j} + \frac{\partial \tilde{u}_{j(0)}}{\partial x_i} \Big) \Big], \end{aligned} \tag{36b}$$

$$\begin{aligned} &\tilde{u}_{j(0)} \frac{\partial \tilde{\tau}_{(1)}}{\partial x_j} + (\tilde{\omega}_{(0)} \tilde{u}_{j(0)} + \tilde{u}_{j(1)}) \frac{\partial \tilde{\tau}_{(0)}}{\partial x_j} - \frac{2}{5} \tilde{u}_{j(0)} \frac{\partial \tilde{P}_{(1)}}{\partial x_j} \\ &\quad = \frac{1}{5} \gamma_1 \Big(\frac{\partial \tilde{u}_{i(0)}}{\partial x_j} + \frac{\partial \tilde{u}_{j(0)}}{\partial x_i} \Big)^2 + \frac{1}{2} \frac{\partial^2}{\partial x_j^2} \Big(\gamma_2 \tilde{\tau}_{(1)} + \frac{1}{2} \gamma_5 \tilde{\tau}_{(0)}^2 \Big), \end{aligned} \tag{36c}$$

$$\tilde{\omega}_{(1)} = \tilde{P}_{(1)} - \tilde{\tau}_{(1)} - \tilde{\omega}_{(0)} \tilde{\tau}_{(0)}, \tag{36d}$$

where γ_2, ..., γ_5 as well as γ_1 that has already appeared in Eq. (22b) are the constants the values of which depend on the molecular model. For hard-sphere molecules,

$$\left.\begin{aligned} \gamma_2 &= 1.922284, \qquad \gamma_3 = 1.947906, \\ \gamma_4 &= 0.635021, \qquad \gamma_5 = 0.961142, \end{aligned}\right\} \tag{37}$$

and for the BGK model,

$$\gamma_2 = \gamma_3 = \gamma_4 = \gamma_5 = 1. \tag{38}$$

The γ_2 is related to the thermal conductivity λ_0 as

$$\lambda_0 = (5\sqrt{\pi}/4) \gamma_2 R p_0 (2RT_0)^{-1/2} l_0. \tag{39}$$

3.2.2 - Slip boundary conditions

In accordance with the situation considered here, we assume the velocity $\boldsymbol{v}_w$ and temperature T_w of the boundary to be of the form $\boldsymbol{v}_w = (2RT_0)^{1/2} \varepsilon \tilde{\boldsymbol{u}}_w$ and $T_w = T_0(1 + \varepsilon \tilde{\tau}_w)$ with $\tilde{\boldsymbol{u}}_w$ and $\tilde{\tau}_w$ being of $O(1)$. Then, the boundary condition for Eqs. (35a)–(35d) and that for Eqs. (36a)–(36d) are, respectively, given by

$$\tilde{\boldsymbol{u}}_{(0)} = \tilde{\boldsymbol{u}}_w, \qquad \tilde{\tau}_{(0)} = \tilde{\tau}_w, \tag{40}$$

$$\begin{cases} \tilde{u}_{i(1)} t_i = -k_0 \Big(\dfrac{\partial \tilde{u}_{i(0)}}{\partial x_j} + \dfrac{\partial \tilde{u}_{j(0)}}{\partial x_i} \Big) n_i t_j - K_1 \dfrac{\partial \tilde{\tau}_{(0)}}{\partial x_i} t_i, \\ \tilde{u}_{i(1)} n_i = 0, \qquad \tilde{\tau}_{(1)} = d_1 \dfrac{\partial \tilde{\tau}_{(0)}}{\partial x_i} n_i. \end{cases} \tag{41}$$

These conditions are essentially the same as Eq. (26) and Eqs. (27a)–(27c).

3.2.3 - Remarks

Equations (35a)–(35b) are the Navier–Stokes equations for an "incompressible" fluid (the meaning of the quotation marks will be explained in the next paragraph). Now, let us consider the compressible Navier–Stokes equations for a gas and insert the expansions (32) and (33), which are equivalent to Mach number expansions because of the relation $\mathrm{Kn} = O(\mathrm{Ma})$. Then, we obtain the trivial equation (34), Eqs. (35a)–(35c) as the (non-trivial) leading-order equations, and, as the next-order ones, the equations almost the same as Eqs. (36a)–(36c), namely, the latter equations with $\gamma_3 = 0$. This difference is attributed to the thermal stress that is not included in Newton's law of stress. But, if we introduce a modified pressure $\tilde{P}^*_{(2)}$ by $\tilde{P}^*_{(2)} = \tilde{P}_{(2)} + (2/3)\gamma_3(\partial^2\tilde{\tau}_{(0)}/\partial x_j^2)$, the effect of the thermal stress is absorbed in the pressure. Therefore, it turns out that $\tilde{\boldsymbol{u}}_{(1)}$, $\tilde{\tau}_{(1)}$, and $\tilde{\omega}_{(1)}$ are not affected by the thermal stress [note that the boundary conditions (40) and (41) do not include $\tilde{P}_{(2)}$]. In other words, the effect of gas rarefaction essentially comes in only through the slip boundary conditions (41), whereas the effect of compressibility appears in Eqs. (36a)–(36c). The $\tilde{\boldsymbol{u}}_{(1)}$, $\tilde{\tau}_{(1)}$, and $\tilde{\omega}_{(1)}$ undergo the Knudsen-layer corrections in the vicinity of the boundary. See [**1, 2, 8**] for the details.

The *true* incompressible Navier–Stokes equations are derived from the compressible Navier-Stokes equations by introducing the condition of incompressibility, which reads $\hat{v}_j(\partial\hat{\rho}/\partial x_j) = 0$ for steady flows. The continuity and momentum equations derived in such a manner are of the same form as Eqs. (35a) and (35b) [with Eq. (34)], respectively. However, the energy equation is not exactly the same as Eq. (35c). More specifically, it is of the same form as Eq. (35c) with γ_2 replaced by $(5/3)\gamma_2$. This is due to the fact that, the work done by the pressure comes in this equation for an ideal gas, whereas it becomes of higher order in the *true* incompressible fluid. In this sense, Eqs. (35a)–(35c) are not exactly the incompressible Navier–Stokes equations. See [**2**] for more details.

The slip boundary condition is often combined with the incompressible Navier–Stokes equations when $\mathrm{Re} = O(1)$. But this combination is *inconsistent*, as is seen from Eqs. (34)–(36d) and boundary conditions (40) and (41). That is, the effect of gas rarefaction and that of compressibility go together.

The mathematical study of the passage from the Boltzmann to the "incompressible" Navier–Stokes equations in the continuum limit had been an important subjects in kinetic theory [**19, 20, 21, 22, 23**]. A crucial point is the parameter setting $\mathrm{Ma} = O(\mathrm{Kn})$ [or the setting in Eq. (32)], which was understood by Sone already in 1971 [**4**] and rediscovered by mathematicians much later. The complete proof of the passage was given by Golse and Saint-Raymond rather recently [**23**].

3.3 - *The case of* $\mathrm{Re} \sim 1$ *with finite temperature variations*

Let us consider the case where the temperature variation of the system is not small and the boundary is at rest (the gas is at rest with a uniform pressure at infinity when an infinite domain is considered). We use the dimensionless density $\hat{\rho}$, flow velocity $\hat{\boldsymbol{v}}$, temperature $\hat{T}$, and pressure $\hat{p}$ defined in Eq. (1). In this situation, one can seek the overall solution consistently in the following form [**7, 1, 2,** 8]: with $\varepsilon = (\sqrt{\pi}/2)\,\mathrm{Kn}$,

$$\hat{H} = \hat{H}_{(0)} + \hat{H}_{(1)}\varepsilon + \cdots, \quad (\hat{H} = \hat{\rho},\ \hat{T},\ \text{or}\ \hat{p}), \tag{42a}$$

$$\hat{\boldsymbol{v}} = \hat{\boldsymbol{v}}_{(1)}\varepsilon + \cdots. \tag{42b}$$

Note that the series of the velocity $\hat{\boldsymbol{v}}$ starts from the first order. Since $\hat{\boldsymbol{v}} = O(\varepsilon)$ or $O(\mathrm{Kn})$, $\mathrm{Re} = O(1)$ also in this case. The leading-order fluid-dynamic type equations are for $(\hat{\rho}_{(0)}, \hat{T}_{(0)}, \hat{\boldsymbol{v}}_{(1)}, \hat{p}_{(2)})$ with $\hat{p}_{(0)}$ and $\hat{p}_{(1)}$ being constant (see Ref. [**7**]). Their momentum equation contains the non-Newtonian stress terms (the thermal stress terms) explicitly. The no-jump condition for $\hat{T}_{(0)}$ and the thermal-creep slip condition for $\hat{\boldsymbol{v}}_{(1)}$, proportional to the temperature gradient along the boundary, are the appropriate boundary conditions for the equations. This fluid-dynamic type system shows that the following two types of flow [of $O(\mathrm{Kn})$] are induced by the effect of the temperature: (i) the thermal creep flow [see Sec. 3.1.4; note that the temperature gradient is not small in the present case] and (ii) the nonlinear thermal stress flow. The latter, which was first pointed out by Kogan *et al.* [**24, 25**], is induced in the gas when the space between isothermal surfaces vary along them [**7**].

Next we consider the continuum limit, the limit where Kn (or ε) tends to zero. Then, we have $\hat{\boldsymbol{v}} \to 0$, $\hat{p} \to const$, and $\hat{T} \to \hat{T}_{(0)}$, that is, the flows (i) and (ii) vanish in this limit. However, $\hat{T}_{(0)}$ is determined together with $\hat{\boldsymbol{v}}_{(1)}$, which is of $O(1)$, by the fluid-dynamic type system irrespective of ε. This means that, although the flow itself vanishes in the continuum limit, it still has a finite effect on the temperature field in this limit. In other words, the behavior of the gas in the continuum limit is affected by the flow that does not exist in the limit. This effect was pointed out in [**7**] and termed the *ghost effect* afterward. Now let us consider the same problem using the (compressible) Navier–Stokes equations and the no-slip condition that are commonly accepted as the correct system for the continuum limit. Then, we have $\hat{\boldsymbol{v}} = 0$ and $\hat{p} = const$ again, but $\hat{T}$ is determined by the steady heat-conduction equation without any effect from the velocity of $O(\varepsilon)$. That is, the Navier–Stokes system cannot describe the ghost effect and therefore does not give the correct temperature field in the continuum limit. This fact reveals an essential defect contained in the classical fluid dynamics (for a gas). The ghost effect and the invalidity of the classical fluid dynamics in the continuum limit are discussed in detail in subsequent papers by Sone

[**7, 26, 27, 28**]. Afterward, the effect has been viewed more comprehensively as a consequence of the singular nature of the continuum limit, and new types of ghost effect, such as the surprising effect of infinitesimal curvature of the boundary, have been pointed out and clarified [**29, 30, 31, 32**]. The reader is referred to [**2**] for the detailed description of the ghost effect.

3.4 - *The case of* $\mathrm{Ma} \sim 1$

The case of high-speed flows where the Mach number is of the order of unity, i.e., $\mathrm{Ma} = O(1)$ [thus, $\mathrm{Re} = O(\mathrm{Kn}^{-1}) \gg 1$ from Eq. (18)], is studied by Sone *et al.* [**9**]. In this case, the leading-order (Kn^0-order) flow field is described by the (compressible) Euler equations plus the compressible and viscous boundary-layer equations with the no-slip boundary condition. The next order in the flow field is of $O(\sqrt{\mathrm{Kn}})$, instead of $O(\mathrm{Kn})$. The physical quantities of this order are governed by the perturbed Euler equations and the equations of boundary-layer type with the slip boundary condition composed of the velocity slip due to the shear of the flow and the temperature jump due to the temperature gradient normal to the boundary. (The solution of this perturbed system undergoes the Knudsen-layer correction.) Except for the slip boundary condition (and the Knudsen-layer correction), the non Navier–Stokes effect does not appear up to this order.

4 - Flows at intermediate Knudsen numbers: numerical approaches

As we have seen in Sec. 3 (see Secs. 3.1.4 and 3.3), the fact that gas flows are induced by temperature fields without the help of external forces is one of the typical effects of gas rarefaction. In this and the following sections, we investigate such flows for general Knudsen numbers (i.e., in the transition regime), with special interest in internal flows.

The most fundamental flow in this category would be the thermal transpiration, the flow induced through a long pipe (or channel) with a uniform temperature gradient along the pipe wall. This flow is often discussed together with the Poiseuille flow, the flow caused through a long pipe by a uniform pressure gradient imposed along the pipe axis. Since these flows are particularly important in microscale applications, we leave them for the later sections (in particular, Sec. 7) and consider other types of flow in the present section.

As mentioned in Secs. 3.1.4 and 3.3, three types of flow, i.e., the thermal creep flow, the thermal stress slip flow, and the nonlinear thermal stress flow, are induced by the temperature field when the Knudsen number is small. This fact was clarified

by the asymptotic theory described in Sec. 3. However, it should be noted that the theory is based on the assumption that the local Knudsen number, the local mean free path divided by the local length scale of variation of physical quantities, is uniformly small. This means that the radius of curvature of the boundary should be much larger than the mean free path, and the boundary condition specified on the boundary should be smooth enough. If this condition is not fulfilled, there is a possibility that flows other than the above three types are caused by the temperature field even when the Knudsen number is small. We will give two such examples here: the flow induced by a heated (or cooled) sharp edge (thermal edge flow) and the flow induced by a discontinuous wall temperature.

Since analytical approaches are not available for such flows (even for small Knudsen numbers), we must rely on numerical approaches, as in the case of general flows in the transition regime. In regard to the two examples, we briefly mention two typical numerical methods for the transition regime, the direct simulation Monte Carlo (DSMC) method and a finite-difference method.

4.1 - *Thermal edge flow: DSMC method*

We first give a brief outline of the DSMC method and then come back to the thermal edge flow.

4.1.1 - Brief outline of DSMC

The DSMC method, which was first proposed by G. A. Bird [**33**], is a stochastic and particle method. It was originally introduced on the basis of physical intuition. Although the limitations of available computer capacity restricted actual computations to rather rough ones, the method was widely used in applications because of its simplicity and adaptability. Nowadays, however, its relation to the Boltzmann equation is clarified mathematically [**34, 2**], and the progress of computers enables us to apply it to the numerical analysis of fundamental and delicate problems that require great accuracy. This method has been developed and improved by many scientists and engineers including Bird himself (e.g., [**35, 36, 37, 38**]). As the result, there exist many variations of the method. However, none of them alters the basic framework of Bird's method. In this section, we give a brief outline of the computational procedure of this method. The reader is referred to [**39, 40**] for mathematical arguments.

Unlike in Secs. 2 and 3, we use, in this subsection, dimensional variables and assume that the gas molecules are subject to an external force $\boldsymbol{F}(\boldsymbol{X}, \boldsymbol{\xi}, t)$ per unit mass [correspondingly, a term $\mathrm{Fr}^{-1}\partial(\hat{F}_j \hat{f})/\partial\zeta_j$ should be added to the left-hand side

of the dimensionless Boltzmann equation (6), where $\hat{F}_i = F_i/F_0$, F_0 is the magnitude of the reference force per unit mass, and $\mathrm{Fr} = 2RT_0/LF_0$ is the Froude number].

Let us consider the initial and boundary value problem of the Boltzmann equation in a finite domain. We assume that the interaction between gas molecules is expressed by a spherically symmetric intermolecular force with a finite influence range of radius d_m (for hard-sphere molecules, d_m is the diameter of a molecule). The outline of the process of computation is as follows.

(i) We divide the gas region under consideration into S small regions, which are usually called cells. Let the volume of the lth cell be $V_{(l)}$ ($l = 1, 2, ..., S$).

(ii) We allot $N_{(l)}$ particles to the lth cell, where $N_{(l)}$ is chosen to be proportional to the volume of the cell $V_{(l)}$ and to the density $\rho^{(0)}_{(l)}$ at a representative point in the cell at the initial time, that is,

$$N_{(l)} = \rho^{(0)}_{(l)} V_{(l)}/C_0 m, \tag{43}$$

where m is the mass of a gas molecule, and C_0 is a constant that is common to all the cells. The positions of the particles are distributed randomly in the cell, whereas their velocities are distributed according to the initial velocity distribution.

(iii) We assume that all the particles in the gas region are numbered from 1 to N ($N = \sum_{l=1}^{S} N_{(l)}$) and denote by $\boldsymbol{X}^{(n)}$ and $\boldsymbol{\xi}^{(n)}$ the position and the velocity of the nth particle, respectively. For a small time step Δt, we change the position and the velocity of each particle from $\boldsymbol{X}^{(n)}$ and $\boldsymbol{\xi}^{(n)}$ to $\boldsymbol{X}^{(n)} + \boldsymbol{\xi}^{(n)}\Delta t$ and $\boldsymbol{\xi}^{(n)} + \boldsymbol{F}^{(n)}\Delta t$, where $\boldsymbol{F}^{(n)} = \boldsymbol{F}(\boldsymbol{X}^{(n)}, \boldsymbol{\xi}^{(n)}, t)$ with t being the time of the present stage. The particles that go out from the gas region in this change are removed, but new particles are cast in the region from the boundary according to the boundary condition there. Here, recounting the number of the particles in each cell, we take the new number as $N_{(l)}$ anew. The particles should be renumbered in this stage because their total number may have changed.

(iv) The collision process of the particles in each cell is computed independently from other cells. Let us consider the lth cell (with volume $V_{(l)}$). To a pair of the particles with velocities $\boldsymbol{\xi}^{(j)}$ and $\boldsymbol{\xi}^{(k)}$, we assign the following probability $P^{(j,k)}_{(l)}$ for their collision:

$$\begin{aligned} P^{(j,k)}_{(l)} &= (C_0\Delta t/V_{(l)}) \int_{\text{all } \boldsymbol{e}} B(|(\boldsymbol{\xi}^{(k)} - \boldsymbol{\xi}^{(j)})\cdot\boldsymbol{e}|, |\boldsymbol{\xi}^{(k)} - \boldsymbol{\xi}^{(j)}|)\, \mathrm{d}\Omega(\boldsymbol{e}) \\ &= \pi d_m^2 C_0 |\boldsymbol{\xi}^{(k)} - \boldsymbol{\xi}^{(j)}| \Delta t/V_{(l)}. \end{aligned} \tag{44}$$

Here, $B = B_0\hat{B}$, with $B_0 = 4\sqrt{\pi} d_m^2 \sqrt{RT_0}$, is the dimensional counterpart of $\hat{B}$ in Eq. (7) [B_0 is related to the mean free path l_0 as $l_0 = (8RT_0/\pi)^{1/2}(m/\rho_0 B_0)$

$= (\sqrt{2}\pi d_m^2 \rho_0/m)^{-1}$; note that this relation, which is of the same form as for hard-sphere molecules, is more general]. We first choose $M_{(l)}$ pairs randomly from the $N_{(l)}(N_{(l)}-1)/2$ pairs in the cell, where $M_{(l)}$ is a number such that

$$M_{(l)} \ll N_{(l)}(N_{(l)}-1)/2, \tag{45}$$

$$M_{(l)} - [N_{(l)}(N_{(l)}-1)/2] \max P_{(l)}^{(j,k)} \gg 1. \tag{46}$$

Then, for each of $M_{(l)}$ pairs, we determine whether it collides or not according to the elevated probability $P_{M(l)}^{(j,k)}$ for their collision, i.e.,

$$P_{M(l)}^{(j,k)} = [N_{(l)}(N_{(l)}-1)/2M_{(l)}]P_{(l)}^{(j,k)}. \tag{47}$$

The determination of the collision pairs by the above two steps instead of the single step by the use of Eq. (44) is a time-saving procedure, which is efficient and legitimated when $P_{(l)}^{(j,k)}$ is small. For the pair that was judged to collide, we select a unit vector $\boldsymbol{e}$ assuming that the probability for $\boldsymbol{e}$ lying in the solid-angle element $\mathrm{d}\Omega(\boldsymbol{e})$ is

$$(\pi d_m^2)^{-1}|\boldsymbol{\xi}^{(k)} - \boldsymbol{\xi}^{(j)}|^{-1} B(|(\boldsymbol{\xi}^{(k)} - \boldsymbol{\xi}^{(j)}) \cdot \boldsymbol{e}|,\ |\boldsymbol{\xi}^{(k)} - \boldsymbol{\xi}^{(j)}|)\, \mathrm{d}\Omega(\boldsymbol{e}), \tag{48}$$

and replace the velocities of the pair $(\boldsymbol{\xi}^{(j)},\ \boldsymbol{\xi}^{(k)})$ by $(\boldsymbol{\xi}^{(j)} + [(\boldsymbol{\xi}^{(k)} - \boldsymbol{\xi}^{(j)}) \cdot \boldsymbol{e}]\boldsymbol{e}$, $\boldsymbol{\xi}^{(k)} - [(\boldsymbol{\xi}^{(k)} - \boldsymbol{\xi}^{(j)}) \cdot \boldsymbol{e}]\boldsymbol{e})$. The velocities of the pair that does not collide are left unchanged. With the new velocities $\boldsymbol{\xi}^{(j)}$, we construct the velocity distribution function f at the lth cell at time $t + \Delta t$ as

$$f = (mC_0/V_{(l)}) \sum_{j \in V_{(l)}} \delta(\boldsymbol{\xi} - \boldsymbol{\xi}^{(j)}), \tag{49}$$

where $\delta(\boldsymbol{\xi})$ is the (three-dimensional) delta function, and $j \in V_{(l)}$ indicates that the sum is taken for all j corresponding to the particles contained in the lth cell. Using Eq. (49) in the definitions of the macroscopic variables [i.e., the dimensional counterparts of Eq. (2)], we obtain their expressions at the lth cell, e.g.,

$$\rho = mC_0 N_{(l)}/V(l), \tag{50}$$

$$\mathbf{v} = (1/N_{(l)}) \sum_{j \in V_{(l)}} \boldsymbol{\xi}^{(j)}, \tag{51}$$

$$T = (1/3RN_{(l)}) \sum_{j \in V_{(l)}} (\boldsymbol{\xi}^{(j)} - \boldsymbol{v}) \cdot (\boldsymbol{\xi}^{(j)} - \boldsymbol{v}). \tag{52}$$

We carry out the above procedure for all the cells.

(v) With the new positions in process (iii) and new velocities in process (iv) of the particles, we go back to process (iii).

We repeat the processes (iii) – (v) until the necessary time is reached.

The method described above is shown to be mathematically consistent with the Boltzmann equation as well as physically natural. That is, the velocity distribution function thus obtained converges to the solution of the corresponding initial and boundary value problem of the Boltzmann equation in the limit as $N_{(l)} \to \infty$ and $D_{(l)} \to \infty$ ($D_{(l)}$ is the linear dimension of the lth cell; thus $V_{(l)} \sim D_{(l)}^3$ for the cell with a regular shape) for each cell and as $\Delta t \to 0$ [with the condition $|\boldsymbol{\xi}^{(j)}|_{\max}\Delta t < O(D_{(l)})$ in each cell] in the following sense: any moments of f of the form (49) in each cell become arbitrarily close to the corresponding moments of the solution of the Boltzmann equation (weak convergence) (see Appendix B of [**2**] for the details).

This method is basically a time-dependent one. Therefore, when we deal with a steady problem, we pursue the time evolution starting from an appropriately chosen initial condition and regard the steady state obtained after a long time as the solution. However, in the actual computation, where the available number of particles and that of cells are restricted by computer capacity, the true steady state is never reached even after a long time, that is, the macroscopic variables as well as the velocity distribution function always show large temporal fluctuations. Therefore, the steady state is judged to have been established if the averages of the macroscopic variables over a certain time interval (consisting of a large number of time steps) are independent of the choice of the interval. We usually compute the average of the fluctuating *steady* solution over a great number of time steps and regard the result as the desired steady solution. Although we can obtain a smooth and seemingly reasonable solution by means of the time averaging, the averaging process has not been validated so far. For a time-dependent problem, for which the time averaging cannot be used, the accurate numerical solution is still very difficult to obtain by this method.

4.1.2 - Thermal edge flow

Since the DSMC method is quite simple as a solution method for the Boltzmann equation, it has widely been used in technological applications. Here, we rather give an example of a new type of basic flow discovered by using DSMC method, that is, a flow induced around the edges of a uniformly heated or cooled plate (thermal edge flow) [**41, 42**].

Let us consider the geometry shown in Fig. 1 (a), that is, a rarefied gas is confined in a square container kept at a uniform temperature T_0, and a flat plate (with length L and without thickness) kept at another uniform temperature T_1 is set in the middle of the container. The gas is subject to no external force. We assume that the gas molecules are reflected according to the diffuse reflection condition on the plate as well as on the wall of the container and that the problem is two dimensional. In this

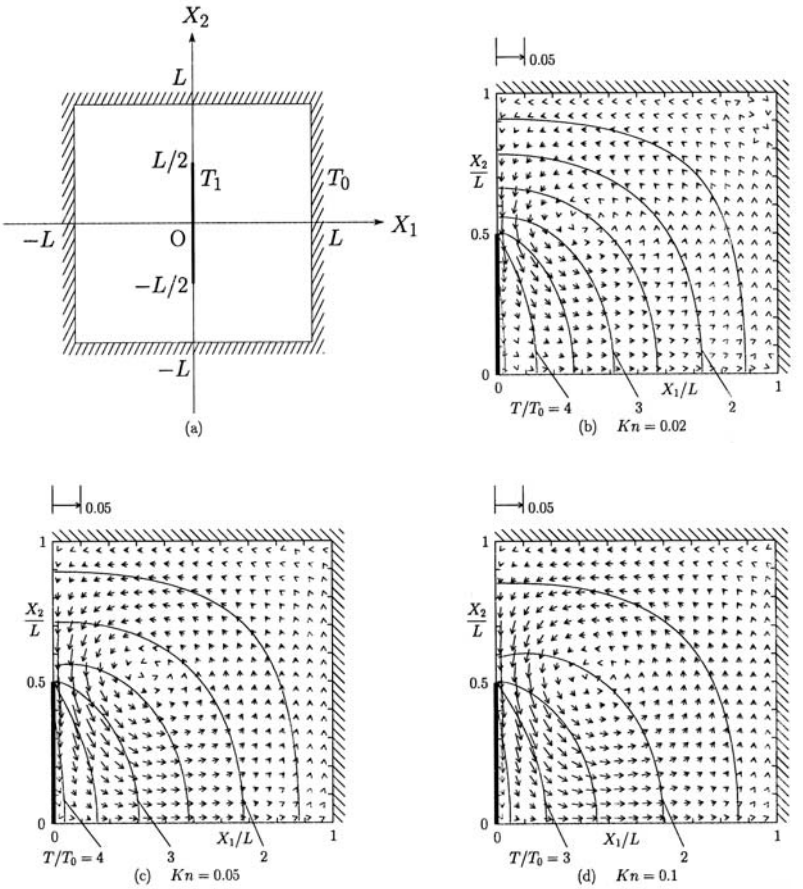

Fig. 1. Flow induced around the edge of a uniformly heated plate [**42**] (by courtesy of Prof. Y. Sone). (a) a uniformly heated (or cooled) plate in a square container, and (b)–(c) the induced gas flow and the isothermal lines in the first quadrant for $T_1/T_0 = 5$. (b) $Kn = 0.02$, (c) $Kn = 0.05$, (d) $Kn = 0.1$. The arrow indicates the flow velocity vector $(v_1, v_2)/(2RT_0)^{1/2}$ at its starting point, and its length corresponding to 0.05 is shown in the figure.

situation, a steady flow is induced in the gas. An example of the flow, obtained by the DSMC method for hard-sphere molecules in [**42**], is shown in Fig. 1. To be more specific, the flow velocity field and isothermal lines in the first quadrant for $T_1/T_0 = 5$ is shown for relatively small Knudsen numbers in Figs. 1 (b)–(d), where $\mathrm{Kn} = \ell_0/L$ is the Knudsen number, and ℓ_0 is the mean free path of the gas molecules in the equilibrium state at rest with temperature T_0 and density ρ_0 (the mean density over the gas region).

In this problem, the thermal creep (cf. Sec. 3.1.4) is not expected because the temperature of each boundary is uniform. On the other hand, since the space between

isothermal lines vary along them, the nonlinear thermal stress flow (cf. Sec. 3.3) can be induced. However, it can be shown by a numerical computation that the vortical flow caused by the nonlinear thermal stress flow is opposite to that of the flow in Fig. 1. This means that the flow field is dominated by another type of flow that causes the circulating flow of Fig. 1. As is seen from the fact that the flow is locally intense at the edge, this flow is caused by the effect of the edge. Although the temperature of the plate is uniform, the abrupt temperature variation near the edge produces a steep temperature gradient in the gas along the plate there. Because of this temperature gradient, the same mechanism as the thermal creep flow works, and a flow is induced. According to a rough estimate based on the temperature field obtained from the Laplace equation, the flow speed [normalized by $(2RT_0)^{1/2}$] is of the order of $\mathrm{Kn}^{1/2}$ for small Kn [**42**]. Therefore, the flow, though localized at the edge, has a stronger effect than the thermal creep and nonlinear thermal stress flows of $O(\mathrm{Kn})$. The flow is strongest at around $\mathrm{Kn} = 0.1$ and decays relatively fast as Kn increases. It vanishes in the free-molecular limit [**43, 1, 2**]. Sone and Yoshimoto performed a simple but interesting experiment that demonstrates the flow by means of the rotation of a tiny windmill placed near the edge of a heated plate in a low-pressure chamber [**42**]. It should be mentioned that, quite recently, new types of thermal pump and gas separator exploiting this flow were proposed (see Sec. 5).

4.2 - *Flow induced by a discontinuous wall temperature: finite-difference method*

In this subsection, we discuss another type of flow, the flow induced by a discontinuous wall temperature. We start with short remark on the finite-difference method.

4.2.1 - Remark on finite-difference method

In contrast to the DSMC method, some deterministic solution methods have also been proposed for the Boltzmann equation. Concerning the finite-difference method, some accurate computations were carried out by Ohwada for spatially one-dimensional problems [**44, 45**]. The method can, in principle, be extended to more general cases. However, if we require the same degrees of accuracy, such extension is still not practical. Therefore, the use of the model Boltzmann equations, such as the BGK model [Eq. (6) with Eq. (12)], is a powerful tool for accurate computations of two- and three-dimensional problems. In the BGK model, the computation of the complicated gain term of the original Boltzmann equation is reduced to simple computations of the macroscopic quantities in the local Maxwellian. Furthermore, in the spatially two-dimensional case where the velocity distribution function is,

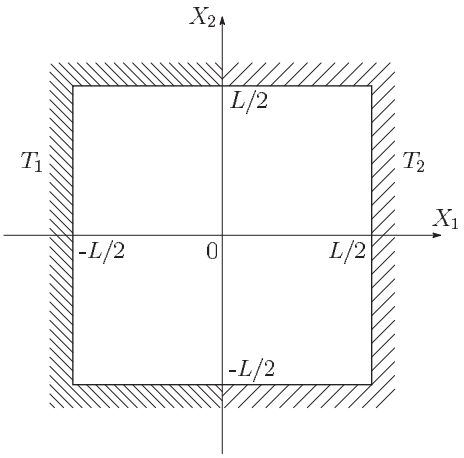

Fig. 2. Rarefied gas in a two-dimensional square container with a discontinuous wall temperature.

say, of the form $\hat{f}(\hat{t}, x_1, x_2, \zeta_i)$, one can eliminate the ζ_3 variable by integrating Eq. (6) with Eq. (12) and that multiplied by ζ_3^2 with respect to ζ_3 over its whole range. As the result, one obtains two coupled integro-differential equations of the form similar to Eq. (6) with Eq. (12) for the following marginal velocity distribution functions:

$$\hat{g} = \int_{-\infty}^{\infty} \hat{f}(\hat{t}, x_1, x_2, \zeta_i)\mathrm{d}\zeta_3, \qquad \hat{h} = \int_{-\infty}^{\infty} \zeta_3^2 \hat{f}(\hat{t}, x_1, x_2, \zeta_i)\mathrm{d}\zeta_3. \tag{53}$$

Similarly, in the spatially one-dimensional case where $\hat{f} = \hat{f}(\hat{t}, x_1, \zeta_i)$, one can eliminate ζ_2 and ζ_3 variables [**46**]. In the case of cylindrical and spherical symmetry, similar reduction can be done. Exploiting these properties of the BGK model, we can devise more sophisticated finite-difference schemes than in the case of the original Boltzmann equation. The following is one of such examples.

4.2.2 - Flow caused by a discontinuous wall temperature

Let us consider a gas confined in a two-dimensional square container $-L/2 < X_1 < L/2$, $-L/2 < X_2 < L/2$, where X_i is the rectangular coordinate system (Fig. 2). (The dimensional variables are used in Sec. 4.2.2.) The left and right halves of the wall of the container are kept at different uniform temperatures T_1 and T_2, respectively, so that the temperatures of the top and bottom walls are discontinuous at their respective middle points ($X_1 = 0$, $X_2 = \pm L/2$). External forces are assumed to be absent. In this situation, a steady gas flow is induced in the

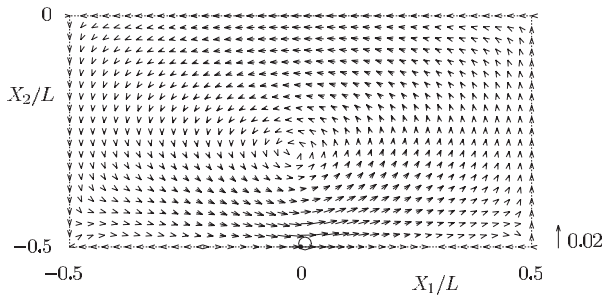

(a) Kn = 0.2

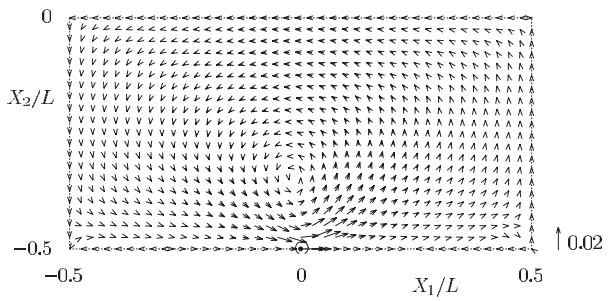

(b) Kn = 0.02

Fig. 3. Flow induced in the lower half of the container for $T_2/T_1 = 2$. (a) Kn = 0.2, (b) Kn = 0.02. The arrow indicates the two-dimensional flow velocity vector $(v_1, v_2)/(2RT_1)^{1/2}$ at its starting point. The scale of $(v_1^2 + v_2^2)^{1/2}/(2RT_1)^{1/2} = 0.02$ is shown in the figure. The symbol • indicates the point of discontinuity of the temperature of the bottom wall, and ○ indicates the point with the maximum flow speed.

container by the effect of the discontinuities of the wall temperature. The flow was analyzed in [**47**] numerically by an accurate finite-difference method on the basis of the BGK model [Eq. (6) with Eq. (12)] and the diffuse reflection boundary condition [Eqs. (16a) and (16b) with $a = 1$], and the features of the flow were clarified for a wide range of the Knudsen number.

Some examples of the flow field are shown in Fig. 3, where Kn= l_0/L is the Knudsen number and l_0 is the mean free path of the gas molecules in the equilibrium state at rest whose temperature is T_1 and density is the average density of the gas in the container. Since the flow is symmetric with respect to X_1-axis, the lower half of the container ($X_2 < 0$) is shown in the figure. A flow is induced from the colder to the hotter part along the bottom wall near the point of discontinuity, and it causes an overall circulating flow. The maximum flow

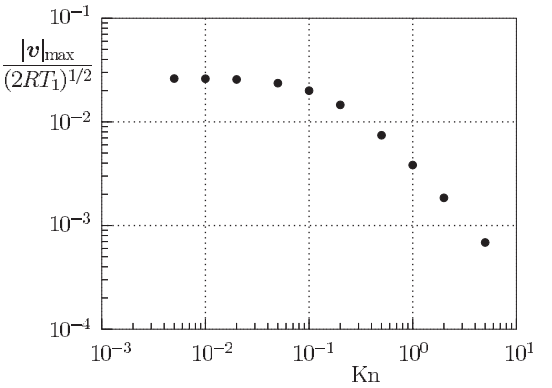

Fig. 4. Maximum flow speed $|\boldsymbol{v}|_{\max}$ in the gas versus the Knudsen number for $T_2/T_1 = 2$.

speed in the container versus the Knudsen number is shown in Fig. 4. The maximum speed tends to approach a finite value as the Knudsen number goes to zero. However, the detailed computation shows that the region with appreciable flow tends to shrink to the point of discontinuity of the wall temperature as the Knudsen number becomes small. Therefore, the overall flow in the container vanishes nonuniformly in the continuum limit (i.e., for any small Knudsen number, there is a small region where there is a gas flow with a finite speed).

The difficulty in the finite-difference analysis of the present problem comes from the fact that the discontinuity of the wall temperature causes the discontinuity of the velocity distribution function in the gas. Let us consider the velocity distribution function of the gas molecules leaving the bottom wall ($X_2 = -L/2$). At the point of discontinuity of the wall temperature, the limit from the left is prescribed by the boundary condition with temperature T_1, whereas the limit from the right is prescribed by that with temperature T_2. Therefore, these two limits, in general, do not coincide for any fixed molecular velocity (ξ_1, ξ_2) $(\xi_2 > 0)$. This discontinuity propagates in the gas in the direction of (ξ_1, ξ_2), i.e., along the characteristic of the (steady) Boltzmann equation $(\xi_1 \partial f/\partial X_1 + \xi_2 \partial f/\partial X_2 = \cdots)$. Therefore, at a point (X_1, X_2) in the gas, the velocity distribution function is generally discontinuous in the direction $\xi_1/\xi_2 = X_1/(X_2 + L/2)$ in the $\xi_1\xi_2$ plane. It is easily shown that the discontinuity attenuates over the distance of the order of the molecular free path in its propagation because of the effect of molecular collisions [**48**]. The discontinuity point of the boundary temperature is also a singular point for the macroscopic variables in the sense that their limiting values at the point are different depending on the direction of approach. The finite-difference scheme used here, which is essentially the same as that developed in [**49**], is a combination of a standard finite-difference method and a

characteristic method, capable of describing the discontinuity in the velocity distribution function. Its original version was proposed in [**50, 51**] and had been developed in subsequent papers [**52, 53, 54, 55, 56**].

5 - Knudsen compressor and its variants

In the present section, we discuss the potential applications of the thermally-induced flows, such as the thermal transpiration (or thermal creep) and the thermal-edge flow, of a rarefied gas. Here introduced is the applications to compressors and gas separators. We shall begin with a thought experiment on a simple compressor making use of the thermal transpiration.

Consider a straight pipe with a gradient of temperature along its surface. If the pipe is a capillary tube or the gas pressure is low enough, the thermal transpiration from one end to the other takes place because the Knudsen number in the system is no longer small. Thus, if the pipe connects two reservoirs as depicted in Fig. 5, the pressure of the gas in one of the reservoirs becomes lower than in the other. The achieved difference of pressure is determined by the competition between the gas transport by the thermal transpiration and the backward flow caused by the induced pressure difference (the Poiseuille flow). In this way, even a simple straight pipe works as a compressor (or pump) if a gradient of temperature is given along its surface. It is a basic idea of thermally-driven compressors to be discussed below.

Since the driving mechanism of the above straight pipe pump is the temperature gradient, the better performance can be achieved by increasing the magnitude of temperature gradient or by lengthening the pipe with keeping the magnitude of temperature gradient. However, both requires the large difference of temperatures between the extreme ends of the pipe, and the straightforward application of the above idea is practically difficult. The necessity of avoiding the

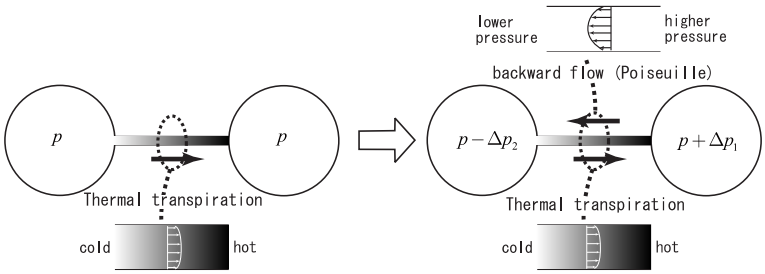

Fig. 5. Sketch of a primitive thermally-driven compressor and its basic concept. The shade of the pipe represents the imposed temperature distribution.

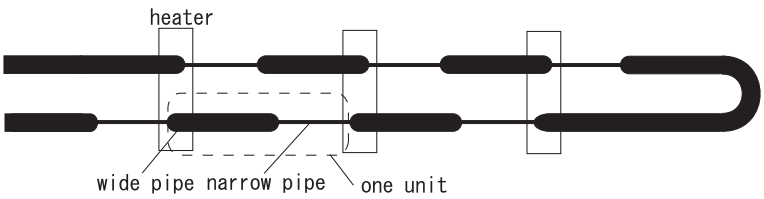

Fig. 6. Schematic of the original Knudsen compressor [**57**].

limitless increase of temperature for a real application leads to the idea of a pump of cascade structure.

As early as 1910, Knudsen made up a simple but cleverly designed device, which we now call the Knudsen compressor [**57**]. His original device is a cascade of units composed of a narrow and a wide glass tube with a heater at each junction of neighboring units (Fig. 6). The heater arrangement and the natural cooling make a temperature variation along the pipe shell. With this device, he actually demonstrated a compression ratio of ten at a low absolute pressure levels. However, little attention has been turned to his device for a long time, and it is just in the last decade that the device becomes a target of intensive studies in the modern kinetic theory in the connection to the development of micromechanical engineering. We should refer to [**58, 59**] as a trigger for the revival (or may be said "as rediscovery") of the Knudsen compressor in the middle of 90s in the community of rarefied gas dynamics.

5.1 - *One-way flow in a channel with a periodic temperature distribution*

Sone, Waniguchi and Aoki [**59**] studied the behavior of a rarefied gas in a two-dimensional channel with a periodic temperature distribution. The configuration is shown in Fig. 7. Assuming the behavior to be periodic, they demonstrated the oc-

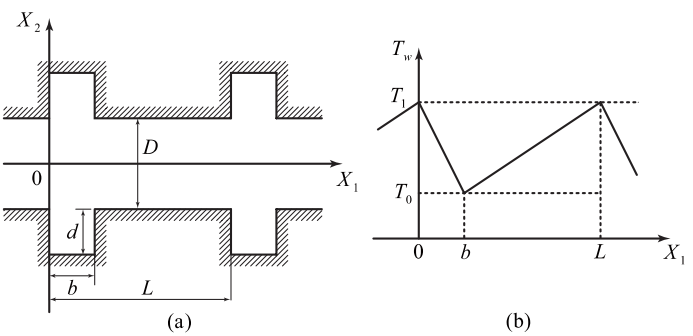

Fig. 7. Channel configuration and distribution of surface temperature T_w.

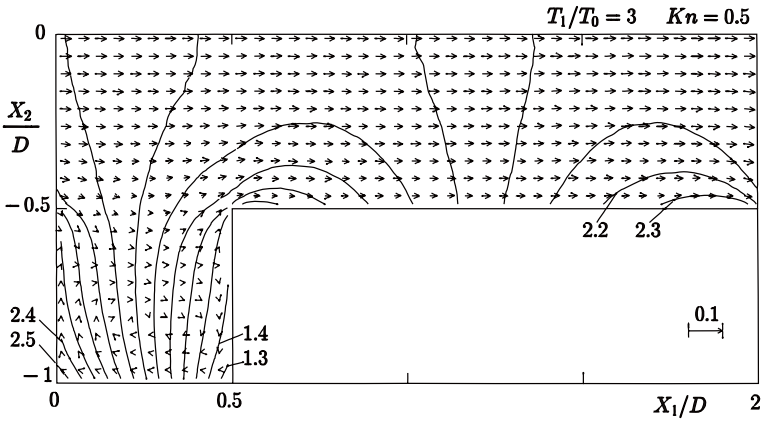

Fig. 8. Induced one-way flow and temperature field in the channel of Fig. 7 ($L/D = 2$, $b/D = 1/2$, $d/D = 1/2$, $T_1/T_0 = 3$, Kn $= 0.5$; a hard-sphere gas). The arrows indicate the flow velocity $\boldsymbol{v}$ at their starting points; the scale of 0.1 of $|\boldsymbol{v}|/(2RT_0)^{1/2}$ is shown at the right bottom of the figure. The solid curves indicate the isothermal lines $T/T_0 = 1.3,\ 1.4, \ldots,\ 2.5$. The Knudsen number is defined by $\mathrm{Kn} = \ell_{\mathrm{av}}/D$ with ℓ_{av} being the mean free path in the equilibrium state at rest with the density ρ_{av} averaged over the channel. The field is symmetric with respect to $X_2 = 0$ and only the lower half part is shown.

currence of one-way flow in the channel by the DSMC computations for a hard-sphere gas under the assumption of diffuse reflection of molecules on the channel surface. Figure 8 shows an example of the induced flow and temperature field in the gas. The induced mass flux through the channel is shown by closed circles in Fig. 9 as a function of the Knudsen number. They also demonstrated the pumping effect of the channel by performing the DSMC computations for the systems of up to 10 units

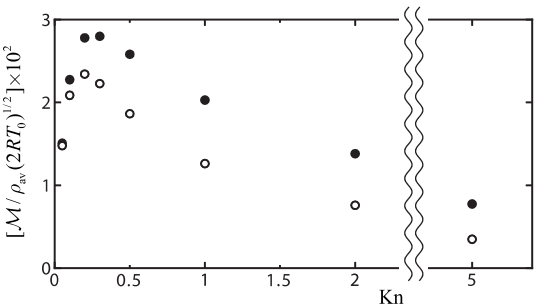

Fig. 9. Mass flux $\mathcal{M}$ through the channel for the same parameters as in Fig. 8 except the Knudsen number. Closed circles indicate the mass-flow rate $\mathcal{M}D$ through the two-dimensional channel with unit width in X_3 direction [**59**]; open circles the mass-flow rate $\mathcal{M}\pi(D/2)^2$ through the channel of circular cross-section [**60**].

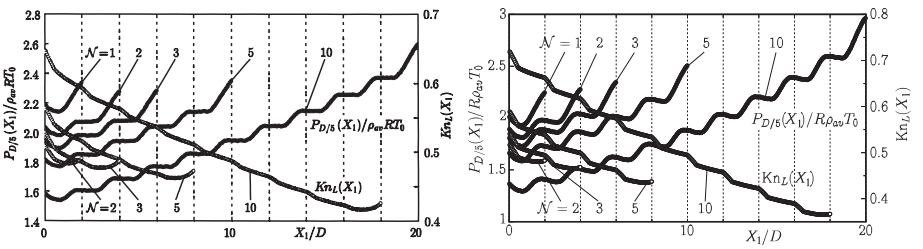

(a) two-dimensional channel (b) cylindrical channel

Fig. 10. Pumping effect of the channel with the same parameters as Fig. 8 except the Knudsen number. Here, $P_{D/5}$ is the average of the local pressure in the central part of the channel: $P_{D/5} = (5/D)\int_{-D/10}^{D/10} p(X_1, X_2)dX_2$ in (a) and $P_{D/5} = 2(10/D)^2 \int_0^{D/10} p(X_1, r)rdr$ in (b); $\mathrm{Kn}_L(X_1)$ is the semi-local Knudsen number at X_1 defined on the basis of the mean free path at the average density over the interval $(X_1, X_1 + L)$. $\mathcal{N}$ is the number of units in the cascade system.

with closed ends for various Knudsen numbers. Figure 10(a) shows an example of the pumping effect. They further presented a diagram from which one can estimate the compression ratio by a given (much larger) number of cascade units.

The case of the channel of cylindrical pipe with the corresponding configuration was studied in [**60**], results of which are shown in Fig. 9 by open circles and in Fig. 10(b). As is seen from Fig. 9, the induced flow under the periodic condition is weaker. Nevertheless, the pumping effect is found to be stronger [compare Fig. 10(b) with 10(a)]. This is due to the lower conductance of the cylindrical channel against the pressure difference because of the larger fraction of surface to volume.

In the configuration of the channel, the change of width is essential. In fact, it was demonstrated in [**59, 60**] by the DSMC computations that in the case of a simple straight channel with a periodic temperature distribution, a circulating flow is induced in each part of the unit and there is no mass flux through the channel. No mass flux in the case of the straight pipe is also verified experimentally [**61, 62**]. Golse [**1**] gave a rigorous mathematical proof of this fact in the linear regime where the variation of the imposed temperature is small. In summary, a mere periodic temperature is not enough to induce a one-way flow; a coupling of the periodic temperature with the width variation is essential.

5.2 - *Variants of the Knudsen compressor*

5.2.1 - The first category

As remarked at the end of Sec. 5.1, the essential feature of the Knudsen compressor is the combination of a periodic temperature distribution and the change of

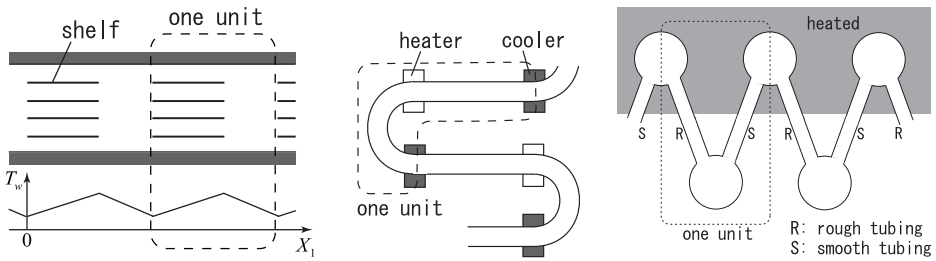

Fig. 11. Variants of the Knudsen compressor in the first category: (a) channel with shelves, (b) curvature compressor, (c) accommodation pump.

geometry in the unit device. Each unit is composed of two channels of different width with a gradient of temperature opposite to each other. In each part a flow of thermal transpiration is induced, but the direction is opposite. The induced flows in different parts cancel out each other, but the cancellation is not complete and the one-way flow occurs. The incomplete cancellation is due to the difference of channel width between the parts. Since the flow conductance depends on the width of channel, the incomplete cancellation may be reinterpreted as a consequence of the conductance change in the unit. In Fig. 10, the pressure changes in such a way to support the above interpretation: the pressure changes steeper at narrow parts of the channel. In the meantime, the flow conductance depends also on factors other than the width, such as the geometry of the cross-section, curvature, surface material of the channel. The reinterpretation suggests alternative ways to make compressors similar to the original Knudsen compressor. We shall call the compressors devised in this way the variants of the Knudsen compressor in the first category in this manuscript.

The compressor of a straight channel with shelves experimentally studied in [**62, 63**] would be considered as an (immediate) outcome of the above reinterpretation. In this compressor, in place of alternative arrangement of narrow and wide part, used is a channel of uniform width equipped with shelves periodically [Fig. 11(a)]; the part with shelves plays the same role as the narrow part in the original Knudsen compressor in an enhanced manner.[1] The prototype compressor fabricated and tested in the USC group may be considered as the same type (e.g., [**64**]).

[1] The gradient of temperature is imposed to shelves too. Thus, the part with shelves is not only of lower conductance (against the backward flow by a pressure difference) but also equipped with more driving parts of the thermal transpiration.

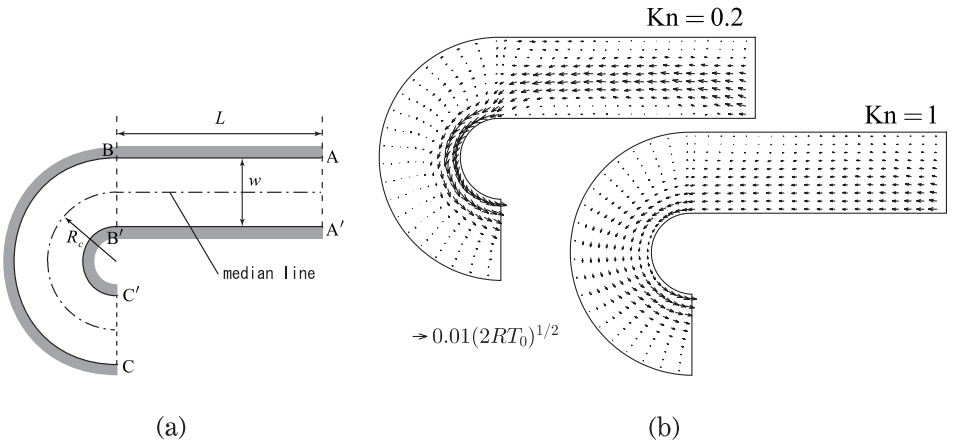

Fig. 12. Curvature compressor of two-dimensional channel and induced flow: (a) configuration of unit. (b) flow induced in the unit in the case of the ring-shape arrangement of two units ($T_1/T_0 = 3$, $L/R_c = \pi$, $R_c/w = 1$; a hard-sphere gas). In (b), the arrows indicate the flow velocity $\boldsymbol{v}$ at their starting points; the scale of $0.01(2RT_0)^{1/2}$ of $|\boldsymbol{v}|$ is shown at the left bottom of the figure. Kn is the Knudsen number defined by $\mathrm{Kn} = \ell_{\mathrm{av}}/w$ with ℓ_{av} being the mean free path in the equilibrium state at rest with the density ρ_{av} averaged over the ring.

Recently proposed idea of the compressor using the effect of curvature of channel [**65, 66**] (the curvature compressor, for short) also arose from the above reinterpretation. It is a compressor consisting of alternatively arranged straight and curved channels with a periodic temperature distribution [Fig. 11(b)]. Figure 12(a) shows the configuration of the unit studied in [**65**]. The unit consists of a straight and a semi-circular two-dimensional channel of a uniform width w, where the temperature of the channel surface T_w is kept at T_0 at the positions B and B′ and at $T_1 (> T_0)$ at the positions A, A′, C, and C′ and changes linearly with the distance from A (A′) to B (B′) and from B (B′) to C (C′). Figure 12(b) shows an example of the induced flow in the ring-shape arrangement of two units where the positions A and A′ of one unit are respectively connected to C and C′ of the other unit. The ring-shape arrangement corresponds to the periodic arrangement in the case of the original Knudsen compressor. Thus, the induced flow implies the pumping effect of the unit. In fact, the pumping effect of the snaky arrangement of units like Fig. 11(b) was demonstrated in [**65**]. As is clear from Figs. 8 and 12(b), the induced flow in the ring channel is much weaker, and so is the pumping effect by a single unit compared to the original Knudsen compressor. Nevertheless, the curvature compressor is attractive because of its dramatically simple structure. This feature would allow us to make a huge cascade, which compensates for the low performance of a single unit.

The so-called accommodation pump [**67**] may also be regarded as a variant in the first category. It is a compressor consisting of a channel with alternatively arranged rough and smooth surfaces [Fig. 11(c)]. Here, the change of the surface roughness causes the change of conductance.[2] The name of the accommodation pump comes from the fact that the surface roughness is represented by the accommodation coefficient appearing in the kinetic boundary condition. Rather recently, Hudson and Bartel [**68**] investigated the capability of the accommodation pumps numerically by the DSMC method.

5.2.2 - The second category

The driving force of the original Knudsen compressor and its variants in the first category is the thermal transpiration. Recently a compressor using the thermal-edge flow (Sec. 4.1.2) as a driving force has been proposed by Sugimoto and Sone [**69**], which we shall call the thermal-edge compressor following the reference. It may be considered as a variant of the Knudsen compressor in the sense that the driving force is a thermal gas-kinetic effect. However, the difference of the driving force should be reminded; thus we separate it from the first category.

The unit device of the thermal-edge compressor is a channel equipped with arrays of heated and unheated plates [Fig. 13(a)]. In the compressor, the arrays in the unit are arranged close to each other so that the strong temperature gradient is established in the gas near the inside edges. Then, the thermal-edge flow induced near there is superior to that near the outside edges, forming a one-way flow in the direction from the unheated to the heated arrays of plates. Fig. 13(b) shows an example of the temperature field in the gas and induced flow obtained by the DSMC computation for a hard-sphere gas.

In the original Knudsen compressor, one has to maintain the gradient of temperature along the channel wall, which accompanies a heat flow there. It means that a part of the supplied energy is consumed outside of the system. The advantage of the thermal-edge compressor is the absence of the energy loss of this kind, because the heated part is separated from the outside. Thus the energy efficiency is considerably improved.

---

[2] Qualitatively speaking, the rough tubing would have the same effect as the shelf part of the channel with shelves, i.e., the lower conductance against the back flow by a pressure difference and the enhanced thermal transpiration.

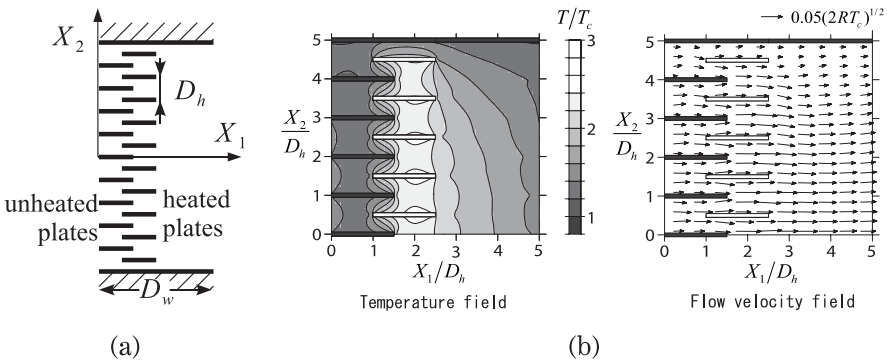

Fig. 13. Thermal-edge compressor of two-dimensional channel (by courtesy of Prof. H. Sugimoto). (a) Configuration of the unit device. (b) Temperature field and induced flow in the upper half of the unit in the case of its periodic arrangement obtained by the DSMC computation ($T_h/T_c = 3$, Kn $= 1$; hard-sphere gas). In (b), T_c and T_h are the temperature of the unheated and heated plates and Kn is the Knudsen number defined by Kn $= \ell_{\rm av}/D_h$ with $\ell_{\rm av}$ being the mean free path in the equilibrium state at rest with the average density $\rho_{\rm av}$ over the unit. Specific values of geometric parameters are obvious from the figure. The arrows in the right figure in (b) indicate the flow velocity $\boldsymbol{v}$ at their starting points; the scale of $0.05(2RT_c)^{1/2}$ is shown at the top of the figure. The field is symmetric with respect to $X_2 = 0$ and only the upper half part is shown in (b).

5.3 - *New feasibility as a gas separator*

We have introduced, so far, the Knudsen compressor and its variants, together with numerical data showing their features. Originally, they were designed and studied aiming at their capability as a compressor (or a pump, a flow controller). Recently a new feasibility of the use for the gas separation has been reported in [**70, 71**], which we shall describe below.

Consider two different species of gas, say gas A and gas B, at the same pressure and temperature. The Knudsen number in the system of gas A is different from that in the system of gas B, because the viscosity (or the mean free path of a molecule determined from it) depends on gas species even at the same temperature and pressure. On the other hand, as is expected from Fig. 9, the compression ratio of the Knudsen compressor depends on the Knudsen number. Therefore, even in the same condition, the achieved compression ratio differs from species to species, which suggests a feasibility of the compressor as a separator of gas mixtures. It should be noted, however, that the interaction between different species is not taken into account in the above preliminary consideration. The interaction diminishes the difference of flow velocities between species; the feasibility raised above is not obvious and should be examined carefully.

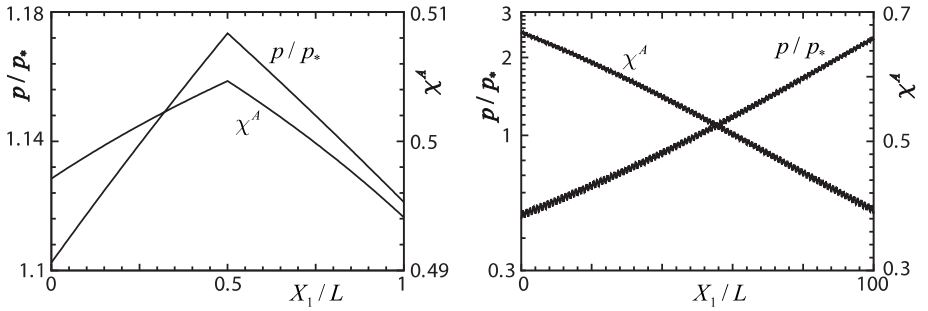

Fig. 14. Pumping and separation effect in the Knudsen compressor of two-dimensional channel with the configuration in Fig. 7 on the basis of the fluid system with transport coefficients based on the McCormack kinetic model for a binary mixture of hard-sphere gases, gas A and gas B ($b/L = 1/2$, $d/D = 1$, $T_1/T_0 = 1.3$, Kn $= 1$). Two species gases of the same amount are put inside, and the ratio of molecular mass is $m^B/m^A = 2$ and that of diameter $d^B/d^A = 1$. Here, $p(X_1)$ and $\chi^A(X_1)$ denote respectively the pressure of the total mixture and concentration of species A averaged over the cross-section at X_1; p_* is the pressure defined by $p_* = n_{\rm av}kT_0$ with $n_{\rm av}$ being the average molecular number density of total mixture; Kn is the reference Knudsen number defined on the basis of the mean free path in a pure gas A with number density $n_{\rm av}$ in the equilibrium state at rest with temperature T_0.

The feasibility of the original Knudsen compressor, including the compressor with shelves, was investigated in [**70**] on the basis of the fluid-dynamic system derived from the Boltzmann system for binary gas mixtures. The derivation of the former is the issue of Sec. 6; here we merely mention (i) that it is derived from the Boltzmann system by an asymptotic analysis of the so-called narrow channel approximation [$D, d \ll b, L$ in Fig 7(a)]; (ii) that it is a spatially one-dimensional convection-diffusion equation for the partial pressures of individual species averaged over the cross-section of the channel; (iii) that it covers the entire range of the Knudsen number.

Figure 14 shows an example of the numerical results based on the fluid system for the cascade of units with the configuration in Fig. 7(a) ($b/L = 1/2$, $d/D = 1$, $T_1/T_0 = 1.3$). In the simulation, both ends of the cascade are closed, and two species, gas A and gas B (the diameter of a molecule is common but the mass is different, i.e., $m^B/m^A = 2$), of the same amount are put. Thus the deviation of the concentration χ^A of species A from 0.5 is the measure of separation effect. As is seen from the figure, the use of the compressor as a gas separator is promising. The saw-tooth distribution in the one-hundred unit system can be understood from the distribution in the one unit system.

In the meantime, the modeling at the level of the kinetic equation turned out to have a decisive impact on the proper estimate of the separation effect. In fact, the

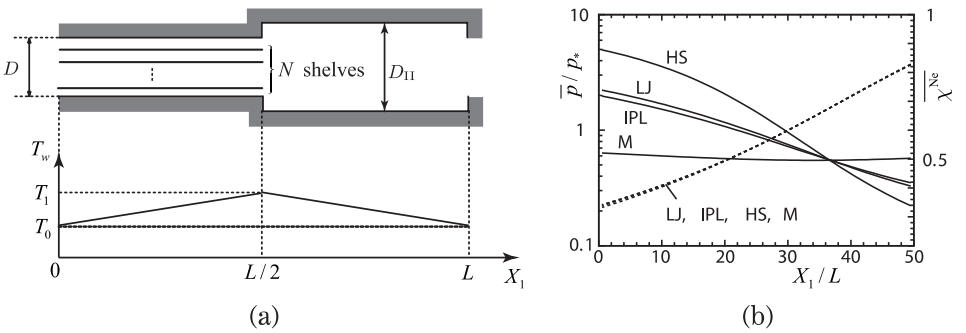

Fig. 15. Model dependence of the pumping and separation effects: the performance of the 50-unit system with closed ends for the Ne–Ar mixture of the same amount (Kn = 1). (a) Configuration of the unit and wall temperature T_w. (b) Distribution of the pressure $\bar{p}$ and concentration $\chi^{\rm Ne}$ averaged in respective units ($D_{\rm II}/D = 5$, $N = 5$, $T_1/T_0 = 1.3$). In (b), $\chi^{\rm Ne}$ is indicated by solid lines and $\bar{p}/p_*$ by dashed lines; HS, LJ, IPL, and M represent the results for the hard-sphere, Lenard-Jones (12-6) potential, inverse-power law potential, and Maxwell molecular model, respectively. See the caption of Fig. 14 for the definition of the reference Knudsen number Kn and pressure p_*.

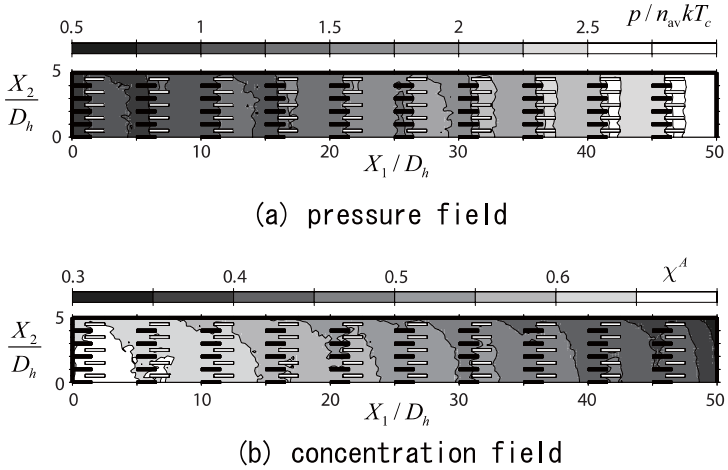

Fig. 16. Pumping and separation effects by the 10-unit system of the thermal-edge compressor with the configuration in Fig. 13 ($T_h/T_c = 3$, Kn = 0.5; a binary mixture of hard sphere gases of the same amount; ratios of molecular mass and diameter: $m^B/m^A = 10$ and $d^B/d^A = 1$): (a) pressure p of the total mixture, (b) concentration χ^A of species A. See the caption of Fig. 14 for the definition of Kn and $n_{\rm av}$. The field is symmetric with respect to $X_2 = 0$ and only the upper half part is shown.

fluid system with transport coefficients based on the Maxwell molecular model gives pessimistic results in the corresponding situation. The contradicting results between the hard-sphere and Maxwell models required further studies on the dependence of estimate on the choice of molecular model. Figure 15 shows partial results of those studies, which includes the hard-sphere, Maxwell, inverse power law, and more realistic Lenard-Jones (12-6) potential molecular models based on the McCormack kinetic model Boltzmann equation. It is clear from the figure that the modeling by use of the celebrated Maxwell molecules is decisively unfavorable for describing the separation effect. It makes a marked contrast to its capability for the description of pumping effect.

The feasibility in the case of the thermal-edge compressor was also investigated [**71**]. In this reference, the DSMC computations are carried out mainly for hard sphere gases, and the results are promising as shown in Fig. 16. On the other hand, the decisive defect of the modeling by the use of the Maxwell molecular model was also observed as in [**70**].

6 - Fluid-dynamic systems for the Knudsen compressors

In Sec. 5, we have introduced the Knudsen compressors with numerical results obtained mainly by the DSMC method. The DSMC method is a stochastic and most commonly used numerical method for simulating rarefied gas flows; advantageous is its simplicity and highly flexibility to complicated geometries, chemical reactions, etc. However, there is a drawback: it actually suffers from a large stochastic noise because of the limited number of simulation particles in a single shot of simulation. Some averaging process, i.e., the time average in a single shot or the ensemble average of independent shots, is inevitable to secure the sample size enough to take out the necessary information buried in the noise with reasonable accuracy. In view of this nature, there are two factors that make the DSMC simulation expensive in the study of the Knudsen compressors. The first is that, as is clear from the figures in Sec. 5, the thermally induced flows in the Knudsen compressors are of small Mach number. It makes the required level of noise reduction severer than the case of transonic or supersonic flows. The second is the cascade structure of the compressors: the required number of simulation particles increases in proportion to the number of units in a cascade. Since the statistical noise decays with the rate of $\sqrt{N}$ with N being the sample size, there is no hope to perform the DSMC computations for large cascades. In facts, it took several months by the use of a MPI parallel computing system in order to obtain some of the data in Fig. 10.

The diagram in [**59, 60, 65**] for the estimate of the pumping effect in a large number cascade from the data of a small number cascade for various Knudsen numbers is one of the ways to bypass the difficulty addressed above. Another way is, of course, taking an alternative method. For instance, for small Knudsen numbers, the fluid dynamic system can be derived from the Boltzmann system, and the use of the former for numerical simulations should drastically reduce the computational cost with higher accuracy. The approach in [**73**] is the one in this direction.

Usually the fluid dynamic description makes sense only in the regime of small Knudsen number. However, under an additional assumption on the configuration of the compressors, it is possible to derive such a fluid dynamic system from the Boltzmann that can describe gas flows for the entire range of the Knudsen number. To be more specific, the additional assumption is that the physical quantities vary moderately along the channel and the ratio of the channel width to its length is small enough. The so-called narrow channel approximation under this assumption enables us to derive that system. In the present section, we shall give the outline of its construction.

The construction to be presented is based on the method by Aoki and Degond [**74**], in which a simplified BGK-type linear kinetic equation is used for the sake of mathematical rigor in the course of discussions. Here, we shall consider the case of binary gas mixtures in the original Knudsen compressor of two-dimensional channel depicted in Fig. 7(a). We shall show the derivation from the Boltzmann equation with the diffuse reflection boundary-condition on the channel walls, following [**70**]. It is the simplest setting of the problem, except for treating a gas mixture not a single-species gas, with retaining all the essence of rarefied gas flows. The reader is refer to [**75**] for additional aspects such as more general boundary conditions, channels with an arbitrary cross-section, and to [**66**] for the case of curvature compressor.

There are two main steps in the construction of the fluid dynamic system. In the first step, we consider a gas in an infinitely long straight channel whose surface temperature varies slowly in space along the channel in the scale of the channel width. In the situation, we introduce the so-called diffusion scaling and derive a fluid dynamic equation of convection-diffusion type in that channel. Each unit of the compressor is composed of two straight channels of different uniform width. In the second step, assuming these channels to be long enough, we derive the connection condition at the junction for the fluid dynamic equations in the respective channels. The fluid dynamic system for the Knudsen compressor is then constructed by the connection of the convection-diffusion equations in neighboring subunit channels at junctions by the use of that condition.

6.1 - *The first step*

6.1.1 - Problem and formulation

Consider a binary mixture of two-species gases, say species A and species B, in a straight two-dimensional channel of uniform width oriented to the direction of X_1, where X_i's are the Cartesian space coordinates (Fig. 17). The channel walls are separated by a distance D and are located at $X_2 = \pm D/2$. The temperatures of the walls may vary along the channel, i.e., in the direction of X_1, but are constant both in time t and in coordinate X_3. They are supposed to take a common value at the same location in X_1 and will be denoted by $T_{\rm w}(X_1)$. There is no external force. We will investigate the behavior of the mixture in the channel by assuming that

1. The behavior of the mixture can be described by the Boltzmann equation for binary gas mixtures.
2. The gas molecules are reflected diffusely on the surface of the walls.
3. The characteristic length of the variation of the wall temperature, L, is much larger than the separation distance D.

The first assumption implies that the mean free path of a molecule ℓ is comparable to the separation distance D, i.e., $\ell \sim D$. The third implies that the state of the mixture would change in the scale of L, not of D, in the direction of X_1. And, since $\ell \sim D \ll L$, the molecules undergo innumerable collisions with both other molecules and the walls when traveling in that direction until its surroundings change appreciably.

Let us denote by $\boldsymbol{\xi} = (\xi_1, \xi_2, \xi_3)$ the molecular velocity and by $f^a(t, \boldsymbol{X}, \boldsymbol{\xi})$ the velocity distribution function of molecules of a-species gas ($a = \mathrm{A}, \mathrm{B}$). In the

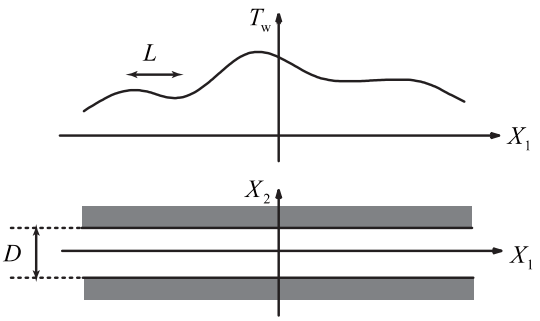

Fig. 17. Two-dimensional straight channel with wall temperature variation.

sequel, the Greek letters α and β will be symbolically used to denote the gas species, i.e., $\{\alpha,\beta\}=\{\mathrm{A},\mathrm{B}\}$. The Boltzmann equation and the boundary condition are written as

$$\frac{\partial f^\alpha}{\partial t}+\xi_1\frac{\partial f^\alpha}{\partial X_1}+\xi_2\frac{\partial f^\alpha}{\partial X_2}=J^{\mathrm{B}\alpha}(f^{\mathrm{B}},f^\alpha)+J^{\mathrm{A}\alpha}(f^{\mathrm{A}},f^\alpha), \tag{54a}$$

$$f^\alpha=\sigma_{2\pm}\left(f^\alpha(\boldsymbol{\xi});\frac{m^\alpha}{2kT_{\mathrm{w}}}\right)M\left(\boldsymbol{\xi};\frac{m^\alpha}{2kT_{\mathrm{w}}}\right),\quad \xi_2\lessgtr 0,\quad X_2=\pm\frac{D}{2}, \tag{54b}$$

where m^α is the mass of a molecule of species α, k the Boltzmann constant, $\sigma_{2\pm}$ a constant (in $\boldsymbol{\xi}$) depending on the arguments defined by

$$\sigma_{i\pm}(f(\boldsymbol{\xi});a)=\pm 2(\pi a)^{1/2}\int\limits_{\xi_i\gtrless 0}\xi_i f(\boldsymbol{\xi})\mathrm{d}^3\xi\qquad (i=1,2),$$

with $\mathrm{d}^3\xi=\mathrm{d}\xi_1\mathrm{d}\xi_2\mathrm{d}\xi_3$ and M the normalized Maxwellian given by

$$M(\boldsymbol{\xi};a)=\left(\frac{a}{\pi}\right)^{3/2}\exp(-a|\boldsymbol{\xi}|^2).$$

In Eq. (54b), the argument $\boldsymbol{\xi}$ of f^α is explicitly shown in order to indicate the variable of integration in the definition of $\sigma_{2\pm}$, while the other arguments t, X_1 and X_2 are suppressed for conciseness. We shall follow this convention in the sequel. $J^{\beta\alpha}$'s in Eq. (54a) are the collision integrals defined by

$$J^{\beta\alpha}(f,g)=\int(f'_*g'-f_*g)B^{\beta\alpha}\left(\frac{|\boldsymbol{e}\cdot\boldsymbol{V}|}{|\boldsymbol{V}|},|\boldsymbol{V}|\right)\mathrm{d}\Omega(\boldsymbol{e})\mathrm{d}^3\xi_*,$$

$$f'_*=f(\boldsymbol{\xi}'_*),\qquad g'=g(\boldsymbol{\xi}'),\qquad f_*=f(\boldsymbol{\xi}_*),\qquad g=g(\boldsymbol{\xi}),$$

$$\boldsymbol{\xi}'=\boldsymbol{\xi}+\frac{\mu^{\beta\alpha}}{m^\alpha}(\boldsymbol{e}\cdot\boldsymbol{V})\boldsymbol{e},\qquad \boldsymbol{\xi}'_*=\boldsymbol{\xi}_*-\frac{\mu^{\beta\alpha}}{m^\beta}(\boldsymbol{e}\cdot\boldsymbol{V})\boldsymbol{e},$$

$$\mu^{\beta\alpha}=\frac{2m^\alpha m^\beta}{m^\alpha+m^\beta},\qquad \boldsymbol{V}=\boldsymbol{\xi}_*-\boldsymbol{\xi},$$

where $\boldsymbol{e}$ is a unit vector, $\mathrm{d}\Omega(\boldsymbol{e})$ the solid angle element in the direction of $\boldsymbol{e}$ and $\mathrm{d}^3\xi_*=\mathrm{d}\xi_{*1}\mathrm{d}\xi_{*2}\mathrm{d}\xi_{*3}$. $B^{\beta\alpha}$ is a nonnegative function of its arguments whose functional form is determined by the molecular interaction between species β and α. It has the symmetry property of $B^{\mathrm{BA}}=B^{\mathrm{AB}}$ because of the law of action and reaction. The integration in the definition of $J^{\beta\alpha}$ is carried out over the all directions of $\boldsymbol{e}$ and over the whole space of $\boldsymbol{\xi}_*$. The initial- and boundary-value problem for the binary gas mixture in the channel is formulated by Eq. (54) supplemented by an initial condition.

6.1.2 - Scaling and dimensionless description

We are concerned with the solution which varies in the scale of L in the X_1-direction. Since the Mach number Ma of the flow thermally induced by the kinetic effect is of $O(\ell/L)$, it is natural to take the quantity L^2/cD with c being the sound speed as the time scale of variation because of the relation

$$\text{time scale} = \frac{\text{characteristic length}}{\text{representative flow speed}} = \frac{L}{c\,\mathrm{Ma}} = O\left(\frac{L^2}{c\,\ell}\right) \sim O\left(\frac{L^2}{c\,D}\right).$$

Thus we introduce the following dimensionless variables:

$$s = t/t_*, \qquad x_1 = X_1/L, \qquad x_2 = X_2/D_*, \qquad \boldsymbol{\zeta} = \boldsymbol{\xi}/(2kT_*/m^{\mathrm{A}})^{1/2},$$
$$\hat{f}^a = f^a/[n_*(2kT_*/m^{\mathrm{A}})^{-3/2}], \qquad \hat{T}_{\mathrm{w}} = T_{\mathrm{w}}/T_*,$$

where n_* is the reference molecular number density, T_* the reference temperature, p_* the reference pressure defined by $p_* = n_* k T_*$ and

$$t_* = \frac{L^2}{(2kT_*/m^{\mathrm{A}})^{1/2} D_*}.$$

The references n_* and T_* are to be chosen in a certain proper manner. In the above, the reference length scale is different in the X_1- and X_2-directions. The length scale D_* in the X_2-direction is a constant of $O(D)$, i.e., the ratio $a_* = D/D_*$ is of $O(1)$. This choice of reference length is simply for the convenience of the later discussions on the connection of channels of different widths. For the time being, if prefer, one may put $D_* = D$ or $a_* = 1$. Further, we introduce the following dimensionless quantities:[3]

$$\varepsilon = D_*/L, \qquad \hat{m}^a = m^a/m^{\mathrm{A}}, \qquad K^{\beta a} = B_*^{\beta a}/B_*^{\mathrm{AA}}, \qquad \mathrm{K}_* = \ell_*/D_*,$$

where

$$\ell_* = \frac{1}{n_* B_*^{\mathrm{AA}}} \sqrt{\frac{2kT_*}{m^{\mathrm{A}}}}, \tag{55}$$

$$B_*^{\beta a} = \frac{\sqrt{\pi}}{2} \int M\left(\boldsymbol{\xi}_*; \frac{m^\beta}{2kT_*}\right) M\left(\boldsymbol{\xi}; \frac{m^a}{2kT_*}\right) B^{\beta a}\left(\frac{|\boldsymbol{e}\cdot\boldsymbol{V}|}{|\boldsymbol{V}|}, |\boldsymbol{V}|\right) \mathrm{d}\Omega(\boldsymbol{e}) \mathrm{d}^3\xi_* \mathrm{d}^3\xi. \tag{56}$$

Here ℓ_* is the reference mean free path of a molecule and K_* is the corresponding reference Knudsen number.

---

[3] The integral in the right-hand side of Eq. (56) does not remain finite in general. In the case, in place of $B_*^{\beta a}$'s defined by Eq. (56), one should use as $B_*^{\beta a}$'s those constants that are chosen properly and satisfy the symmetry property $B_*^{\mathrm{AB}} = B_*^{\mathrm{BA}}$. See the Appendix A of [**70**] for specific examples.

With the dimensionless quantities introduced above, the original Boltzmann system is recast as

$$\varepsilon^2\partial_s\hat{f}^a+\varepsilon\,\zeta_1\partial_{x_1}\hat{f}^a+\zeta_2\partial_{x_2}\hat{f}^a=\frac{1}{\mathrm{K}_*}\sum_{\beta=\mathrm{A},\mathrm{B}}K^{\beta a}\hat{J}^{\beta a}(\hat{f}^\beta,\hat{f}^a), \tag{57a}$$

$$\hat{f}^a=\sigma_{2\pm}\left(\hat{f}^a(\boldsymbol{\zeta});\frac{\hat{m}^a}{\hat{T}_\mathrm{w}}\right)M\left(\boldsymbol{\zeta};\frac{\hat{m}^a}{\hat{T}_\mathrm{w}}\right),\qquad \zeta_2\lessgtr 0,\qquad x_2=\pm\frac{a_*}{2}, \tag{57b}$$

where

$$\hat{J}^{\beta a}(f,g)=\int(f'_*g'-f_*g)b^{\beta a}\left(\frac{|\boldsymbol{e}\cdot\hat{\boldsymbol{V}}|}{|\hat{\boldsymbol{V}}|},|\hat{\boldsymbol{V}}|\right)\mathrm{d}\Omega(\boldsymbol{e})\mathrm{d}^3\boldsymbol{\zeta}_*, \tag{58a}$$

$$f'_*=f(\boldsymbol{\zeta}'_*),\qquad g'=g(\boldsymbol{\zeta}'),\qquad f_*=f(\boldsymbol{\zeta}_*),\qquad g=g(\boldsymbol{\zeta}), \tag{58b}$$

$$\boldsymbol{\zeta}'=\boldsymbol{\zeta}+\frac{\hat{\mu}^{\beta a}}{\hat{m}^a}(\boldsymbol{e}\cdot\hat{\boldsymbol{V}})\boldsymbol{e},\qquad \boldsymbol{\zeta}'_*=\boldsymbol{\zeta}_*-\frac{\hat{\mu}^{\beta a}}{\hat{m}^\beta}(\boldsymbol{e}\cdot\hat{\boldsymbol{V}})\boldsymbol{e}, \tag{58c}$$

$$\hat{\mu}^{\beta a}=\frac{2\hat{m}^a\hat{m}^\beta}{\hat{m}^a+\hat{m}^\beta},\qquad \hat{\boldsymbol{V}}=\boldsymbol{\zeta}_*-\boldsymbol{\zeta},\qquad b^{\beta a}=\frac{B^{\beta a}}{B^{\beta a}_*}. \tag{58d}$$

Here again, the system (57) must be supplemented by a dimensionless initial condition.

It should be noted that ε is a small parameter by the third assumption in Sec. 6.1.1 and that it arises in the first two terms of the left-hand side of the scaled Boltzmann equation (57a). We shall seek the moderately varying solution of the system (57) in a power series of ε.

Before proceeding, we introduce here the notation and definition of the macroscopic quantities. The average molecular number density, mass density, pressure, temperature, and flow velocity of species a are respectively denoted by $n_*\hat{n}^a$, $m^\mathrm{A}n_*\hat{\rho}^a$, $p_*\hat{p}^a$, $T_*\hat{T}^a$, and $(2kT_*/m^\mathrm{A})^{1/2}\hat{\boldsymbol{v}}^a$; the average molecular number density, mass density, pressure, temperature, and barycentric flow velocity of the mixture are by $n_*\hat{n}$, $m^\mathrm{A}n_*\hat{\rho}$, $p_*\hat{p}$, $T_*\hat{T}$, and $(2kT_*/m^\mathrm{A})^{1/2}\hat{\boldsymbol{v}}$. The quantities with $\hat{}$ are defined as follows:

$$\hat{n}^a=\int\hat{f}^a\mathrm{d}^3\boldsymbol{\zeta},\qquad \hat{\rho}^a=\hat{m}^a\hat{n}^a,\qquad \hat{n}^a\hat{v}^a_i=\int\zeta_i\hat{f}^a\mathrm{d}^3\boldsymbol{\zeta}\qquad (i=1,2), \tag{59a}$$

$$\hat{p}^a=\hat{n}^a\hat{T}^a=\frac{2}{3}\int|\boldsymbol{\zeta}-\hat{\boldsymbol{v}}^a|^2\hat{m}^a\hat{f}^a\mathrm{d}^3\boldsymbol{\zeta}, \tag{59b}$$

$$\hat{n}=\hat{n}^\mathrm{A}+\hat{n}^\mathrm{B},\qquad \hat{\rho}=\hat{\rho}^\mathrm{A}+\hat{\rho}^\mathrm{B}, \tag{59c}$$

$$\hat{\rho}\hat{\boldsymbol{v}}=\hat{\rho}^\mathrm{A}\hat{\boldsymbol{v}}^\mathrm{A}+\hat{\rho}^\mathrm{B}\hat{\boldsymbol{v}}^\mathrm{B},\qquad \hat{p}=\hat{n}\hat{T}=\sum_{a=\mathrm{A},\mathrm{B}}\left(\hat{p}^a+\frac{2}{3}\,\hat{\rho}^a|\hat{\boldsymbol{v}}^a-\hat{\boldsymbol{v}}|^2\right). \tag{59d}$$

The concentration (or the molar fraction) χ^a of species a is written as $\chi^a = \hat{n}^a/\hat{n}$.

6.1.3 - Asymptotic analysis

Now we seek the moderately varying solution $\hat{f}^a$ to the system (57) in a power series of ε:

$$\hat{f}^a = \hat{f}^a_{(0)} + \hat{f}^a_{(1)}\varepsilon + \cdots.$$

Corresponding to the expansion of $\hat{f}^a$, we expand the macroscopic quantities as

$$\hat{n}^a = \hat{n}^a_{(0)} + \hat{n}^a_{(1)}\varepsilon + \cdots, \quad \hat{\boldsymbol{T}}^a = \hat{\boldsymbol{T}}^a_{(0)} + \hat{\boldsymbol{T}}^a_{(1)}\varepsilon + \cdots, \quad \text{etc.}$$

The expressions of the coefficient functions $\hat{n}^a_{(0)}$, $\hat{n}^a_{(1)}$, $\hat{\boldsymbol{T}}^a_{(0)}$, $\hat{\boldsymbol{T}}^a_{(1)}$, etc. in terms of $\hat{f}^a_{(0)}$,$\hat{f}^a_{(1)}$, etc. are obtained by substituting the expansions into Eq. (59) and by equating like powers of ε. We omit these expressions for conciseness.

Substituting the expansion of $\hat{f}^a$ into the system (57) and equating like powers of ε lead to the following series of problems for $\hat{f}^a_{(0)}$,$\hat{f}^a_{(1)}$, $\cdots$:

$\underline{O(\varepsilon^0)}$

$$\zeta_2 \partial_{x_2} \hat{f}^a_{(0)} = \frac{1}{\mathrm{K}_*} \sum_{\beta=\mathrm{A},\mathrm{B}} K^{\beta a} \hat{J}^{\beta a}(\hat{f}^\beta_{(0)}, \hat{f}^a_{(0)}), \tag{60a}$$

$$\hat{f}^a_{(0)} = \sigma_{2\pm}\left(\hat{f}^a_{(0)}(\boldsymbol{\zeta}); \frac{\hat{m}^a}{\hat{T}_\mathrm{w}}\right) M\left(\boldsymbol{\zeta}; \frac{\hat{m}^a}{\hat{T}_\mathrm{w}}\right), \qquad \zeta_2 \lessgtr 0, \quad x_2 = \pm\frac{a_*}{2}, \tag{60b}$$

$\underline{O(\varepsilon^1)}$

$$\zeta_1 \partial_{x_1} \hat{f}^a_{(0)} + \zeta_2 \partial_{x_2} \hat{f}^a_{(1)} = \frac{1}{\mathrm{K}_*} \sum_{\beta=\mathrm{A},\mathrm{B}} K^{\beta a}[\hat{J}^{\beta a}(\hat{f}^\beta_{(0)}, \hat{f}^a_{(1)}) + \hat{J}^{\beta a}(\hat{f}^\beta_{(1)}, \hat{f}^a_{(0)})], \tag{61a}$$

$$\hat{f}^a_{(1)} = \sigma_{2\pm}\left(\hat{f}^a_{(1)}(\boldsymbol{\zeta}); \frac{\hat{m}^a}{\hat{T}_\mathrm{w}}\right) M\left(\boldsymbol{\zeta}; \frac{\hat{m}^a}{\hat{T}_\mathrm{w}}\right), \qquad \zeta_2 \lessgtr 0, \ x_2 = \pm\frac{a_*}{2}, \tag{61b}$$

$\underline{O(\varepsilon^2)}$

$$\begin{aligned} &\partial_s \hat{f}^a_{(0)} + \zeta_1 \partial_{x_1} \hat{f}^a_{(1)} + \zeta_2 \partial_{x_2} \hat{f}^a_{(2)} \\ &\qquad = \frac{1}{\mathrm{K}_*} \sum_{\beta=\mathrm{A},\mathrm{B}} K^{\beta a}[\hat{J}^{\beta a}(\hat{f}^\beta_{(0)}, \hat{f}^a_{(2)}) + \hat{J}^{\beta a}(\hat{f}^\beta_{(2)}, \hat{f}^a_{(0)}) + \hat{J}^{\beta a}(\hat{f}^\beta_{(1)}, \hat{f}^a_{(1)})], \end{aligned} \tag{62a}$$

$$\hat{f}^a_{(2)} = \sigma_{2\pm}\left(\hat{f}^a_{(2)}(\boldsymbol{\zeta}); \frac{\hat{m}^a}{\hat{T}_\mathrm{w}}\right) M\left(\boldsymbol{\zeta}; \frac{\hat{m}^a}{\hat{T}_\mathrm{w}}\right), \qquad \zeta_2 \lessgtr 0, \ x_2 = \pm\frac{a_*}{2}, \tag{62b}$$

and so on. This series of problems can be solved from the lowest order.

The leading order solution: the solution of the problem (60), in which s and x_1 occur as parameters, is the following bi-Maxwellian independent of x_2:

$$\hat{f}^a_{(0)} = \hat{n}^a_{(0)}(s,x_1)\, M(\boldsymbol{\zeta}; \frac{\hat{m}^a}{\hat{T}_{\rm w}(x_1)}) = \frac{\hat{n}^a_{(0)}(s,x_1)}{(\pi \hat{T}_{\rm w}(x_1)/\hat{m}^a)^{3/2}} \exp\Big(-\frac{\hat{m}^a|\boldsymbol{\zeta}|^2}{\hat{T}_{\rm w}(x_1)}\Big). \tag{63}$$

The proof is a straightforward extension of that in [**76**] to gas mixtures and is omitted here. From Eq. (63), the coefficient functions $\hat{n}^a_{(0)}, \hat{p}^a_{(0)}$, etc. at $O(\varepsilon^0)$ are independent of x_2; in particular, the following relations hold:

$$\hat{\boldsymbol{v}}^a_{(0)} = \hat{\boldsymbol{v}}_{(0)} = 0, \quad \hat{T}^a_{(0)} = \hat{T}_{(0)} = \hat{T}_{\rm w}(x_1).$$

The first relation is due to the present scaling taking into account the situation described in the first paragraph of Sec. 6.1.2. The second relation yields the following expressions for $\hat{p}^a_{(0)}$ and $\hat{p}_{(0)}$:

$$\hat{p}^a_{(0)} = \hat{n}^a_{(0)} \hat{T}_{\rm w}, \quad \hat{p}_{(0)} = \hat{n}_{(0)} \hat{T}_{\rm w}.$$

It should be noted that $\hat{n}^a_{(0)}$'s in the expression (63) remain undetermined at the present stage.

The first order solution : the problem (61) is linear in $\hat{f}^a_{(1)}$, and the solution can be expressed as

$$\hat{f}^a_{(1)} = \hat{n}_{(0)} M\left(\boldsymbol{\zeta}; \frac{\hat{m}^a}{\hat{T}_{\rm w}}\right) \big(\phi^a_{\rm e} + a_* \phi^a_{\rm P} \partial_{x_1} \ln \hat{p}_{(0)} + a_* \phi^a_{\rm T} \partial_{x_1} \ln \hat{T}_{\rm w} + a_* \phi^a_\chi \partial_{x_1} \chi^{\rm A}_{(0)} \big), \tag{64}$$

where $\phi^a_{\rm e}$ and ϕ^a_J $(J = {\rm P},\, {\rm T},\, \chi)$ are functions of s, x_1, y, $\boldsymbol{c}$ with $y = x_2/a_*$ and $\boldsymbol{c} = \boldsymbol{\zeta}/\sqrt{\hat{T}_{\rm w}}$; $\phi^a_{\rm e}$ is the solution of the problem

$$c_2 \partial_y \phi^a_{\rm e} = \frac{1}{\rm K} \sum_{\beta={\rm A,B}} K^{\beta a} L^{\beta a}_{\hat{T}_{\rm w}}(\chi^a_{(0)} \phi^\beta_{\rm e}, \chi^\beta_{(0)} \phi^a_{\rm e}), \tag{65a}$$

$$\phi^a_{\rm e} = \sigma_{2\pm}(\phi^a_{\rm e}(\boldsymbol{c}) M(\boldsymbol{c}; \hat{m}^a); \hat{m}^a), \qquad c_2 \lessgtr 0,\ y = \pm\frac{1}{2}, \tag{65b}$$

and is even with respect to c_1, while ϕ^a_J's $(J = {\rm P},\, {\rm T},\, \chi)$ are the solutions of the independent three problems

$$c_2 \partial_y \phi^a_J = \frac{1}{\rm K} \sum_{\beta={\rm A,B}} K^{\beta a} L^{\beta a}_{\hat{T}_{\rm w}}(\chi^a_{(0)} \phi^\beta_J, \chi^\beta_{(0)} \phi^a_J) - I^a_J, \quad (J = {\rm P},\, {\rm T},\, \chi), \tag{66a}$$

$$\phi^a_J = 0, \qquad c_2 \lessgtr 0,\ y = \pm\frac{1}{2}, \tag{66b}$$

with

$$I^a_{\rm P} = c_1 \chi^a_{(0)}, \quad I^{\rm A}_\chi = c_1, \quad I^{\rm B}_\chi = -c_1, \quad I^a_{\rm T} = \chi^a_{(0)} c_1 \Big(\hat{m}^a |\boldsymbol{c}|^2 - \frac{5}{2} \Big),$$

and are odd with respect to c_1. Here,

$$L_\tau^{\beta\alpha}(f,g)=\int (f_*'+g'-f_*-g)M(\boldsymbol{c}_*;\hat{m}^\beta)b_\tau^{\beta\alpha}\left(\frac{|\boldsymbol{e}\cdot\boldsymbol{C}|}{|\boldsymbol{C}|},|\boldsymbol{C}|\right)\mathrm{d}\Omega(\boldsymbol{e})\mathrm{d}^3c_*,$$

$$f_*'=f(\boldsymbol{c}_*'),\qquad g'=g(\boldsymbol{c}'),\qquad f_*=f(\boldsymbol{c}_*),\qquad g=g(\boldsymbol{c}),$$

$$\boldsymbol{c}'=\boldsymbol{c}+\frac{\hat{\mu}^{\beta\alpha}}{\hat{m}^\alpha}(\boldsymbol{e}\cdot\boldsymbol{C})\boldsymbol{e},\qquad \boldsymbol{c}_*'=\boldsymbol{c}_*-\frac{\hat{\mu}^{\beta\alpha}}{\hat{m}^\beta}(\boldsymbol{e}\cdot\boldsymbol{C})\boldsymbol{e},$$

$$\boldsymbol{C}=\boldsymbol{c}_*-\boldsymbol{c},\qquad b_\tau^{\beta\alpha}\left(\frac{|\boldsymbol{e}\cdot\boldsymbol{C}|}{|\boldsymbol{C}|},|\boldsymbol{C}|\right)=\frac{1}{\sqrt{\tau}}\,b^{\beta\alpha}\left(\frac{|\boldsymbol{e}\cdot\boldsymbol{C}|}{|\boldsymbol{C}|},\sqrt{\tau}\,|\boldsymbol{C}|\right),$$

and K is the local Knudsen number defined by

$$\mathrm{K}(s,x_1,a_*)=\frac{\mathrm{K}_*}{a_*\,\hat{n}_{(0)}(s,x_1)}=\frac{\mathrm{K}_*\hat{T}_{\mathrm{w}}(x_1)}{a_*\,\hat{p}_{(0)}(s,x_1)}.$$

It should be noted that s and x_1 occur as parameters through $\chi_{(0)}^{\mathrm{A}}$, $\hat{T}_{\mathrm{w}}$, and K in the above problems. Further, the solution ϕ_{e}^a of the problem (65) is independent of both y and c_i, which can be proved by the use of the *non-positivity* of the linearized collision operator (see [**77**] and Appendix A.12 in [**2**]). On the other hand, ϕ_{P}^a, ϕ_{T}^a and ϕ_χ^a are, respectively, the solutions for the three elemental flow problems: the flow caused by the pressure gradient (Poiseuille flow), the flow by the temperature gradient (thermal transpiration) and the flow by the concentration gradient.

In summary, $\hat{f}_{(1)}^a$ can be expressed, in terms of the solutions of elemental problems ϕ_{e}^a, ϕ_{P}^a, ϕ_{T}^a and ϕ_χ^a, as

$$\begin{aligned}\hat{f}_{(1)}^a=\hat{n}_{(0)}M\left(\boldsymbol{\zeta};\frac{\hat{m}^a}{\hat{T}_{\mathrm{w}}}\right)\Big(&\phi_{\mathrm{e}}^a(\mathrm{K},\chi_{(0)}^{\mathrm{A}},\hat{T}_{\mathrm{w}})+a_*\phi_{\mathrm{P}}^a(y,\boldsymbol{c};\mathrm{K},\chi_{(0)}^{\mathrm{A}},\hat{T}_{\mathrm{w}})\partial_{x_1}\ln\hat{p}_{(0)}\\&+a_*\,\phi_{\mathrm{T}}^a(y,\boldsymbol{c};\mathrm{K},\chi_{(0)}^{\mathrm{A}},\hat{T}_{\mathrm{w}})\partial_{x_1}\ln\hat{T}_{\mathrm{w}}+a_*\,\phi_\chi^a(y,\boldsymbol{c};\mathrm{K},\chi_{(0)}^{\mathrm{A}},\hat{T}_{\mathrm{w}})\partial_{x_1}\chi_{(0)}^{\mathrm{A}}\Big),\end{aligned}\tag{68}$$

and the corresponding coefficient functions of the macroscopic quantities at the first order of ε are obtained as follows:

$$\hat{n}_{(1)}^a=\hat{n}_{(0)}\int\phi_{\mathrm{e}}^aM(\boldsymbol{c};\hat{m}^a)\mathrm{d}^3c=\hat{n}_{(0)}\phi_{\mathrm{e}}^a,\tag{69}$$

$$\hat{n}_{(0)}^a\hat{v}_{1(1)}^a=a_*\,\hat{n}_{(0)}\sqrt{\hat{T}_{\mathrm{w}}}(u_{\mathrm{P}}^a\partial_{x_1}\ln\hat{p}_{(0)}+u_{\mathrm{T}}^a\partial_{x_1}\ln\hat{T}_{\mathrm{w}}+u_\chi^a\partial_{x_1}\chi_{(0)}^{\mathrm{A}}),\tag{70}$$

$$u_J^a=\int c_1\phi_J^a(\boldsymbol{c})M(\boldsymbol{c};\hat{m}^a)\mathrm{d}^3c\qquad(J=\mathrm{P},\mathrm{T},\chi),\tag{71}$$

$$\hat{v}_{2(1)}^a=\hat{v}_{3(1)}^a=\hat{T}_{(1)}^a=0.\tag{72}$$

The second order and the conservation law of the number of particles: we can proceed in the same way as the previous orders. However, our purpose is to derive

the equation describing the behavior of the gas at the leading order, say the quantities $n^a_{(0)}$ which are left undetermined at the previous stages. Then, it is enough to consider the conservation law of the number of particles in the system (62). The specific procedure is the following.

We first integrate Eq. (62a) with respect to $\boldsymbol{\zeta}$ in its whole space and with respect to x_2 from $-a_*/2$ to $a_*/2$ to have

$$a_*\,\partial_s \hat{n}^a_{(0)} + \partial_{x_1} \int_{-\frac{a_*}{2}}^{\frac{a_*}{2}} \hat{n}^a_{(0)} \hat{v}^a_{1(1)} \mathrm{d}x_2 + \Big[\int \zeta_2 \hat{f}^a_{(2)} \mathrm{d}^3\zeta \Big]_{x_2=-\frac{a_*}{2}}^{x_2=\frac{a_*}{2}} = 0.$$

The last term on the left-hand side vanishes because of the boundary condition (62b). Consequently, substituting Eq. (70) into the second term and using the relation between y and x_2, we obtain

$$\partial_s \hat{n}^a_{(0)} + \partial_{x_1} \mathcal{J}^a = 0, \tag{73a}$$

$$\mathcal{J}^a = a_* \left(\mathcal{M}^a_{\mathrm{P}} \partial_{x_1} \ln \hat{p}_{(0)} + \mathcal{M}^a_{\mathrm{T}} \partial_{x_1} \ln \hat{T}_{\mathrm{w}} + \mathcal{M}^a_{\chi} \partial_{x_1} \chi^{\mathrm{A}}_{(0)} \right) \frac{\hat{p}_{(0)}}{\sqrt{\hat{T}_{\mathrm{w}}}}, \tag{73b}$$

where

$$\mathcal{M}^a_J(\mathrm{K}, \chi^{\mathrm{A}}_{(0)}, \hat{T}_{\mathrm{w}}) = \int_{-\frac{1}{2}}^{\frac{1}{2}} u^a_J \mathrm{d}y \qquad (J = \mathrm{P}, \mathrm{T}, \chi). \tag{73c}$$

The physical meaning of $\mathcal{J}^a$ is the particle flux N^a_f of species a through the channel nondimensionalized by the factor of $n_* D\,\varepsilon (2kT_*/m^{\mathrm{A}})^{1/2}$. Since $\hat{p}_{(0)} = \hat{n}_{(0)} \hat{T}_{\mathrm{w}}$ and $\chi^{\mathrm{A}}_{(0)} \equiv \hat{n}^{\mathrm{A}}_{(0)}/\hat{n}_{(0)} = \hat{n}^{\mathrm{A}}_{(0)}/(\hat{n}^{\mathrm{A}}_{(0)} + \hat{n}^{\mathrm{B}}_{(0)})$, Eq. (73) is a closed set of equations for $\hat{n}^{\mathrm{A}}_{(0)}$ and $\hat{n}^{\mathrm{B}}_{(0)}$.

6.2 - *The second step: connection problem*

Now we consider a binary gas mixture in the channel composed of two elemental channels, say element I and element II, of different uniform widths connected at $X_1 = 0$ with sharing the center line (Fig. 18). The width D_{I} of element I is smaller than that of element II, D_{II}. The temperature T_{w} of the channel walls is kept constant in time and depends only on X_1, i.e., $T_{\mathrm{w}}(X_1)$. At the junction ($X_1 = 0$), the temperature T_{w} is continuous, but its gradient may be discontinuous in general. We assume that in each element the behavior of the gas mixture can be described by the Boltzmann equation and the velocity distribution function is continuous at the junction. We also assume the diffuse reflection boundary condition on the walls.

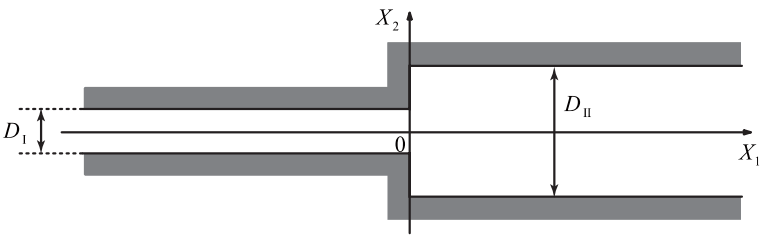

Fig. 18. Connection of two channels with different width.

By the use of the same reference quantities as in Sec. 6.1, we have the dimensionless description of the problem in the following form: for $x_1 \lessgtr 0$

$$\varepsilon^2 \partial_s F^a + \varepsilon \zeta_1 \partial_{x_1} F^a + \zeta_2 \partial_{x_2} F^a = \frac{1}{\mathrm{K}_*} \sum_{\beta=\mathrm{A,B}} K^{\beta a} \hat{J}^{\beta a}(F^\beta, F^a), \tag{74a}$$

$$F^a = \sigma_{2\pm}(F^a(\boldsymbol{\zeta}); \frac{\hat{m}^a}{\hat{T}_{\rm w}}) M(\boldsymbol{\zeta}; \frac{\hat{m}^a}{\hat{T}_{\rm w}}), \quad \zeta_2 \lessgtr 0, \ x_2 = \pm \frac{a_J}{2}, \tag{74b}$$

and at the junction ($x_1 = 0$)

$$F^a = \sigma_{1-}\left(F^a(\boldsymbol{\zeta}); \frac{\hat{m}^a}{\hat{T}_{\rm w}}\right) M\left(\boldsymbol{\zeta}; \frac{\hat{m}^a}{\hat{T}_{\rm w}}\right), \quad \zeta_1 > 0, \ \frac{a_{\rm I}}{2} < |x_2| < \frac{a_{\rm II}}{2}, \tag{75a}$$

$$F^a(s, x_1 = 0_-, x_2, \boldsymbol{\zeta}) = F^a(s, x_1 = 0_+, x_2, \boldsymbol{\zeta}), \quad |x_2| < \frac{a_{\rm I}}{2}, \tag{75b}$$

where $J = \mathrm{I}$ for $x_1 < 0$ and $J = \mathrm{II}$ for $x_1 > 0$ in Eq. (74b) and

$$a_{\rm I} = D_{\rm I}/D_*, \quad a_{\rm II} = D_{\rm II}/D_*.$$

Here, we denote the dimensionless distribution function by F^a in order to avoid the confusion with the solution $\hat{f}^a$ of the problem in Sec. 6.1.

As is readily seen, $\hat{f}^a_{(0)}$ solves the problem (74) and (75) with ε being zero if

$$\hat{n}^a_{(0)}(s, x_1 = 0_-) = \hat{n}^a_{(0)}(s, x_1 = 0_+). \tag{76}$$

That is, as far as the order of ε^0 is concerned, one can construct the solution of the present problem by the solution of the problem in Sec. 6.1 with the continuity condition (76). However, if one proceeds further, the same is not true any more; for instance, $\hat{f}^a_{(1)}$ does not satisfy the diffuse reflection condition at the junction [see Eq. (75a)]. We have to introduce the correction g^a to $\hat{f}^a$ and represent the solution F^a in the form

$$F^a = \hat{f}^a + g^a. \tag{77}$$

Here the correction function g^a is supposed to change rapidly in x_1, i.e., $\partial_{x_1} g^a = O(g^a)/\varepsilon$, and to be appreciable only in the vicinity of the junction. As in

Sec. 6.1.3, we expand g^a in a power series of ε. Since $\hat{f}^a_{(0)}$ solves the problem at the zero-th order, this expansion starts from the first order:

$$g^a = g^a_{(1)}\varepsilon + g^a_{(2)}\varepsilon^2 + \cdots.$$

Substituting Eq. (77) with the expansions of $\hat{f}^a$ and g^a into Eqs. (74) and (75) and equating like powers of ε lead to a series of boundary-value problems for $g^a_{(1)}, g^a_{(2)}, \cdots$. With the stretched coordinate z defined by $z = x_1/\varepsilon$, the boundary-value problem for $g^a_{(1)}$ can be described as follows: for $z \lessgtr 0$

$$\zeta_1 \partial_z g^a_{(1)} + \zeta_2 \partial_{x_2} g^a_{(1)} = \frac{1}{\mathrm{K}_*} \sum_{\beta=\mathrm{A,B}} K^{\beta a}[\hat{J}^{\beta a}(\hat{f}^\beta_{(0)\pm}, g^a_{(1)}) + \hat{J}^{\beta a}(g^\beta_{(1)}, \hat{f}^a_{(0)\pm})], \tag{78a}$$

$$g^a_{(1)} = \sigma_{2\pm}\left(g^a_{(1)}(\boldsymbol{\zeta}); \frac{\hat{m}^a}{\hat{T}_\mathrm{w}}\right) M\left(\boldsymbol{\zeta}; \frac{\hat{m}^a}{\hat{T}_\mathrm{w}}\right), \qquad \zeta_2 \lessgtr 0,\ x_2 = \pm\frac{a_J}{2}, \tag{78b}$$

at the junction ($z = 0$)

$$g^a_{(1)} = \sigma_{1-}(g^a_{(1)}(\boldsymbol{\zeta}) + \hat{f}^a_{(1)+}(\boldsymbol{\zeta}); \frac{\hat{m}^a}{\hat{T}_\mathrm{w}}) M(\boldsymbol{\zeta}; \frac{\hat{m}^a}{\hat{T}_\mathrm{w}}) - \hat{f}^a_{(1)+}, \quad \zeta_1 > 0,\ \frac{a_\mathrm{I}}{2} < |x_2| < \frac{a_\mathrm{II}}{2}, \tag{79a}$$

$$g^a_{(1)}(s, z = 0_-, x_2, \boldsymbol{\zeta}) + \hat{f}^a_{(1)-} = g^a_{(1)}(s, z = 0_+, x_2, \boldsymbol{\zeta}) + \hat{f}^a_{(1)+}, \quad |x_2| < \frac{a_\mathrm{I}}{2}, \tag{79b}$$

and at a far distance from the junction ($|z| \to \infty$)

$$g^a_{(1)} \to 0, \tag{80}$$

where $J = \mathrm{I}$ for $z < 0$ and $J = \mathrm{II}$ for $z > 0$ in Eq. (78b) and $\hat{f}^a_{(0)\pm}$ and $\hat{f}^a_{(1)\pm}$ represent their values at $x_1 = 0_\pm$. In Eq. (78a), $\hat{f}^a_{(0)+}$ is for $z > 0$ and $\hat{f}^a_{(0)-}$ for $z < 0$. It should be noted that in Eq. (78b), as well as in Eq. (79a), $\hat{T}_\mathrm{w}$ denotes the dimensionless temperature at the junction ($x_1 = 0$).

Now, we consider the necessary condition for the solution to exist. The condition is no other than the conservation law of the number of particles; it provides, together with the continuity condition (76), the connection condition at the junction for the set of fluid-dynamic equations (73). The specific procedure is the following.

We first integrate Eq. (78) with respect to $\boldsymbol{\zeta}$ in its whole space and with respect to x_2 from $-a_\mathrm{I}/2$ to $a_\mathrm{I}/2$ for $z < 0$ and from $-a_\mathrm{II}/2$ to $a_\mathrm{II}/2$ for $z > 0$ to have

$$\partial_z \int_{-a_\mathrm{I}/2}^{a_\mathrm{I}/2} \int \zeta_1 g^a_{(1)} \mathrm{d}^3\zeta \mathrm{d}x_2 = 0, \quad z < 0,$$

$$\partial_z \int_{-a_\mathrm{II}/2}^{a_\mathrm{II}/2} \int \zeta_1 g^a_{(1)} \mathrm{d}^3\zeta \mathrm{d}x_2 = 0, \quad z > 0,$$

where the property of the collision terms and the diffuse reflection condition (78b) have been taken into account. The resulting equations, with the aid of the condition (80), lead to

$$\int_{-a_{\rm I}/2}^{a_{\rm I}/2}\int \zeta_1 g^a_{(1)}(s, z=0_-, x_2, \boldsymbol{\zeta}) {\rm d}^3\zeta {\rm d}x_2 = 0, \tag{81a}$$

$$\int_{-a_{\rm II}/2}^{a_{\rm II}/2}\int \zeta_1 g^a_{(1)}(s, z=0_+, x_2, \boldsymbol{\zeta}) {\rm d}^3\zeta {\rm d}x_2 = 0. \tag{81b}$$

In the meantime, from condition (79), $g^a_{(1)}$ must satisfy

$$\int_{a_{\rm I}/2 < |x_2| < a_{\rm II}/2}\int \zeta_1 [g^a_{(1)}(s, z=0_+, x_2, \boldsymbol{\zeta}) + \hat{f}^a_{(1)+}] {\rm d}^3\zeta {\rm d}x_2 = 0, \tag{82}$$

and

$$\int_{-a_{\rm I}/2}^{a_{\rm I}/2}\int \zeta_1 [g^a_{(1)}(s, z=0_-, x_2, \boldsymbol{\zeta}) + \hat{f}^a_{(1)-}] {\rm d}^3\zeta {\rm d}x_2 = \int_{-a_{\rm I}/2}^{a_{\rm I}/2}\int \zeta_1 [g^a_{(1)}(s, z=0_+, x_2, \boldsymbol{\zeta}) + \hat{f}^a_{(1)+}] {\rm d}^3\zeta {\rm d}x_2. \tag{83}$$

Combining the conditions (81)–(83) all together, we have

$$\int_{-a_{\rm I}/2}^{a_{\rm I}/2}\int \zeta_1 \hat{f}^a_{(1)-} {\rm d}^3\zeta {\rm d}x_2 = \int_{-a_{\rm II}/2}^{a_{\rm II}/2}\int \zeta_1 \hat{f}^a_{(1)+} {\rm d}^3\zeta {\rm d}x_2,$$

which is finally reduced to

$$a_{\rm I}\mathcal{J}^a(s, x_1=0_-) = a_{\rm II}\mathcal{J}^a(s, x_1=0_+). \tag{84}$$

In summary, the set of Eqs. (76) and (84) is the connection condition at the junction for the fluid-dynamic set of equations (73).

6.3 - *Fluid dynamic system for the Knudsen compressor*

In deriving the connection condition in Sec. 6.2, the two channels are assumed to share the center line. However, this restriction can be readily removed, resulting in no influence on the condition. It is due to the facts that $\hat{n}^a_{(0)}$ and $\mathcal{J}^a$ do not depend

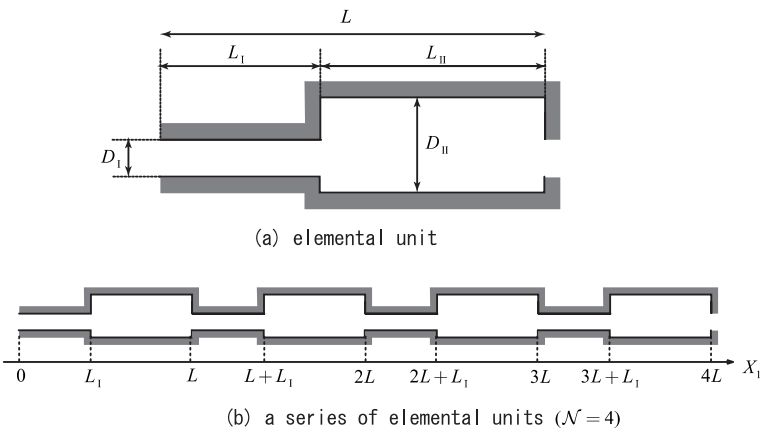

Fig. 19. Schematic of the Knudsen compressor.

on x_2. Here, we summarize the fluid-dynamic system for the Knudsen compressor with the configuration in Fig. 19. The reader is referred to [**70**] for the system of more general configuration shown in Fig. 15(a).

Considered is the Knudsen compressor composed of $\mathcal{N}$ elemental units of length L arranged in the X_1-direction as depicted in Fig. 19. The elemental unit is composed of two subunits, subunit I of length $L_{\rm I}$ and width $D_{\rm I}$ and subunit II of length $L_{\rm II}$ and width $D_{\rm II}$, where $L = L_{\rm I} + L_{\rm II}$ and $D_{\rm I} \le D_{\rm II}$. They do not necessarily share the center line. The temperature $T_{\rm w}$ of the wall is constant in time and depends only on X_1. The temperature $T_{\rm w}(X_1)$ varies smoothly in each subunit, is continuous at junctions and is periodic with period L, i.e., $T_{\rm w}(X_1) = T_{\rm w}(X_1 + L)$ $[0 \le X_1 \le (\mathcal{N}-1)L]$.

If individual elemental channels are long enough, i.e., $D_{\rm I}/L_{\rm I} \ll 1$ and $D_{\rm II}/L_{\rm II} \ll 1$, the behavior of the mixture in the Knudsen compressor can be described by the set of fluid-dynamic equations (73) for the individual elemental channels with the connection conditions (76) and (84). The whole system is the following:

In the subunit I: for $j < x_1 < j + (L_{\rm I}/L)$ $(j = 0, 1, \ldots, \mathcal{N}-1)$

$$\partial_s \hat{n}_{\rm I}^a + \partial_{x_1} \mathcal{J}_{\rm I}^a = 0, \tag{85a}$$

$$\begin{aligned} \mathcal{J}_{\rm I}^a = a_{\rm I} \Big(& \mathcal{M}_{\rm P}^a(\mathrm{K}_{\rm I}, \chi_{\rm I}^{\rm A}, \hat{T}_{\rm w}) \partial_{x_1} \ln \hat{p}_{\rm I} \\ & + \mathcal{M}_{\rm T}^a(\mathrm{K}_{\rm I}, \chi_{\rm I}^{\rm A}, \hat{T}_{\rm w}) \partial_{x_1} \ln \hat{T}_{\rm w} + \mathcal{M}_{\chi}^a(\mathrm{K}_{\rm I}, \chi_{\rm I}^{\rm A}, \hat{T}_{\rm w}) \partial_{x_1} \chi_{\rm I}^{\rm A} \Big) \hat{n}_{\rm I} \sqrt{\hat{T}_{\rm w}} \,, \end{aligned} \tag{85b}$$

In the subunit II: for $j+(L_{\rm I}/L)<x_1<j+1$ $(j=0,1,\dots,\mathcal{N}-1)$

$$\partial_s \hat{n}^a_{\rm II}+\partial_{x_1}\mathcal{J}^a_{\rm II}=0, \tag{86a}$$

$$\begin{aligned}\mathcal{J}^a_{\rm II}=a_{\rm II}\Big(&\mathcal{M}^a_{\rm P}({\rm K}_{\rm II},\chi^{\rm A}_{\rm II},\hat{T}_{\rm w})\partial_{x_1}\ln\hat{p}_{\rm II}\\&+\mathcal{M}^a_{\rm T}({\rm K}_{\rm II},\chi^{\rm A}_{\rm II},\hat{T}_{\rm w})\partial_{x_1}\ln\hat{T}_{\rm w}+\mathcal{M}^a_{\chi}({\rm K}_{\rm II},\chi^{\rm A}_{\rm II},\hat{T}_{\rm w})\partial_{x_1}\chi^{\rm A}_{\rm II}\Big)\hat{n}_{\rm II}\sqrt{\hat{T}_{\rm w}}\,,\end{aligned} \tag{86b}$$

At junctions: at $x_1=(L_{\rm I}/L),\ j,\ (L_{\rm I}/L)+j$ $(j=1,\dots,\mathcal{N}-1)$

$$\hat{n}^a_{\rm I}=\hat{n}^a_{\rm II},\quad a_{\rm I}\mathcal{J}^a_{\rm I}=a_{\rm II}\mathcal{J}^a_{\rm II}. \tag{87}$$

Here $\hat{n}^a_{\rm I}$, $\chi^{\rm A}_{\rm I}$, $\hat{p}_{\rm I}$, and $\hat{n}_{\rm I}$ denote $\hat{n}^a_{(0)}$, $\chi^{\rm A}_{(0)}(=\hat{n}^{\rm A}_{(0)}/\hat{n}_{(0)})$, $\hat{p}_{(0)}(=\hat{n}_{(0)}\hat{T}_{\rm w})$, and $\hat{n}_{(0)}(=\hat{n}^{\rm A}_{(0)}+\hat{n}^{\rm B}_{(0)})$ in subunit I, and the counterparts with subscript II those in subunit II. ${\rm K}_{\rm I}$ and ${\rm K}_{\rm II}$ are the local Knudsen numbers in the subunits I and II defined by

$${\rm K}_{\rm I}=\frac{\hat{T}_{\rm w}}{a_{\rm I}\hat{p}_{\rm I}}{\rm K}_*,\quad {\rm K}_{\rm II}=\frac{\hat{T}_{\rm w}}{a_{\rm II}\hat{p}_{\rm II}}{\rm K}_*.$$

$\mathcal{J}^a_{\rm I}$ denotes the dimensionless particle flux of species a through the subunit I nondimensionalized by $n_*D_{\rm I}\,\varepsilon\,(2kT_*/m^{\rm A})^{1/2}$; $\mathcal{J}^a$ the counterparts through the subunit II nondimensionalized by $n_*D_{\rm II}\,\varepsilon\,(2kT_*/m^{\rm A})^{1/2}$.

With initial conditions for $\hat{n}^a_{\rm I}$ and $\hat{n}^a_{\rm II}$ and with proper boundary conditions at the both ends of the compressor (at $x_1=0$ and $\mathcal{N}$), we can pursue the time evolution of the behavior of the mixture by the use of (85)–(87). The simplest reasonable conditions at the extreme ends of the compressor would be the following:

1. Open end (or the end connected to a reservoir huge enough): the molecular number densities of respective species are given.
2. Closed end: there are no particle fluxes of respective species.

6.4 - *Summary and some other possibilities*

In summary, the problem is reduced to solving the system (85)–(87), i.e., the set of convection-diffusion equations and their connection conditions, supplemented by a macroscopic initial condition and boundary conditions at the extreme ends. However, in order to complete the system, we have to prepare the transport coefficients M^a_J $(J={\rm P},\ {\rm T},\ \chi)$ beforehand. It can be done numerically by solving the elementary flow problems (the flows caused by the gradient of pressure, temperature, and concentration in an infinitely long straight channel) for the linearized Boltzmann system (66). It is the issue of the next section. The reduction of the original kinetic problem to the elementary linear problems is the primary advantage of the present approach.

Essentially, there is no difficulty in solving the fluid-dynamic system (85)–(87) itself. The results in Figs. 14 and 15 are obtained by solving time-independent problems of that system (or the counterpart for more general configuration in the case of Fig. 15) with the closed end condition, where the references are chosen as $D_* = D_{\rm I}(= D)$ and $T_* = T_0$. The transport coefficients prepared on the basis of the McCormack model have been used there.

Incidentally, motivated by the periodic structure of the compressor (both in geometry and in temperature distribution), Aoki and Degond [**74**] proposed a further simplified fluid-dynamic system by the use of the homogenization method, which describes the change of the gas state in much larger scale than the unit length L (the change in the scale of L is treated as the rapid variation in the homogenization procedure). For the specific procedure in the case of the full Boltzmann equation (not the simplified BGK model in [**74**]), the reader is referred to [**75**]. Recently, Charrier and Dubroca [**76**] derived a fluid-dynamic system describing gas flows in porous media by the use of homogenization method directly from the kinetic description (without passing through the intermediate fluid description as in [**74, 75**]). Corresponding approach to the Knudsen compressors may be considered.

7 - Numerical analysis of elementary flow problems with the view of preparing transport coefficients

In the course of analysis in Sec. 6.1.3, there occurred three elementary flow problems (66), i.e., the problems of the pressure-driven, temperature-driven, and concentration-driven flows in a straight channel. The solutions of the problems are included as the transport coefficients $\mathcal{M}_J^a$ ($J = \mathrm{P}, \mathrm{T}, \chi$; $a = \mathrm{A}, \mathrm{B}$) in the final fluid-dynamic system (85)–(87) summarized in Sec. 6.3. The physical meaning of those coefficients is the (dimensionless) particle flux of species a in the respective problems. In order to make use of the fluid-dynamic system (85)–(87), one has to prepare a numerical table of the fluxes beforehand by solving the problems (66) for various values of the Knudsen number, concentration, and temperature [K, $\chi_{(0)}^{\rm A}$, and $\hat{T}_{\rm w}$ in (66a)]. Then, during the numerical solution process of the system (85)–(87), one draws the desired data from those tables typically by interpolation, since the Knudsen number and concentration are the local quantities varying with position and time in the system. The tables are desired to cover the entire range of the Knudsen number ($0 < \mathrm{K} < \infty$) and concentration ($0 \le \chi_{(0)}^{\rm A} \le 1$) and a wide range of the temperature $\hat{T}_{\rm w}$. We shall call those tables that meet these requirement the *complete* flux tables or the flux database. In the present section, we shall introduce the works on three elementally flow problems performed in our group, in view of the preparation of the complete flux tables.

7.1 - *Solutions of the linearized Boltzmann equation*

7.1.1 - The state of the art

Nowadays, the solutions of the problems (66) on the basis of the linearized Boltzmann equation are available [**78**] for a wide range of the Knudsen number. The first numerical solution of the linearized Boltzmann equation for hard-sphere gases was reported by Sone, Ohwada, and Aoki [**79**] in the study of the temperature-jump problem. The method developed in this reference, which they call the *numerical kernel method*, has been applied to many fundamental flow problems for single-species rarefied gases [**81, 82, 83, 84, 17, 85, 53, 55, 86, 87,** 88], including the Poiseuille flow and thermal transpiration [**80**]. The extension of the method to the case of gas mixtures was initiated in [**89**] and later applied to various Knudsen-layer problems for mixtures [**90, 91, 92, 93**]. The work reported in [**78**] has been done as the continuation of the project in Kyoto aiming at providing standard solutions of the Boltzmann equation for fundamental rarefied gas flows. We shall give below a brief outline of the analysis.

With the aid of the spherical symmetry of the collision integral, we first see the solution ϕ_J^a of the problem (66) to be sought in the form:

$$\phi_J^a(y, \boldsymbol{c}) = (c_1/c_\rho)\psi_J^a(y, c_2, c_\rho), \qquad c_\rho = (c_1^2 + c_3^2)^{1/2},$$

and ψ_J^a is the solution of a boundary-value problem, which is symbolically written as

$$c_2\partial_y \begin{bmatrix} \psi_J^{\mathrm{A}} \\ \psi_J^{\mathrm{B}} \end{bmatrix} = \frac{1}{\mathrm{K}} \begin{bmatrix} -\nu^{\mathrm{A}} + C^{AA} & C^{BA} \\ C^{AB} & -\nu^{\mathrm{B}} + C^{BB} \end{bmatrix} \begin{bmatrix} \psi_J^{\mathrm{A}} \\ \psi_J^{\mathrm{B}} \end{bmatrix} - \begin{bmatrix} \mathcal{I}_J^{\mathrm{A}} \\ \mathcal{I}_J^{\mathrm{B}} \end{bmatrix}, \tag{88a}$$

$$\psi_J^a = 0, \quad \text{for } c_2 \lessgtr 0, \ y = \pm\frac{1}{2}, \tag{88b}$$

with

$$\mathcal{I}_{\mathrm{P}}^a = c_\rho\chi_{(0)}^a, \quad \mathcal{I}_{\mathrm{T}}^a = c_\rho\chi_{(0)}^a\left(\hat{m}^a|\boldsymbol{c}|^2 - \frac{5}{2}\right), \quad \mathcal{I}_\chi^{\mathrm{A}} = c_\rho, \quad \mathcal{I}_\chi^{\mathrm{B}} = -c_\rho, \tag{88c}$$

where ν^a are functions of $|\boldsymbol{c}|\left(= \sqrt{c_2^2 + c_\rho^2}\right)$ depending on $\hat{T}_{\mathrm{w}}$ and $\chi_{(0)}^{\mathrm{A}}$, while $C^{\beta a}$ are those linear integral operators depending on $\hat{T}_{\mathrm{w}}$ and $\chi_{(0)}^{\mathrm{A}}$ that work on ψ_J^β:

$$C^{\beta a}\psi_J^\beta(y, c_2, c_\rho) = \int \mathcal{K}^{\beta a}(c_2, c_\rho; \hat{c}_2, \hat{c}_\rho)\psi_J^\beta(y, \hat{c}_2, \hat{c}_\rho)d\hat{c}_2 d\hat{c}_\rho. \tag{89}$$

In the actual computation, we truncate the infinite regions of c_2 and c_ρ ($-\infty < c_2 < \infty, 0 \le c_\rho < \infty$) at $\sqrt{\hat{m}^a}|c_2| = C_2$ and $\sqrt{\hat{m}^a}c_\rho = C_\rho$ with C_2 and C_ρ being

finite positive constants sufficiently large.[4] Then, we arrange grid points in the finite region of (y, c_2, c_ρ) and denote them by $(y^{(i)}, c_2^{(j)}, c_\rho^{(k)})$, where $i = -N_y, \ldots, N_y$, $j = -N_2, \ldots, N_2$, $k = 0, \ldots, N_\rho$ with N_y, N_2 and N_ρ being certain positive constants and with $y^{(0)} = 0$ and $c_2^{(0)} = 0$. The solution is obtained iteratively by the use of the following finite-difference scheme:

$$c_2^{(j)} \begin{bmatrix} \partial_y \psi^{\mathrm{A}} \\ \partial_y \psi^{\mathrm{B}} \end{bmatrix}_{ijk}^{(n)} = \frac{-1}{\mathrm{K}} \begin{bmatrix} \nu_{jk}^{\mathrm{A}} \psi_{ijk}^{\mathrm{A}(n)} \\ \nu_{jk}^{\mathrm{B}} \psi_{ijk}^{\mathrm{B}(n)} \end{bmatrix} + \frac{1}{\mathrm{K}} \begin{bmatrix} C^{AA}\psi^{\mathrm{A}} + C^{BA}\psi^{\mathrm{B}} \\ C^{AB}\psi^{\mathrm{A}} + C^{BB}\psi^{\mathrm{B}} \end{bmatrix}_{ijk}^{(n-1)} - \begin{bmatrix} \mathcal{I}^{\mathrm{A}} \\ \mathcal{I}^{\mathrm{B}} \end{bmatrix}_{jk}, \tag{90}$$

where we suppressed the subscript J for the simplicity of notation; $\psi_{ijk}^{a(n)}$ denotes the value of ψ^a at the n-th step of iteration at the grid point of $(y^{(i)}, c_2^{(j)}, c_\rho^{(k)})$; and h_{jk} with $h = \nu^a, \mathcal{I}^a$ denotes the value of h at the point $(c_2^{(j)}, c_\rho^{(k)})$. In the above scheme, the derivative terms $\partial_y \psi^a$ are approximated typically by second-order upwind scheme. The essential part of the *numerical kernel* method is the way of approximation of the second term on the right-hand side. The method is conceptually simple. We introduce a set of basis functions $B_{lm}^a(\hat{c}_2, \hat{c}_\rho)$ such that the sum

$$\sum_{l=-N_2}^{N_2} \sum_{m=0}^{N_\rho} B_{lm}^a(\hat{c}_2, \hat{c}_\rho) \psi^a(y, \hat{c}_2^{(l)}, \hat{c}_\rho^{(m)})$$

yields a quadratic interpolation of the discrete data $\{\psi^a(y, \hat{c}_2^{(l)}, \hat{c}_\rho^{(m)})\}$ in every two intervals of grid points with respect to both $\hat{c}_2$ and $\hat{c}_\rho$.[5] Hence, we regard the sum as the approximation of the function $\psi^a(y, \hat{c}_2, \hat{c}_\rho)$ and substitute it to (89) to have the expression of the second term on the right-hand side of (90):

$$\begin{bmatrix} C^{AA}\psi^{\mathrm{A}} + C^{BA}\psi^{\mathrm{B}} \\ C^{AB}\psi^{\mathrm{A}} + C^{BB}\psi^{\mathrm{B}} \end{bmatrix}_{ijk}^{(n-1)} = \sum_{l=-N_2}^{N_2} \sum_{m=0}^{N_\rho} \begin{bmatrix} C_{jklm}^{AA} & C_{jklm}^{BA} \\ C_{jklm}^{AB} & C_{jklm}^{BB} \end{bmatrix} \begin{bmatrix} \psi^{\mathrm{A}} \\ \psi^{\mathrm{B}} \end{bmatrix}_{ilm}^{(n-1)},$$

where

$$C_{jklm}^{\beta a} = \int \mathcal{K}^{\beta a}(c_2^{(j)}, c_\rho^{(k)}; \hat{c}_2, \hat{c}_\rho) B_{lm}^\beta(\hat{c}_2, \hat{c}_\rho) d\hat{c}_2 d\hat{c}_\rho.$$

Note that $C_{jklm}^{\beta a}$ is independent of ψ^a and can be computed beforehand. Once $C_{jklm}^{\beta a}$ is

---

[4] Typically C_2 and C_ρ are chosen to be $4.5 \sim 6$.

[5] As will be demonstrated later in Fig. 21, ψ^a is discontinuous at $c_2 = 0$ on the wall $\left(y = \pm \frac{1}{2}\right)$. The interpolation in terms of the basis functions is made properly by taking into account the discontinuity. Incidentally, the quadratic interpolation is not obligatory. One may consider basis functions that yield, for instance, a linear or cubic interpolation, if it is preferable.

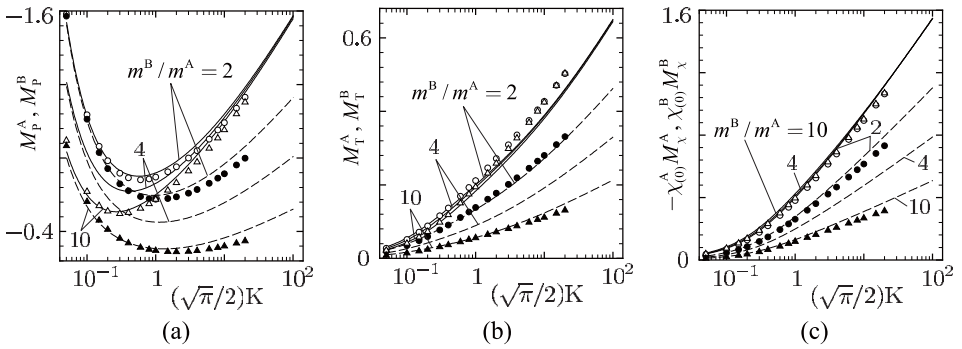

Fig. 20. Particle fluxes of respective species in a binary mixture of hard-sphere gases in the case of $m^{\rm B}/m^{\rm A}=2$, 4, and 10, $d^{\rm B}/d^{\rm A}=1$, and $\chi_{(0)}^{\rm A}=0.5$. Here, M_J^a ($J={\rm P},\ {\rm T},\ \chi$; $a={\rm A},\ {\rm B}$) is a function of K defined by $M_J^a=\mathcal{M}_J^a({\rm K},\chi_{(0)}^{\rm A}=0.5,\hat{T}_{\rm w}=1)$. The results for the linearized Boltzmann equation at eighteen points of K obtained in [**78**] are shown by circles ($m^{\rm B}/m^{\rm A}=2$) and triangles ($m^{\rm B}/m^{\rm A}=10$). The open symbols ○ and △ indicate the results for species A, while the closed symbols ● and ▲ those for species B. The solid and dashed lines respectively indicate the results of species A and B for the McCormack model Boltzmann equation for hard-sphere gases. In the case of hard sphere gases, $\mathcal{M}_J^a({\rm K},\chi_{(0)}^{\rm A},\hat{T}_{\rm w})$ is recovered by the formula $\mathcal{M}_J^a({\rm K},\chi_{(0)}^{\rm A},\hat{T}_{\rm w})=M_J^a\left({\rm K}\sqrt{\hat{T}_{\rm w}},\chi_{(0)}^{\rm A}\right)$.

prepared, we can compute the collision integral by a simple multiplication (and sum) of matrices in the iterative process, which can be performed efficiently particularly on vector computer systems.

The particle fluxes thus obtained are shown in Fig. 20 with open and closed symbols. Figure 21 shows the velocity distribution function $\psi_\chi^{\rm A}$ of the concentration-driven flow problem for three representative Knudsen numbers. The reader is referred to [**78, 94**] for more detailed descriptions and data.

7.1.2 - Prospect for the complete flux tables

By the method explained in Sec. 7.1.1, one can obtain the solutions for a wide range of the Knudsen number. There is, however, a practical upper and lower limits of the Knudsen number if the method is applied to in a straightforward way. The difficulty in the regime of small Knudsen number comes from the following facts:

(i) the slow convergence of the solution.

(ii) the velocity distribution function close to the local Maxwellian. Substitution of the nearly Maxwellian in the collision integrals results in the output of small data, which is magnified by the factor of $\rm K^{-1}$. This means that the small deviation from the Maxwellian should be well-captured in order to retain the accuracy of computation.

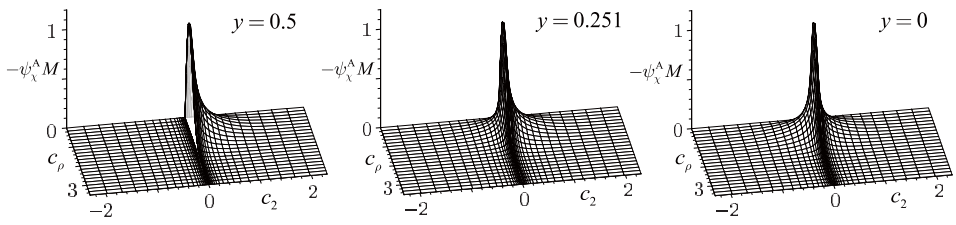

(a) K=10.53

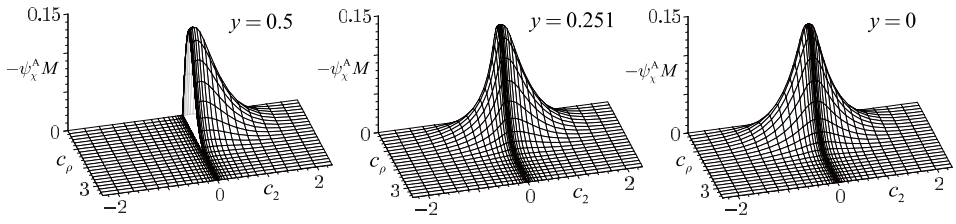

(b) K=1.053

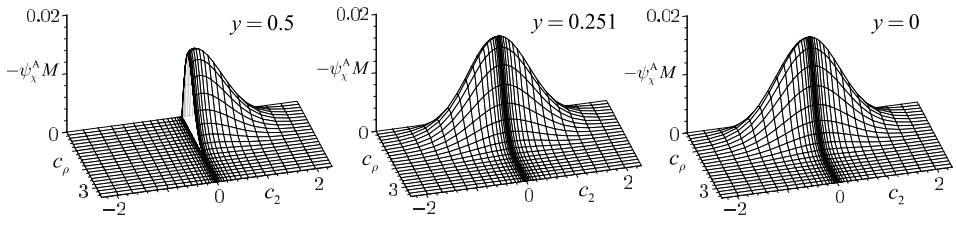

(c) K=0.1053

Fig. 21. Velocity distribution function $\psi_\chi^{\mathrm{A}} M(|\boldsymbol{c}|, 1)$ for the concentration-driven flow at three points in the gas in the case of $m^{\mathrm{B}}/m^{\mathrm{A}} = 2$, $d^{\mathrm{B}}/d^{\mathrm{A}} = 1$, $\chi_{(0)}^{\mathrm{A}} = 0.5$, and $\hat{T}_{\mathrm{w}} = 1$ (hard sphere gases). (a) $\mathrm{K} = 10.53$, (b) $\mathrm{K} = 1.053$, and (c) $\mathrm{K} = 0.1053$. The position in the y coordinate is shown at the top right corner in each figure. Note the discontinuity at $c_2 = 0$ on the wall $y = 0.5$.

These features are not peculiar to the present problems, but generally appear in solving the kinetic equation. On the other hand, the difficulty in the regime of large Knudsen number is rather specific to the present problems. As is seen from Fig. 21, the velocity distribution function ψ_χ^{A} becomes steep for large Knudsen numbers. This feature is common to the three problems irrespective of the component species (i.e., to ψ_J^a with $J = \mathrm{P}, \mathrm{T}, \chi$ and $a = \mathrm{A}, \mathrm{B}$), and is enhanced as the Knudsen number increases. For the preparation of flux tables that cover the regime of large Knudsen

number, special attention should be paid to the arrangement of grid points in numerical computations, since the Knudsen number can be indefinitely large.

The difficulty in the regime of small Knudsen number can be overcome by the use of the asymptotic theory established by Sone [**3, 1, 2**]. In the course of the analysis, one has to solve, numerically, the half-space problems of the linearized Boltzmann equation, but the solutions of the problems are now available [**89, 90, 91**]. On the other hand, up to this moment, the difficulty in the regime of large Knudsen number has not yet been well-handled. Recently, however, there was a progress on the flux estimate of the thermal transpiration for single-species hard-sphere gases by Chen, Chen, Liu, and Sone [**95**]. It had been known for the BGK model equation that the flux grows with the rate of ln K as $K \to \infty$ [**96, 97, 98**]. They proved the same growing rate of ln K for the linearized Boltzmann equation. Thanks to the constructive way of the analysis, the dominant term is explicitly given, so that it should be possible numerically to obtain accurate flux data for very large Knudsen numbers from that explicit term.

In summary, it would be realized in the near future, though still difficult (or too tough due to high computational costs) at present, to provide the flux tables that cover the entire range of the Knudsen number on the basis of the linearized Boltzmann equation.

7.2 - *Solutions of the model Boltzmann equation and flux-database construction*

At present, the complete flux tables on the basis of the linearized Boltzmann equation are not available. However, there are the counterparts on the basis of the model equations, which have been made use of in the studies of the Knudsen compressors.

The complete flux tables were first provided by Sone and Itakura [**99**] in the study of the Poiseuille flow and thermal transpiration for single-species gases, not only for the two-dimensional channel but also for the circular pipe, on the basis of the BGK equation and diffuse reflection boundary condition. The numerical simulation of the Knudsen compressor in [**75**] has been carried out by the use of their tables. The software package developed (from these tables) by Sone, Itakura, and Handa is available from our web-site.[6] Quite recently we also prepared the corresponding complete flux tables [**100**] on the basis of the ellipsoidal statistical model (ES-BGK model [**103, 104**]) equation. In the case of gas mixtures, the complete flux tables on the basis of the McCormack model equation [**101, 102**]

[6] http://www.users.kudpc.kyoto-u.ac.jp/~a51424/Sone/database-e.html

have been prepared in [**70, 94**] for the three elementary flows in two-dimensional channels.[7]

The model Boltzmann equations are those equations that have a simplified collision integral in place of that of the original Boltzmann equation. This feature gives rise to a lot of benefits in various aspects, which we shall explain in rather abstract way in Sec. 7.2.1. It should be noted, however, that it is not clear a priori whether or not the solution of the model equation is close to that of the original Boltzmann equation. The ability of individual model equations should always be assessed numerically. Our solutions of the Boltzmann equation have been serving as the standard for this purpose.

7.2.1 - Numerical advantages of the model equations

For the problems we are now concerned with, the linearized version of the model Boltzmann equations, such as the BGK, ES-BGK, and polynomial type models (see [**105**] and the references therein), is to be used under the diffuse reflection boundary condition.[8] For the sake of the specific description, we shall explain the advantages coming from the simplified collision integrals in the case of the McCormack model equation. For the BGK and ES-BGK type cases, the situation is much simpler and the reader would find the corresponding descriptions in the literature (e.g., Appendix A.6 of [**2**]).

The collision operator $L^{\beta\alpha}_{\hat{T}_{\rm w}}$ of the McCormack model equation reads

$$L^{\beta\alpha}_{\hat{T}_{\rm w}}(\chi^{\alpha}_{(0)}\phi^{\beta}, \chi^{\beta}_{(0)}\phi^{\alpha}) = M^{\beta\alpha} - C_{\beta\alpha}\phi^{\alpha}, \tag{91a}$$

with

$$\begin{aligned} M^{\beta\alpha} &= C_{\beta\alpha}\omega^{\alpha} \\ &\quad + 2\hat{m}^{\alpha}c_i\left[C_{\beta\alpha}\chi^{\alpha}_{(0)}u^{\alpha}_i + \chi^{\alpha}_{(0)}\chi^{\beta}_{(0)}(u^{\beta}_i - u^{\alpha}_i)\nu^{(1)}_{\beta\alpha} + \left(\frac{\chi^{\alpha}_{(0)}Q^{\beta}_i}{\hat{m}^{\beta}} - \frac{\chi^{\beta}_{(0)}Q^{\alpha}_i}{\hat{m}^{\alpha}}\right)\nu^{(2)}_{\beta\alpha}\right] \\ &\quad + \chi^{\alpha}_{(0)}\left(\hat{m}^{\alpha}|\boldsymbol{c}|^2 - \frac{3}{2}\right)\left(C_{\beta\alpha}\theta^{\alpha} + \frac{\hat{\mu}^{\beta\alpha}}{\hat{m}^{\beta}}(\theta^{\beta} - \theta^{\alpha})\chi^{\beta}_{(0)}\nu^{(1)}_{\beta\alpha}\right) \end{aligned} \tag{91b}$$

---

[7] Fortran subroutine program that promptly provides the flux data for arbitrary values of the Knudsen number and concentration (and for a wide range of temperature) is contained in the online version of [**94**] as an additional supplementary material.

[8] The McCormack model was originally proposed as a model of the linearized Boltzmann equation. Recently, however, Kosuge pointed out that it can be derived by linearization from his polynomial model [**105**] for gas mixtures.

$$+\hat{m}^a\left(c_ic_j-\frac{1}{3}|\boldsymbol{c}|^2\delta_{ij}\right)\left((C_{\beta a}-\chi^\beta_{(0)}\nu^{(3)}_{\beta a})P^a_{ij}+\chi^a_{(0)}\nu^{(4)}_{\beta a}P^\beta_{ij}\right)$$

$$+\frac{4}{5}\hat{m}^a c_i\left(\hat{m}^a|\boldsymbol{c}|^2-\frac{5}{2}\right)\left((C_{\beta a}-\chi^\beta_{(0)}\nu^{(5)}_{\beta a})Q^a_i+\chi^a_{(0)}\nu^{(6)}_{\beta a}Q^\beta_i+\frac{5}{2}\frac{\chi^a_{(0)}\chi^\beta_{(0)}}{\hat{m}^a}(u^\beta_i-u^a_i)\nu^{(2)}_{\beta a}\right),$$

where ω^a, u^a_i, θ^a, P^a_{ij}, and Q^a_i are the following moments of ϕ^a:[9]

$$\omega^a=\int\phi^a M(\boldsymbol{c};\hat{m}^a)d^3c,\qquad \chi^a_{(0)}u^a_i=\int c_i\phi^a M(\boldsymbol{c};\hat{m}^a)d^3c,$$

$$\chi^a_{(0)}\theta^a=\frac{2}{3}\int\left(\hat{m}^a|\boldsymbol{c}|^2-\frac{3}{2}\right)\phi^a M(\boldsymbol{c};\hat{m}^a)d^3c,$$

$$P^a_{ij}=2\hat{m}^a\int c_ic_j\phi^a M(\boldsymbol{c};\hat{m}^a)d^3c,$$

$$Q^a_i=\int c_i\left(\hat{m}^a|\boldsymbol{c}|^2-\frac{5}{2}\right)\phi^a M(\boldsymbol{c};\hat{m}^a)d^3c.$$

The $\nu^{(i)}_{\beta a}$ $(i=1,\dots,6)$ and $C_{\beta a}$ are constants with respect to $\boldsymbol{c}$, depending on $\hat{T}_{\rm w}$ and molecular model; their specific forms are omitted here for the sake of brevity (see, e.g., Appendix A.2 of [**70**]).

The collision integral (91) is *simple*, compared to the original one, in the sense that the dependence of $M^{\beta a}$ on the molecular velocity $\boldsymbol{c}$ is explicitly given, especially in terms of up to the third-order polynomials. This feature drastically reduces the computational cost of the collision integral. Actually, however, further drastic reductions can be made by additional simple arguments, which will be described below.

Chu's method

In spatially one dimensional problems,[10] two components of the molecular velocity can be eliminated from the McCormack model equation. It is due to the facts that $M^{\beta a}$ is a given function of $\boldsymbol{c}$ depending on the low-order moments of ϕ's and that $C_{\beta a}$ in front of ϕ^a in (91a) is independent of $\boldsymbol{c}$. Such a reduction was first introduced by Chu [**46**] in the case of the BGK model equation in the study of the formation of shock wave. The way of reduction is simple: the mere integration of

[9] The moments ω^a, u^a_i, θ^a, P^a_{ij}, and Q^a_i are, respectively, the perturbation parts of the molecular number density, flow velocity, *temperature*, *stress tensor*, and *heat-flow* vector of species a.

[10] A similar reduction can be made for two dimensional problems.

(66a) multiplied by

$$\begin{pmatrix} 1 \\ c_1 \\ c_3 \\ \hat{m}^a c_1^2 \\ \hat{m}^a c_3^2 \\ \hat{m}^a c_1 c_3 \\ \hat{m}^a c_1 (c_1^2 + c_3^2) \\ \hat{m}^a c_3 (c_1^2 + c_3^2) \end{pmatrix} \mathcal{E}^a(c_1) \mathcal{E}^a(c_3),$$

with respect to c_1 and c_3 yields simultaneous integro-differential equations for the marginal velocity distribution function $\boldsymbol{\Phi}^a(y, c_2)$ defined by

$$\boldsymbol{\Phi}^a(y, c_2) = \begin{pmatrix} \Phi_1^a \\ \Phi_2^a \\ \Phi_3^a \\ \Phi_4^a \\ \Phi_5^a \\ \Phi_6^a \\ \Phi_7^a \\ \Phi_8^a \end{pmatrix} = \int_{-\infty}^{\infty} \int_{-\infty}^{\infty} \begin{pmatrix} 1 \\ c_1 \\ c_3 \\ \hat{m}^a c_1^2 \\ \hat{m}^a c_3^2 \\ \hat{m}^a c_1 c_3 \\ \hat{m}^a c_1 (c_1^2 + c_3^2) \\ \hat{m}^a c_3 (c_1^2 + c_3^2) \end{pmatrix} \phi^a \mathcal{E}^a(c_1) \mathcal{E}^a(c_3) dc_1 dc_3,$$

where $\mathcal{E}^a(c) = (\hat{m}^a/\pi)^{1/2} \exp(-\hat{m}^a c^2)$. It is readily understood, though complicated at a glance, by observing that all the moments ω^a, u_i^a, θ^a, P_{ij}^a, and Q_i^a occurring in the collision integrals can be expressed by the moments of $\boldsymbol{\Phi}^a$:

$$\omega^a = \int_{-\infty}^{\infty} \Phi_1^a \mathcal{E}^a(c_2) dc_2, \qquad \chi_{(0)}^a u_2^a = \int_{-\infty}^{\infty} c_2 \Phi_1^a \mathcal{E}^a(c_2) dc_2,$$

$$\chi_{(0)}^a u_1^a = \int_{-\infty}^{\infty} \Phi_2^a \mathcal{E}^a(c_2) dc_2, \qquad \chi_{(0)}^a u_3^a = \int_{-\infty}^{\infty} \Phi_3^a \mathcal{E}^a(c_2) dc_2,$$

$$\chi_{(0)}^a \theta^a = \frac{2}{3} \int \left(\hat{m}^a c_2^2 - \frac{3}{2} \right) \Phi_1^a \mathcal{E}^a(c_2) dc_2 + \frac{2}{3} \int (\Phi_4^a + \Phi_5^a) \mathcal{E}^a(c_2) dc_2,$$

$$P_{11}^a = 2 \int \Phi_4^a \mathcal{E}^a(c_2) dc_2,$$

$$P^a_{12} = 2\hat{m}^a \int c_2 \Phi^a_2 \mathcal{E}^a(c_2) dc_2,$$

$$P^a_{13} = 2 \int \Phi^a_6 \mathcal{E}^a(c_2) dc_2,$$

$$P^a_{22} = 2\hat{m}^a \int c_2^2 \Phi^a_1 \mathcal{E}^a(c_2) dc_2,$$

$$P^a_{23} = 2\hat{m}^a \int c_2 \Phi^a_3 \mathcal{E}^a(c_2) dc_2,$$

$$P^a_{33} = 2 \int \Phi^a_5 \mathcal{E}^a(c_2) dc_2,$$

$$Q^a_1 = \int \Big(\hat{m}^a c_2^2 - \frac{5}{2}\Big) \Phi^a_2 \mathcal{E}^a(c_2) dc_2 + \int \Phi^a_7 \mathcal{E}^a(c_2) dc_2,$$

$$Q^a_2 = \int c_2 \Big(\hat{m}^a c_2^2 - \frac{5}{2}\Big) \Phi^a_1 \mathcal{E}^a(c_2) dc_2 + \int c_2 (\Phi^a_4 + \Phi^a_5) \mathcal{E}^a(c_2) dc_2,$$

$$Q^a_3 = \int \Big(\hat{m}^a c_2^2 - \frac{5}{2}\Big) \Phi^a_3 \mathcal{E}^a(c_2) dc_2 + \int \Phi^a_8 \mathcal{E}^a(c_2) dc_2.$$

By the same procedure, we can formally, in general, transform the boundary condition for ϕ^a into that for $\boldsymbol{\Phi}^a$. In the case of the diffuse reflection condition, the resulting condition is closed with respect to $\boldsymbol{\Phi}^a$, and the problem is reduced to that for $\boldsymbol{\Phi}^a$. Because of the smaller number of independent variables, solving the problem for $\boldsymbol{\Phi}^a$ is numerically much less expensive. Actually, in the case of elementary flow problems (88) that we are concerned with, thanks to the strong symmetry of the problems, only the two components Φ^a_2 and Φ^a_7 are necessary, and the situation is much simpler than that one would expect from the above description (see [**94**]).

Transformation into integral equation for macroscopic quantities

The McCormack model equation with the diffuse reflection condition can be transformed into simultaneous integral equations for macroscopic quantities, which are the low-order moments of ϕ^a. It is due to the form of the collision terms explained in the previous paragraph (Chu's method).

The procedure to obtain the integral equations is simple. We just formally solve the equation (66a) for ϕ^a and then substitute the resulting expression into the definition of the moments ω^a, u^a_i, θ^a, P^a_{ij}, and Q^a_i occurring in the model collision integrals. Actually, in the case of elementary flow problems (88), due to the strong symmetry of the problems, many of the moments vanish and what we finally have is the simultaneous integral equations for u^a_1, P^a_{12}, and Q^a_1, which is

symbolically written as [**94**]

$$\begin{bmatrix} u_1^a(y) \\ P_{12}^a(y) \\ Q_1^a(y) \end{bmatrix} = \int_{-1/2}^{1/2} \left(M_A^a\Big(s, y, \frac{1}{\mathrm{K}}\Big) \begin{bmatrix} u_1^{\mathrm{A}}(s) \\ P_{12}^{\mathrm{A}}(s) \\ Q_1^{\mathrm{A}}(s) \end{bmatrix} + M_B^a\Big(s, y, \frac{1}{\mathrm{K}}\Big) \begin{bmatrix} u_1^{\mathrm{B}}(s) \\ P_{12}^{\mathrm{B}}(s) \\ Q_1^{\mathrm{B}}(s) \end{bmatrix} \right) ds + I^a\Big(y, \frac{1}{\mathrm{K}}\Big).$$

Here M_A^a and M_B^a are 3×3 given matrices, while I^a is a three dimensional given vector; and all of them depend on $\hat{T}_{\mathrm{w}}$ and molecular model, besides the variables in their argument.

Elimination of the velocity distribution function has a decisive advantage. As we have pointed it out in Sec. 7.1.2, the velocity distribution function becomes steeper and steeper as the Knudsen number increases [compare Figs. 21(a), (b), and (c)]. By the use of the integral equations, we can bypass the difficulties in dealing with the steepness of the velocity distribution function numerically in the regime of large Knudsen numbers. Furthermore, from the functional form of the integral kernel matrices M_A^a and M_B^a and the inhomogeneous vector I^a, we can explicitly obtain the asymptotic solutions u_1^a, P_{12}^a, and Q_1^a for large Knudsen numbers, following [**96, 97, 98**]. Thus, we have the explicit expressions of the asymptotic behavior of the fluxes $\mathcal{M}_J^a$ for large Knudsen numbers, which read as follows:

$$\mathcal{M}_{\mathrm{P}}^a = \frac{1}{2\sqrt{\pi \hat{m}^a}} \big[-\ln \mathrm{K} - \frac{3}{2}(1-\gamma) + \ln(\sqrt{\hat{m}^a} C_a) \big] + O(\mathrm{K}^{-1}(\ln \mathrm{K})^2), \tag{92a}$$

$$\mathcal{M}_{\mathrm{T}}^a = \frac{1}{4\sqrt{\pi \hat{m}^a}} \big[\ln \mathrm{K} + \frac{1}{2}(1-3\gamma) - \ln(\sqrt{\hat{m}^a} C_a) \big] + O(\mathrm{K}^{-1}(\ln \mathrm{K})^2), \tag{92b}$$

$$\chi_{(0)}^a \mathcal{M}_\chi^a = \pm \frac{1}{2\sqrt{\pi \hat{m}^a}} \big[-\ln \mathrm{K} - \frac{3}{2}(1-\gamma) + \ln(\sqrt{\hat{m}^a} C_a) \big] + O(\mathrm{K}^{-1}(\ln \mathrm{K})^2), \tag{92c}$$

with

$$C_a = K^{\mathrm{B}a} C_{\mathrm{B}a} + K^{\mathrm{A}a} C_{\mathrm{A}a},$$

where γ is the Euler constant and the $\pm$ in the third equation means $+$ for $a = \mathrm{A}$ and $-$ for $a = \mathrm{B}$. Note that $\mathcal{M}_{\mathrm{P}}^a$, $\mathcal{M}_{\mathrm{T}}^a$, and $\chi_{(0)}^a \mathcal{M}_\chi^a$ depend on $\hat{T}_{\mathrm{w}}$ and $\chi_{(0)}^{\mathrm{A}}$ through C_a in the above expressions.

In this way, the difficulties in the regime of large Knudsen numbers, which have not yet been well-handled in the case of the original Boltzmann equation, are resolved.

7.2.2 - Plan of construction of the complete flux tables

Bearing in mind the advantages of the model equations described in Sec. 7.2.1, we can make a specific plan of the construction of the complete flux tables. In the

case of [**94, 70**], it is as follows:

1. In the regime of small Knudsen number (typically $\mathrm{K} \lesssim 0.01$), make use of the results by the asymptotic theory for small Knudsen numbers.
2. In the regime of intermediate Knudsen number (typically $0.01 \lesssim \mathrm{K} \lesssim 400$), make use of the direct numerical solutions of the problems for the marginal distribution functions Φ_2^a and Φ_7^a by a finite-difference method.
3. In the regime of large Knudsen number (typically $100 \lesssim \mathrm{K} \lesssim 10^6$), make use of the direct numerical solutions of the integral equations for macroscopic quantities.
4. In the regime of much larger Knudsen number (typically $\mathrm{K} \gtrsim 10^6$), make use of the asymptotic solutions (92).

Except for the fourth regime, we have to carry out numerical computations, and it can be done only for discrete values of the parameters K, $\chi_{(0)}^{\mathrm{A}}$, and $\hat{T}_{\mathrm{w}}$ in the elementary flow problems.[11] We chose the discrete values for numerical computations in the following way.

As to $\chi_{(0)}^{\mathrm{A}}$, whose range is $[0, 1]$, we carried out the computations for the values corresponding to the Chebyshev abscissa so that the fluxes for any specified value of $\chi_{(0)}^{\mathrm{A}}$ could be promptly and accurately obtained by the Chebyshev polynomial approximation [by the polynomials of (up to) order 21, $15 \sim 21$, and 8 in the first, second, and third regimes, respectively]. As to K, we properly subdivided the region $0.01 \lesssim \mathrm{K} \lesssim 10^6$ in accordance with the change of fluxes as a function of $\ln \mathrm{K}$ and carried out the computations for the values corresponding to the Chebyshev abscissa (with respect to $\ln \mathrm{K}$, not to K itself) in each subdivided region. As to $\hat{T}_{\mathrm{w}}$, we constructed the flux tables covering the region of $0.5 \leq \hat{T}_{\mathrm{w}} \leq 2$ by performing the computations for five different values. The fluxes for arbitrarily specified value of $\hat{T}_{\mathrm{w}}$ in the region are promptly provided by the spline interpolation.

The complete flux tables thus obtained are shown in Fig. 20 with solid and dashed lines. The reliability of the use of the McCormack model is also assessable from the figure. One of the advantages of the McCormack model is its flexibility about the choice of molecular model, such as the Maxwell, hard-sphere, inverse-power-law potential, Lenard-Jones models. This feature was fully made use of in the study of gas separation in [**70**].

---

[11] In the case of the first regime, the dependence on K is expressed by its power series, and numerically solved are the spatially half-space problems (the so-called Knudsen-layer problems) that contain $\chi_{(0)}^{\mathrm{A}}$ and $\hat{T}_{\mathrm{w}}$ as parameters.

References

[1] Y. SONE, *Kinetic theory and fluid dynamics*, Birkhäuser, Boston 2002; supplementary Notes and Errata, http://hdl.handle.net/2433/66099, Kyoto University Research Information Repository.

[2] Y. SONE, *Molecular gas dynamics: Theory, techniques, and applications*, Birkhäuser, Boston 2007; supplementary Notes and Errata, http://hdl.handle.net/2433/66098, Kyoto University Research Information Repository.

[3] Y. SONE, *Asymptotic theory of flow of rarefied gas over a smooth boundary I,* in Rarefied gas dynamics, L. Trilling and H. Y. Wachman eds., Academic, New York 1969, 243-253.

[4] Y. SONE, *Asymptotic theory of flow of rarefied gas over a smooth boundary II,* in Rarefied gas dynamics, D. Dini ed., Editrice Tecnico Scientifica, Pisa 1971, Vol. II, 737-749.

[5] Y. SONE and K. AOKI, *Steady gas flows past bodies at small Knudsen numbers – Boltzmann and hydrodynamic systems,* Transport Theory Statist. Phys. **16** (1987), 189-199.

[6] Y. SONE, *Asymptotic theory of a steady flow of a rarefied gas past bodies for small Knudsen numbers,* in Advances in kinetic theory and continuum mechanics, R. Gatignol and Soubbaramayer eds., Springer, Berlin 1991, 19-31.

[7] Y. SONE, K. AOKI, S. TAKATA, H. SUGIMOTO and A. V. BOBYLEV, *Inappropriateness of the heat-conduction equation for description of a temperature field of a stationary gas in the continuum limit: examination by a asymptotic analysis and numerical computation of the Boltzmann equation,* Phys. Fluids 8 (1996), 628-638; Erratum: *ibid.* 8 (1996), 841.

[8] Y. SONE, *Theory and numerical analysis of the Boltzmann equation – Theory and analysis of rarefied gas flows –, Lecture Notes* (Dept. of Aeronautics and Astronautics, Graduate School of Engineering, Kyoto University, 1998), Part I, http://hdl.handle.net/2433/65065, Kyoto University Research Information Repository.

[9] Y. SONE, C. BARDOS, F. GOLSE and H. SUGIMOTO, *Asymptotic theory of the Boltzmann system for a steady flow of a slightly rarefied gas with a finite Mach number: general theory,* Eur. J. Mech. B/Fluids **19** (2000), 325-360.

[10] E. H. KENNARD, *Kinetic theory of gases,* McGraw-Hill, New York 1938.

[11] Y. SONE, *Thermal creep in rarefied gas,* J. Phys. Soc. Jpn. **21** (1966), 1836-1837.

[12] T. OHWADA, Y. SONE and K. AOKI, *Numerical analysis of the shear and thermal creep flows of a rarefied gas over a plane wall on the basis of the linearized Boltzmann equation for hard-sphere molecules,* Phys. Fluids A **1** (1989), 1588-1599.

[13] Y. SONE, *A simple demonstration of a rarefied gas flow induced over a plane wall with a temperature gradient,* Phys. Fluids A **3** (1991), 997-998.

[14] Y. SONE, K. SAWADA and H. HIRANO, *A simple experiment on the strength of thermal creep flow of a rarefied gas over a flat wall,* Eur. J. Mech. B/Fluids **13** (1994), 299-303.

[15] Y. SONE, *Flow induced by thermal stress in rarefied gas,* Phys. Fluids **15** (1972), 1418-1423.

[16] Y. SONE and S. TANAKA, *Thermal stress slip flow induced in rarefied gas between noncoaxial circular cylinders,* in Theoretical and applied mechanics, F. P. J. Rimrott and B. Tabarrok eds., North-Holland, Amsterdam 1980, 405-416.

[17] T. OHWADA and Y. SONE, *Analysis of thermal stress slip flow and negative thermophoresis using the Boltzmann equation for hard-sphere molecules,* Eur. J. Mech. B/Fluids **11** (1992), 389-414.

[18] F. GOLSE and C. D. LEVERMORE, *Stokes-Fourier and acoustic limits for the Boltzmann equation: convergence proofs*, Comm. Pure Appl. Math. **55** (2002), 336-393.

[19] A. DE MASI, R. ESPOSITO and J. L. LEBOWITZ, *Incompressible Navier-Stokes and Euler limits of the Boltzmann equation,* Comm. Pure Appl. Math. **42** (1989), 1189-1214.

[20] C. BARDOS, F. GOLSE and C. D. LEVERMORE, *Sur les limites asymptotiques de la théorie cinétique conduisant à la dynamique des fluides incompressibles,* C. R. Acad. Sci. Paris Sér. I. Math. **309** (1989), 727-732.

[21] C. BARDOS, F. GOLSE and C. D. LEVERMORE, *Fluid dynamic limits of kinetic equations. I. Formal derivations,* J. Stat. Phys. **63** (1991), 323-344.

[22] C. BARDOS, F. GOLSE and C. D. LEVERMORE, *Fluid dynamic limits of kinetic equations II convergence proofs for the Boltzmann equation,* Comm. Pure Appl. Math. **46** (1993), 667-753.

[23] F. GOLSE and L. SAINT-RAYMOND, *The Navier-Stokes limit of the Boltzmann equation for bounded collision kernels,* Invent. Math. **155** (2004), 81-161.

[24] V. S. GALKIN, M. N. KOGAN and O. G. FRIDLENDER, *Free convection in a gas in the absence of external forces,* Fluid Dynamics **6** (1971), 448-457.

[25] M. N. KOGAN, V. S. GALKIN and O. G. FRIDLENDER, *Stresses produced in gasses by temperature and concentration inhomogeneities. New types of free convection,* Sov. Phys. Usp. **19** (1976), 420-428.

[26] Y. SONE, S. TAKATA and H. SUGIMOTO, *The behavior of a gas in the continuum limit in the light of kinetic theory: the case of cylindrical Couette flows with evaporation and condensation,* Phys. Fluids 8 (1996), 3403-3413; Erratum: *ibid.* **10** (1998), 1239.

[27] Y. SONE, *Continuum gas dynamics in the light of kinetic theory and new features of rarefied gas flows,* in Rarefied gas dynamics, C. Shen ed., Peking University Press, Beijing 1997, 3-24.

[28] Y. SONE, *Flows induced by temperature fields in a rarefied gas and their ghost effect on the behavior of a gas in the continuum limit,* Annu. Rev. Fluid Mech. **32** (2000), 779-811.

[29] Y. SONE and T. DOI, *Bifurcation of and ghost effect on the temperature field in the Bénard problem of a gas in the continuum limit,* Phys. Fluids **15** (2003), 1405-1423; Erratum: *ibid.* **15** (2003), 2786.

[30] Y. SONE, M. HANDA and T. DOI, *Ghost effect and bifurcation in a gas between coaxial circular cylinders with different temperatures,* Phys. Fluids **15** (2003), 2903-2915.

[31] Y. SONE and T. DOI, *Ghost effect of infinitesimal curvature in the plane Couette flow of a gas in the continuum limit,* Phys. Fluids **16** (2004), 952-971.

[32] Y. SONE and T. DOI, *Instability of the plane Couette flow by the ghost effect of infinitesimal curvature,* in Rarefied gas dynamics, M. Capitelli ed., AIP, Melville 2005, 258-263.

[33] G. A. BIRD, *Approach to translational equilibrium in a rigid sphere gas,* Phys. Fluids **6** (1963), 1518-1519.

[34] W. WAGNER, *A convergence proof for Bird's direct simulation Monte Carlo method for the Boltzmann equation,* J. Stat. Phys. **66** (1992), 1011-1044.

[35] G. A. BIRD, *Molecular gas dynamics,* Oxford University Press, Oxford 1976.

[36] G. A. BIRD, *Molecular gas dynamics and the direct simulation of gas flows,* Oxford University Press, Oxford 1994.

[37] K. KOURA, *Null-collision technique in the direct-simulation Monte Carlo method,* Phys. Fluids **29** (1986), 3509-3511.

[38] K. NANBU, *Theoretical basis of the direct simulation Monte Carlo method,* in Rarefied gas dynamics, V. Boffi and C. Cercignani eds., Teubner, Stuttgart 1986, Vol. I, 369-383.

[39] C. CERCIGNANI, R. ILLNER and M. PULVIRENTI, *The mathematical theory of dilute gases,* Springer, New York 1994, Chap. 10.

[40] S. RJASANOW and W. WAGNER, *Stochastic numerics for the Boltzmann equation,* Springer, Berlin 2005.

[41] K. AOKI, Y. SONE and N. MASUKAWA, *A rarefied gas flow induced by a temperature field,* in Rarefied gas dynamics, J. Harvey and G. Lord eds., Oxford Univ. Press, Oxford 1995, 35-41.

[42] Y. SONE and M. YOSHIMOTO, *Demonstration of a rarefied gas flow induced near the edge of a uniformly heated plate,* Phys. Fluids **9** (1997), 3530-3534.

[43] Y. SONE, *Highly rarefied gas around a group of bodies with various temperature distributions. II. Arbitrary temperature variation,* J. Méc. Théor. Appl. **4** (1985), 1-14.

[44] T. OHWADA, *Structure of normal shock waves: direct numerical analysis of the Boltzmann equation for hard-sphere molecules,* Phys. Fluids A **5** (1993), 217-234.

[45] T. OHWADA, *Heat flow and temperature and density distributions in a rarefied gas between parallel plates with different temperatures. Finite-difference analysis of the nonlinear Boltzmann equation for hard-sphere molecules,* Phys. Fluids **8** (1996), 2153-2160.

[46] C. K. CHU, *Kinetic-theoretic description of the formation of a shock wave,* Phys. Fluids **8** (1965), 12-22.

[47] K. AOKI, S. TAKATA, H. AIKAWA and F. GOLSE, *A rarefied gas flow caused by a discontinuous wall temperature,* Phys. Fluids **13** (2001), 2645-2661.

[48] Y. SONE and S. TAKATA, *Discontinuity of the velocity distribution function in a rarefied gas around a convex body and the S layer at the bottom of the Knudsen layer,* Transport Theory Statist. Phys. **21** (1992), 501-530.

[49] K. AOKI, K. KANBA and S. TAKATA, *Numerical analysis of a supersonic rarefied gas flow past a flat plate,* Phys. Fluids **9** (1997), 1144-1161.

[50] Y. SONE and H. SUGIMOTO, *Strong evaporation from a plane condensed phase,* in Adiabatic waves in liquid-vapor systems, G. E. A. Meier and P. A. Thompson eds., Springer, Berlin 1990, 293-304.

[51] K. AOKI, Y. SONE, K. NISHINO and H. SUGIMOTO, *Numerical analysis of unsteady motion of a rarefied gas caused by sudden changes of wall temperature with special interest in the propagation of a discontinuity in the velocity distribution function,* in Rarefied gas dynamics, A. E. Beylich ed., VCH, Weinheim 1991, 222-231.

[52] H. SUGIMOTO and Y. SONE, *Numerical analysis of steady flows of a gas evaporating from its cylindrical condensed phase on the basis of kinetic theory,* Phys. Fluids A **4** (1992), 419-440.

[53] S. TAKATA, Y. SONE and K. AOKI, *Numerical analysis of a uniform flow of a rarefied gas past a sphere on the basis of the Boltzmann equation for hard-sphere molecules,* Phys. Fluids A **5** (1993), 716-737.

[54] Y. SONE and H. SUGIMOTO, *Kinetic theory analysis of steady evaporating flows from a spherical condensed phase into a vacuum*, Phys. Fluids A **5** (1993), 1491-1511.

[55] Y. SONE, S. TAKATA and M. WAKABAYASHI, *Numerical analysis of a rarefied gas flow past a volatile particle using the Boltzmann equation for hard-sphere molecules,* Phys. Fluids **6** (1994), 1914-1928.

[56] Y. SONE and H. SUGIMOTO, *Evaporation of a rarefied gas from a cylindrical condensed phase into a vacuum,* Phys. Fluids **7** (1995), 2072-2085.

[57] M. KNUDSEN, *Eine revision der gleichgewichtsbedingung der gase. Thermische molekularströmung*, Ann. Phys. (Leipzig) **31** (1910), 205-229.

[58] G. PHAM-VAN-DIEP, P. KEELEY, E. P. MUNTZ and D. P.WEAVER, *A micro-mechanical Knudsen compressor*, in Rarefied gas dynamics, J. Harvey and G. Lord eds., Oxford University Press, Oxford 1995, Vol. I, 715-721.

[59] Y. SONE, Y. WANIGUCHI and K. AOKI, *One-way flow of a rarefied gas induced in a channel with a periodic temperature distribution*, Phys. Fluids 8 (1996), 2227-2235.

[60] K. AOKI, Y. SONE, S. TAKATA, K. TAKAHASHI and G. A. BIRD, *One-way flow of a rarefied gas induced in a circular pipe with a periodic temperature distribution*, in Rarefied gas dynamics, T.J. Bartel and M.A. Gallis eds., AIP, Melville 2001, 940-947.

[61] Y. SONE and K. SATO, *Demonstration of a one-way flow of a rarefied gas induced through a pipe without average pressure and temperature gradients*, Phys. Fluids **12** (2000), 1864-1868.

[62] Y. SONE, T. FUKUDA, T. HOKAZONO and H. SUGIMOTO, *Experiment on a one-way flow of a rarefied gas through a straight circular pipe without average temperature and pressure gradients*, in Rarefied gas dynamics, T.J. Bartel and M.A. Gallis eds., AIP, Melville 2001, 948-955.

[63] Y. SONE and H. SUGIMOTO, *Knudsen compressor*, J. Vac. Soc. Jpn. **45** (2002), 138–141.

[64] Y. L. HAN, M. YOUNG, E. P. MUNTZ and G. SHIFLETT, *Knudsen compressor performance at low pressures*, in Rarefied gas dynamics, M. Capitelli ed., AIP, Melville 2005, 162-167.

[65] K. AOKI, P. DEGOND, L. MIEUSSENS, M. NISHIOKA and S. TAKATA, *Numerical simulation of a Knudsen pump using the effect of curvature of the channel*, in Rarefied gas dynamics, M. S. Ivanov and A. K. Rebrov eds., Siberian Branch

of the Russian Academy of Sciences, Novosibirsk 2007, 1079-1084.

[66] K. AOKI, P. DEGOND, L. MIEUSSENS, S. TAKATA and H. YOSHIDA, *A diffusion model for rarefied flows in curved channels*, Multiscale Model. Simul. **6** (2008), 1281-1316.

[67] J. P. HOBSON, *Accommodation pumping – A new principle for low pressures*, J. Vac. Sci. Technol. **7** (1970), 351-357.

[68] M. L. HUDSON and T.J. BARTEL, *DSMC simulation of thermal transpiration and accommodation pumps*, in Rarefied gas dynamics, R. Brun et al. eds., Cépaduès, Toulouse 1999, 719-726.

[69] H. SUGIMOTO and Y. SONE, *Vacuum pump without a moving part driven by thermal edge flow*, in Rarefied gas dynamics, M. Capitelli ed., AIP, Melville 2005, 168-173.

[70] S. TAKATA, H. SUGIMOTO and S. KOSUGE, *Gas separation by means of the Knudsen compressor*, Eur. J. Mech. B/Fluids **26** (2007), 155-181.

[71] H. SUGIMOTO, S. TAKATA and S. KOSUGE, *Gas separation effect of the pump driven by the thermal edge flow*, in Rarefied gas dynamics, M.S. Ivanov and A.K. Rebrov eds., Siberian Branch of the Russian Academy of Sciences, Novosibirsk 2007, 1158-1163.

[72] B.B. HAMEL, *Kinetic model for binary gas mixtures*, Phys. Fluids **8** (1965), 418-425.

[73] C. J. T. LANERYD, K. AOKI, P. DEGOND and L. MIEUSSENS, *Thermal creep of a slightly rarefied gas through a channel with curved boundary*, in Rarefied gas dynamics, M.S. Ivanov and A.K. Rebrov eds., Siberian Branch of the Russian Academy of Sciences, Novosibirsk 2007, 1111-1116.

[74] K. AOKI and P. DEGOND, *Homogenization of a flow in a periodic channel of small section*, Multiscale Model. Simul. **1** (2003), 304-334.

[75] K. AOKI, P. DEGOND, S. TAKATA and H. YOSHIDA, *Diffusion models for Knudsen compressors*, Phys. Fluids **19** (2007), 117103.

[76] P. CHARRIER and B. DUBROCA, *Asymptotic transport models for heat and mass transfer in reactive porous media*, Multiscale Model. Simul. **2** (2003), 124-157.

[77] K. AOKI, C. BARDOS and S. TAKATA, *Knudsen layer for gas mixtures*, J. Stat. Phys. **112** (2003), 629-655.

[78] S. KOSUGE, K. SATO, S. TAKATA and K. AOKI, *Flows of a binary mixture of rarefied gases between two parallel plates*, in Rarefied gas dynamics, M. Capitelli ed., AIP, Melville 2005, 150-155.

[79] Y. SONE, T. OHWADA and K. AOKI, *Temperature jump and Knudsen layer in a rarefied gas over a plane wall: numerical analysis of the linearized Boltzmann equation for hard-sphere molecules*, Phys. Fluids A **1** (1989), 363-370.

[80] T. OHWADA, Y. SONE and K. AOKI, *Numerical analysis of the Poiseuille and thermal transpiration flows between two parallel plates on the basis of the Boltzmann equation for hard-sphere molecules*, Phys. Fluids A **1** (1989), 2042–2049; Erratum: *ibid.* **2** (1990), 639.

[81] T. OHWADA, K. AOKI and Y. SONE, *Heat transfer and temperature distribution in a rarefied gas between two parallel plates with different temperatures: numerical analysis of the Boltzmann equation for a hard sphere molecule*, in Rarefied

gas dynamics: theoretical and computational techniques, E. P. Muntz, D. P. Weaver, D. H. Campbell eds., AIAA, Washington, DC 1989, 70-81.

[82] T. OHWADA, Y. SONE and K. AOKI, *Numerical analysis of the shear and thermal creep flows of a rarefied gas over a plane wall on the basis of the linearized Boltzmann equation for hard-sphere molecules*, Phys. Fluids A **1** (1989), 1588-1599.

[83] Y. SONE, T. OHWADA and K. AOKI, *Evaporation and condensation on a plane condensed phase: numerical analysis of the linearized Boltzmann equation for hard-sphere molecules*, Phys. Fluids A **1** (1989), 1398-1405.

[84] Y. SONE, T. OHWADA and K. AOKI, *Evaporation and condensation of a rarefied gas between its two parallel plane condensed phases with different temperatures and negative temperature-gradient phenomenon: numerical analysis of the Boltzmann equation for hard-sphere molecules*, in Mathematical aspects of fluid and plasma dynamics, Lecture Notes in Mathematics, G. Toscani, V. Boffi, S. Rionero eds., Springer-Verlag, Berlin 1991, Vol. 1460, 186-202.

[85] Y. SONE, S. TAKATA and T. OHWADA, *Numerical analysis of the plane Couette flow of a rarefied gas on the basis of the linearized Boltzmann equation for hard-sphere molecules*, Eur. J. Mech. B/Fluids **9** (1990), 273-288.

[86] S. TAKATA, K. AOKI and Y. SONE, *Thermophoresis of a sphere with a uniform temperature: numerical analysis of the Boltzmann equation for hard-sphere molecules*, in Rarefied gas dynamics: theory and simulations, B. D. Shizgal, D. P. Weaver eds., AIAA, Washington, DC 1994, 626-639.

[87] S. TAKATA and Y. SONE, *Flow induced around a sphere with a non-uniform surface temperature in a rarefied gas, with application to the drag and thermal force problems of a spherical particle with an arbitrary thermal conductivity*, Eur. J. Mech. B/Fluids **14** (1995), 487-518.

[88] S. TAKATA, Y. SONE, D. LHUILLIER and M. WAKABAYASHI, *Evaporation from or condensation onto a sphere: numerical analysis of the Boltzmann equation for hard-sphere molecules*, Computers Math. Appl. **35** (1998), 193-214.

[89] S. TAKATA, *Diffusion slip for a binary mixture of hard-sphere molecular gases: numerical analysis based on the linearized Boltzmann equation*, in Rarefied gas dynamics, T. J. Bartel, M. A. Gallis eds., AIP, Melville 2001, 22-29.

[90] S. TAKATA, S. YASUDA, S. KOSUGE and K. AOKI, *numerical analysis of thermal-slip and diffusion-slip flows of a binary mixture of hard-sphere molecular gases*, Phys. Fluids **15** (2003), 3745-3766.

[91] S. YASUDA, S. TAKATA and K. AOKI, *Numerical analysis of the shear flow of a binary mixture of hard-sphere gases over a plane wall*, Phys. Fluids **16** (2004), 1989-2003.

[92] S. YASUDA, S. TAKATA and K. AOKI, *Evaporation and condensation of a binary mixture of vapors on a plane condensed phase: numerical analysis of the linearized Boltzmann equation*, Phys. Fluids **17** (2005), 047105.

[93] S. TAKATA, K. AOKI, S. KOSUGE and S. YASUDA, *Temperature, pressure, and concentration jumps for a binary mixture of vapors on a plane condensed phase: numerical analysis of the linearized Boltzmann equation*, Phys. Fluids **18** (2006), 067102.

[**94**] S. KOSUGE and S. TAKATA, *Database for flows of binary gas mixtures through a plane microchannel*, Eur. J. Mech. B/Fluids **27** (2008), 444-465.

[**95**] C.-C. CHEN, I.-K. CHEN, T.-P. LIU and Y. SONE, *Thermal transpiration for the linearized Boltzmann equation*, Commun. Pure Appl. Math. **60** (2007), 147-163.

[**96**] H. NIIMI, *Thermal creep flow of rarefied gas between two parallel plates*, J. Phys. Soc. Jpn. **30** (1971), 572-574.

[**97**] C. CERCIGNANI, *Plane Poiseuille flow and Knudsen minimum effect*, in Rarefied gas dynamics, J. A. Laurmann ed., Academic Press, New York 1963, Vol. II, 92-101.

[**98**] C. CERCIGNANI, *Plane Poiseuille flow according to the method of elementary solutions*, J. Math. Anal. Appl. **12** (1965), 254-262.

[**99**] Y. SONE and E. ITAKURA, *Analysis of Poiseuille and thermal transpiration flows for arbitrary Knudsen numbers by a modified Knudsen number expansion method and their database*, J. Vac. Soc. Jpn. **33** (1990), 92-94.

[**100**] K. AOKI, S. TAKATA and K. KUGIMOTO, *Diffusion approximation for the Knudsen compressor composed of circular tubes*, in Rarefied gas dynamics, T. Abe ed., AIP, Melville 2009, 953-958.

[**101**] F. J. MCCORMACK, *Construction of linearized kinetic models for gaseous mixtures and molecular gases*, Phys. Fluids **16** (1973), 2095-2105.

[**102**] C. CERCIGNANI and F. SHARIPOV, *Gaseous mixture slit flow at intermediate Knudsen numbers*, Phys. Fluids A **4** (1992), 1283-1289.

[**103**] L. H. HOLWAY, JR., *Approximation procedures for kinetic theory*, Ph.D. Thesis, Harvard University 1963.

[**104**] L. H. HOLWAY, JR., *New statistical models for kinetic theory: methods of construction*, Phys. Fluids **9** (1966), 1658-1673.

[**105**] S. KOSUGE, *Model Boltzmann equation for gas mixtures: construction and numerical comparison*, Eur. J. Mech. B/Fluids **28** (2009), 170-184.

KAZUO AOKI, SHIGERU TAKATA
Department of Mechanical Engineering and Science
(also Advanced Research Institute for Fluid Science and Engineering)
Graduate School of Engineering, Kyoto University
Kyoto 606-8501, Japan
e-mail: aoki@aero.mbox.media.kyoto-u.ac.jp
e-mail: takata@aero.mbox.media.kyoto-u.ac.jp